Structural basis for interactions of the *Phytophthora sojae* RxLR effector Avh5 with phosphatidylinositol 3-phosphate and for host cell entry

Furong Sun

Dissertation submitted to the faculty of the Virginia Polytechnic Institute and State University in partial fulfillment of the requirements for the degree of

Doctor of Philosophy

in

Chemistry

Committee Chair:

Dr. Daniel G. S. Capelluto

Committee Co-Chair:

Dr. Webster L. Santos

Committee Members:

Dr. David R. Bevan

Dr. Carla V. Finkielstein

Dr. Iuliana Lazar

Dr. Sungsool Wi

April 9th, 2012

Blacksburg, VA

Keywords: Avirulence homolog-5; Phosphatidylinositol 3-phosphate; *Phytophthora sojae*; Protein-lipid interactions.

Structural basis for interactions of the *Phytophthora sojae* RxLR effector Avh5 with phosphatidylinositol 3-phosphate and for host cell entry

Furong Sun

ABSTRACT

Oomycetes, such as *Phytophthora sojae*, are plant pathogens that employ protein effectors that enter host cells to facilitate infection. Plants may overcome infection by recognizing pathogen effectors via intracellular receptors (R proteins) that form part of their defense system. Entry of some effector proteins into plant cells is mediated by conserved RxLR motifs in the effectors and phosphoinositides (PIPs) resident in the host plasma membrane such as phosphatidylinositol 3-phosphate (PtdIns(3)P). Recent reports differ regarding the regions on RxLR effector proteins involved in PIP recognition. To clarify these differences, I have structurally and functionally characterized the *P. sojae* effector, avirulence homolog-5 (Avh5). Using NMR spectroscopy, I demonstrate that Avh5 is helical in nature with a long N-terminal disordered region. Heteronuclear single quantum coherence titrations of Avh5 with the PtdIns(3)P head group, inositol 1,3-bisphosphate (Ins(1,3)P_2), allowed us to identify a C-terminal lysine-rich helical region (helix 2) as the principal lipid-binding site in the protein, with the N-terminal RxLR (RFLR) motif playing a more minor role. Furthermore, mutations in the RFLR motif slightly affected PtdIns(3)P binding, while mutations in the basic helix almost abolished it. Avh5 exhibited moderate affinity for PtdIns(3)P, which increased the thermal stability of the protein. Mutations in the RFLR motif or in the basic region of Avh5 both significantly reduced protein entry into plant and human cells. Both regions independently mediated cell entry via a PtdIns(3)P-dependent mechanism. My findings support a model in which Avh5 transiently interacts with PtdIns(3)P by electrostatic interactions mainly through its positively charged helix 2 region, providing stability to the protein during RFLR-mediated host entry.

Dedication

I sincerely dedicate my dissertation to

My dear parents: Mr. Sun Maoshan & Ms. Fu Jiae

My dear younger sister: Ms. Sun Jingjing

Acknowledgements

“FIVE YEARS” is long enough to change one person. For me, during this period, I have grown up to a lady having tasted the happiness and sorrow in scientific career to some extent. I have no idea of what the long-term impact of this period will impose on my future life, including my career development. However, I firmly believe that the scientific training I have accepted will help me contribute to the society, either in China or in America, in a positive way and that is, enough, from where I stand. To decide to come to the United States for graduate studies is a big decision in my life, and to decide to run to the end is another big decision. Just like a marathon, a lot of people started together at the starting point, many people gave up in the middle, and finally, few people reached the endpoint. Life is long, and nothing is wrong. Whatever choice one person has made is not important, as long as we are able to follow our heart to lead a life in our comfort zone.

Thank you a lot, my parents! Without your understanding and support, I would have been unable to be here. Just like what Confucius said, “While one’s parents are alive, one should not travel to distant places”. Unfortunately, I did not follow his advice. However, I promise I will be back to China in the near future to accompany you to the end!

Thank you a lot, my advisor, Dr. Capelluto! Your patience gave me ample time to grow and your guidance has brought me here!

Thank you a lot, all of my committee members! My first committee meeting was a nightmare, but you never gave up on me!

Thank you a lot, all of the previous and current lab members! Your help kept me progressing!

Thank you a lot, Dr. Deck, Dr. Esker, Dr. Madsen and all of the other Chemistry Faculty at VT! Your presence has made my graduate life more exciting!

Table of Contents

List of Abbreviations:

Avh5: Avirulence homolog-5

BS^3: Bis(Sulfosuccinimidyl) suberate

CD: circular dichroism

DAG: diacylglycerol

dEER: aspartic acid (less conserved), glutamic acid, glutamic acid, arginine

EBD: endosome binding domain

E. coli: *Escherichia coli*

FYVE: Fab1p, YOTB, Vac1p and EEA1

HSQC: heteronuclear single quantum coherence

Ins(1)P: inositol 1-phosphate

Ins(1,3)P_2: inositol 1,3-bisphosphate

Ins(1,4,5)P_3: inositol-1,4,5-trisphosphate

LBA: liposome binding assay

LRR: leucine rich repeats

MAPK: Mitogen-Activated Protein Kinase

MRI: magnetic resonance imaging

NBS: nucleotide binding sites

NMR: nuclear magnetic resonance

OG: N-octyl-β-D-glucopyranoside

PA: phosphatidic acid

PAMP: pathogen-associated molecular pattern

PCR: polymerase chain reaction

PH: pleckstrin homology

PI: phosphatidylinositol

PI3K: phosphoinositide 3-kinase

PI4K: phosphoinositide 4-kinase

PIP: phosphoinositide

PI-PLC: phosphoinositide-specific phospholipase C

PLO: protein lipid overlay

PKB: Protein Kinase B

PtdCho: phosphatidylcholine

PtdEth: phosphatidylethanolamine

PtdIns(3)P: phosphatidylinositol 3-phosphate

PtdIns(3,4)P_2: phosphatidylinositol 3, 4-bisphosphate

PtdIns(3,5)P_2: phosphatidylinositol 3, 5-bisphosphate

PtdIns(3,4,5)P_3: phosphatidylinositol 3, 4, 5-trisphosphate

PtdIns(4)P: phosphatidylinositol 4-phosphate

PtdIns(4)P5K: PtdIns(4)P 5-kinase

PtdIns(4,5)P_2: phosphatidylinositol 4, 5-bisphosphate

PtdIns(5)P: phosphatidylinositol 5-phosphate

PtdSer: phosphatidylserine

PRR: pattern recognition receptor

PTI: PAMP-triggered immunity

PX: phox homology

R: resistance

RNA: ribonucleic acid

RHD4: Root Hair Defective4

RxLR (arginine, any amino acid, leucine, arginine)

SER: Sarco/endoplasmic reticulum

SPR: surface plasmon resonance

List of Figures:

List of Tables:

Chapter 1 INTRODUCTION

1. Research Background

i. *Phytophthora sojae*: Excellent model organism to study oomycete pathogenesis

Oomycetes are usually mistakenly recognized as fungi. They do take after fungi outwardly. However, they are far away from fungi from an evolutionary viewpoint (1). Oomycetes belong to Stramenopiles. Stramenopiles, including oomycetes, chrysophytes, phaeophytes, synurophytes, diatoms, xanthophytes, bicosoecids and slime nets, diverged evolutionarily almost at the same time with animals, plants and fungi (2).

Oomycetes include *Phytophthora megasperma* and *Lagenidium glganteum*, among others (3). Especially, *Phytophthora* species account for the major part of oomycetes. *Phytophthora* species include many agriculturally devastating species, e.g., *Phytophthora sojae* (*P. sojae*), *Phytophthora infestans* (*P. infestans*), and *Phytophthora* ramorum (*P. ramorum*) (4). It has been reported that *Phytophthora* species have caused billions of dollars in losses all over the world each year (1). *P. infestans* leads to potato late blight, which caused the notorious 1846 Ireland potato starvation (5). In fact, even in modern society, potato late blight still has damaging impact on potato yield due to evolved *P. infestans* strains (6). *P. ramorum* causes bleeding cankers and shoot dieback, resulting in the sudden oak death, which seriously threatens the livability of forestry of Europe and North America, especially in the states of California and Oregon (7).

P. sojae attack the underground part of plants, just like what Figure 1 shows, causing the stem rot of adult plants and damping off of young plants (1). The soybean plants and several species of lupin are the attack targets of *P. sojae*. It has been reported that *P. sojae* causes 1 to

2 billion dollar-loss every year worldwide (5). Figure 2 summarizes the life cycle of *P. sojae*, and *P. sojae* includes both sexual and asexual production phases (1). *P. sojae* is defined as hemibiotrophic organism since it exhibits an initial phase of biotrophic growth followed by a transition to necrotrophy (1). Due to the ineffectiveness of conventional medicinal treatment, such as fungicides, novel solutions are urgently needed to be developed to treat *P. sojae*, a

Figure 1. Disease symptoms of *Phytophthora sojae* on soybean. (A) Damping off of seedlings. (B) Stem rot. *Reprinted with permission from* [1].

good representative of oomycete pathogens.

ii. Plant pathogen effector proteins: Good understanding is in urgent need

The effector protein is the core weapon of microbial pathogens. All of the microbial plant pathogens, including bacteria, oomycete and fungi, secrete effector proteins to enhance their virulence towards host plant cells (8). Effector proteins are also called avirulence proteins (Avr

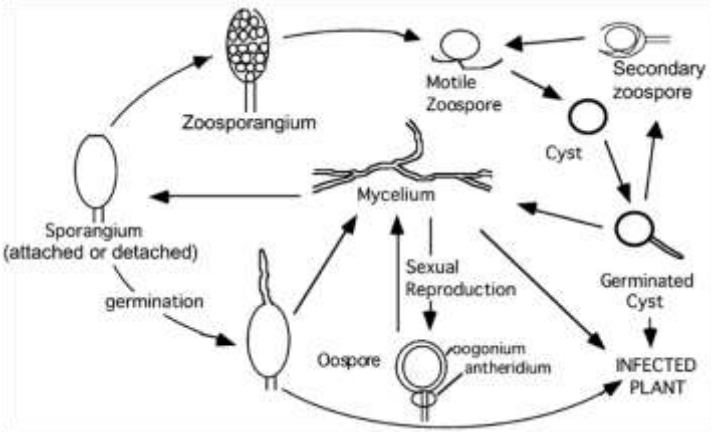

Figure 2. *Phytophthora sojae* life cycle. *Reprinted with permission from* [1].

proteins) in that the pathogen virulence will be abrogated as long as there are cognate resistance proteins encoded by the *R* genes existing inside host cells (9).

How the effector proteins produced by bacteria, fungi and oomycetes, respectively, invade plants is always a significant question to be answered in detail. For bacterial effectors, it has been found that they are directly delivered into the host cell via the type III secretion system (10), while the effector proteins secreted by fungal and oomycete pathogens are delivered inside the host cells via certain translocation motifs (8, 11). For oomycete effector proteins, there are translocation motifs at the N-terminus, called RxLR (arginine, any amino acid, leucine, arginine) and dEER (aspartic acid<less conserved>, glutamic acid, glutamic acid, arginine), employed to mediate effector entry into host cell (8), and such entry is independent of any machinery encoded by the pathogen (5). For fungal effector proteins, there is no obvious RxLR-dEER domain. However, similar translocation motifs are also found (11).

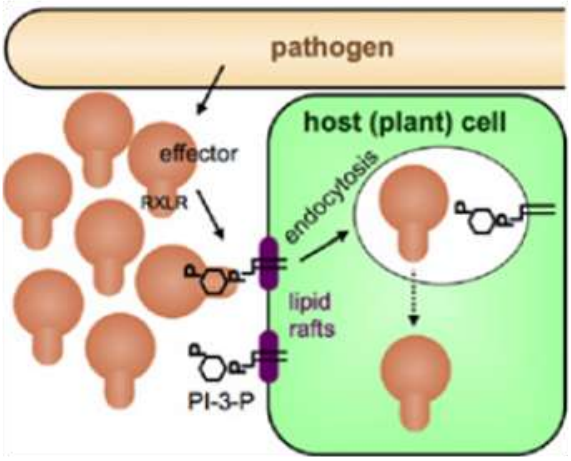

Figure 3. Proposed model for effector entry. Binding of effectors via their RXLR domains to PtdIns(3)P, possibly located in lipid rafts, leads to entry by endocytosis. The mechanism of escape from endosomes is currently unknown. The moderate affinity of the effectors for PtdIns(3)P facilitates binding on the outer surface but dissociation from PtdIns(3)P inside the cell. *Reprinted with permission from* [11].

It is known that effector proteins are responsible for the pathogenesis of pathogens in that they cut off the host plant defense pathway (12). Moreover, the effector proteins produced by oomycete and fungal pathogens have been found to recognize the corresponding resistance protein at the host cytoplasm (13), which indicates that effector proteins must enter the host cell to facilitate pathogenesis. However, how effector proteins enter the host plant cell is still unclear.

According to Tyler and colleagues, the extracellular phosphoinositide, phosphatidylinositol 3-phosphate (PtdIns(3)P), recognizes the N-terminal RXLR and dEER motifs, and such recognition can mediate the effector protein into plant, animal and human cells, respectively (11). As indicated in Figure 3, the oomycete pathogens secret effector proteins with RXLR domain, which recognizes the PtdIns(3)P existing on the outer leaflet of the plant cell plasma membrane, and such recognition mediates the entry of effector proteins into plant host cell possibly via lipid-raft mediated endocytosis (11). Once inside in the cell, the effector protein will be released from the endosome into the cytoplasm to perform pathogenesis, although the escape mechanism is unknown at this point (11). This proposed model for effector entry provides novel insights into the effector protein entry mechanism, and also provides potential solutions to designing therapeutic methods to inhibit the pathogenesis of oomycete pathogens

towards agriculture. However, just one year later, Yaeno and colleagues proposed an alternative model. They found that the conserved, positively charged residues at the C terminus, instead of the RXLR motif at the N terminus, are responsible for PtdIns(3)P recognition, for two effector proteins, one being AVR3a, secreted by *P. capsici*, infecting pepper and cucurbit, as well as Avr1b, the same protein used in Tyler and colleagues' work, secreted by *P. infestans* (14). In addition, they suggested that PtdIns(3)P-mediated effector protein entry into host cell may stabilize the effector protein, which further stabilizes the ubiquitin ligase CMPG1, a critical protein in inhibiting host immunity pathways (14). Therefore, as what Ellis and Dodds have pointed out, there is urgent need to clarify these differences (15). One potential solution is to map the binding site between avirulence proteins and phosphoinositides (15). Additionally, they also suggested that there is need to test the effectiveness of PtdIns(3)P-mediated mutant lacking RXLR domain entry into host cells (15). Those are two urgent problems to be tackled in exploring the basis of plant diseases.

iii. Plant defense mechanism: Looks simple, but actually not

Unlike animals, plants are unable to move. Therefore, plants must find their own way to survive in this competitive world. Especially, how plants protect themselves from external attack, e.g., pathogen invasion, is always an interesting topic. Indeed, after billions of years of evolution, the plant has formulated its own defense system to detect and further combat varied forms of invasion derived from microbial pathogens.

Different from animals, plants do not have an adaptive immune system. Instead, they only have an innate immune system (16). However, it does not affect the strong survivability of plants. According to Dong and Spoel, a well-established immune system can be summarized as three aspects: high specificity, mature self-tolerance and super immune memory (17). The plant

immune system just falls into these three categories via the survival strategies unlike the ones used by animals. Each of the categories will be discussed briefly below.

1). Specificity:

In 1955, H.H. Flor proposed a gene-for-gene model, which states that there may be a cognate resistance (R) protein encoded by the *R* gene inside host plant cells for certain avirulence (AVR) protein encoded by *AVR* gene inside the pathogen genome (18). This model initially suggests the high specificity concerned with the recognition between host plant and its pathogens. Nowadays, this model has been updated by “guard hypothesis”, for it has been revealed that the interaction between R proteins and AVR proteins is not necessarily direct but may also involve the detection of the modification of other proteins (19, 20). Dangl and colleagues reported in 2002 that they have found that RIN4, a binding partner of one of the R proteins, RPM1, in *Arabidopsis*, is manipulated by AvrRpm1 and AvrB secreted by *Pseudomonas syringae*, and such regulation is essential for efficient resistance (21). In addition, Mackey and colleagues have found that also in *Arabidopsis*, the R protein confers resistance via sensing the modifications delivered by RIN4, which is targeted by AvrRpt2 and AvrRpm1 (22). Furthermore, it has been reported that the R proteins share conserved protein sequences to some extent. Yu and colleagues finished the draft sequence of rice genome in 2002, and they have found that more than 600 R proteins are encoded by the rice genome, and all of them share conserved nucleotide binding site and leucine rich repeat (NBS-LRR), which represent common properties of R proteins, in the middle and at the C terminus, respectively (23). In *Arabidopsis*, Meyers and colleagues also discovered similar findings. They have found that around 200 R proteins are encoded by *Arabidopsis* genome, and just like what Yu *et al* have reported, all of the R proteins contain NBS-LRR motifs (24). Both suggest the evolutionary conservation of R proteins in plant cells.

2). Self-tolerance:

Self-tolerance refers to the inability of the organism to induce immune responses to self-produced antigens. To differentiate self and non-self is a basic ability of the immune system (17). The defect in self-tolerance leads to autoimmunity, which causes autoimmune diseases in humans, such as schizophrenia (25) and systemic lupus erythematosus (26). In plants, the immunity system also has the ability to detect modified self. However, self-tolerance can be also compromised. In *Arabidopsis*, it has been found that R proteins are activated by mistakenly recognizing self antigen as non-self antigens, causing autoimmunity, which may lead to hybrid necrosis, with the offspring characterized by sterility and non-viability (27). Furthermore, to tackle autoimmunity, another interesting question to be answered is, in normal states, why do R proteins keep inactive? Currently, studies have correlated the over-expression of R proteins with autoimmunity. Richards and colleagues investigated the hybrid necrosis using multiple *Arabidopsis* wild types, and they found such genetic incompatibility is associated with abnormal activity of R proteins (28). Moreover, Zhang and colleagues have further investigated this phenomenon, and they have found that the down-regulation of transcriptional level of R proteins helps plants to prevent autoimmunity (29).

3). Immune memory:

According to van der Meer and colleagues, not only vertebrates, but also plants and invertebrate animals have long-standing immune memory (30), which suggests they can confer resistance to secondary pathogen attack. It has been reported that the immune memory in plants correlates with the priming of cells (17). Cell priming will cause enhanced resistance to pathogen attack by activating the host plant cell in a sensitized state. Beckers and colleagues have found that in *Arabidopsis*, the inactive proteins of Mitogen-Activated Protein Kinases (MAPK), MAPK3 and MAPK6, is regulated by cell priming, and it is just these inactive forms of

signaling molecules that will be activated by secondary pathogen attack (31). Furthermore, it has been found that epigenetics also plays a role in the plant immune memory. Peterhansel and colleagues have reported that chromatin modification is associated with plant immune memory. They found that the histone acetylation and methylation are involved in cell priming. Finally, in some host plant cells, the immune memory is heritable (32). Hohn and colleagues have reported that in *Arabidopsis*, the homologous recombination of parental plants is inherited by successive generations, and the conferred resistance to environmental stress is not lost in the progeny (33).

iv. Phosphoinositides: Minor, but of importance

Lipids, as major components of the cellular membranes, serve as messenger molecules of critical importance in numerous cellular signaling pathways (34). There are different species of lipids, and phospholipids are the most abundant among them. Phospholipids include phosphatidic acid (PA), phosphatidylcholine (PtdCho), phosphatidylethanolamine (PtdEth), phosphatidylserine (PtdSer), phosphatidylinositol (PI) as well as sphingolipids, all of which participate actively in signal transduction (35). In this section, attention will be focused on PI. PI is composed of a glycerol backbone, connected with two non-polar hydrocarbon chains (one is saturated, while the other is unsaturated, containing *cis*-double bonds) as well as a hydrophilic headgroup, an inositol ring (36). Interestingly, the 3-, 4- and 5- positions of the inositol ring can be phosphorylated with all possible combinations, and such phosphorylated derivatives are called phosphoinositides (PIPs) (35). Currently, there are seven known forms of PIP (phosphatidylinositol 3-phosphate, phosphatidylinositol 4-phosphate, phosphatidylinositol 5-phosphate, phosphatidylinositol 3, 4-bisphosphate, phosphatidylinositol 3, 5-bisphosphate, phosphatidylinositol 4, 5-bisphosphate and phosphatidylinositol 3,4,5-trisphosphate) (37), six of which can be found in plant cells (except for phosphatidylinositol 3,4,5-trisphosphate) (38). Each PIP has its own intracellular locations. Indeed, some PIPs are treated as “identity markers” of

their localized organelles, e.g., PtdIns(3)P is thought as the “identity marker” of endosomes (39). Figure 4 shows the structures of all known PIPs and illustrates the dynamic interconversion between different forms (35). The interconversion is regulated by the corresponding kinases and phosphatases, and some PIPs even have more than one synthesis paths. Figure 5 summarizes the relative level of major acidic phospholipids on cellular membranes in mammalian cells (35). PIP differs in their relative level intracellularly, and such level can be adjusted by external stimuli, which suggests that several PIPs may serve as lipid second messengers. Furthermore, compared to the relative level of other acidic phospholipids, PIPs are almost negligible. However, it is just these negligible phospholipids that play indispensable roles in cellular signaling (40). Each PIP will be discussed briefly.

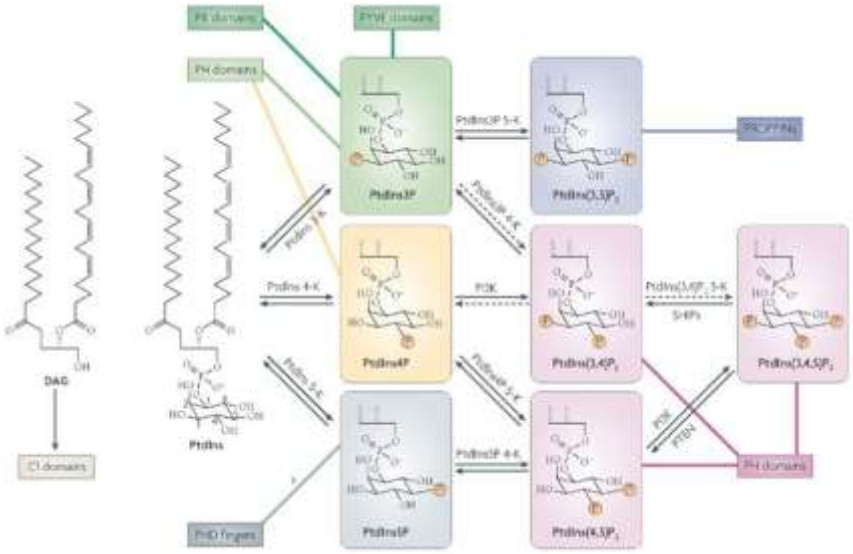

Figure 4. Domains that bind specific lipid targets. The structures and interconversion reactions are shown for all phosphoinositides that are found in mammalian cells. *Reprinted with permission from* [35].

Lipid	Relative level (%)*‡	Fold increase on stimulation
Phosphatidylserine	8.5	1
Phosphatidic acid	1.5	1
Phosphatidylinositol	1.0	1
PtdIns3P	0.002	1§
PtdIns4P	0.05	0.7‖
PtdIns5P	0.002	3–20¶
PtdIns(4,5)P_2	0.05	0.7‖
PtdIns(3,4)P_2	0.0001	10‖
PtdIns(3,5)P_2	0.0001	2–30#

Figure 5. Relative levels of acidic phospholipids in mammalian cells. The main acidic phospholipids in mammalian cells are phosphatidylserine, phosphatidic acid and phosphatidylinositol. The phosphoinositides are much less abundant. Estimated fold increases in the levels of each phosphoinositide in response to selected treatments are also shown. *Reprinted with permission from* [35].

Phosphatidylinositol 3-phosphate (PtdIns(3)P) has attracted much attention during the past decade due to its emerging key functions in regulating numerous vital cellular signaling pathways, especially in membrane trafficking (34). In mammalian cells, PtdIns(3)P is localized on the membranes of early and multivesicular endosomes, while in yeast, other than the endosomes, it is also localized on vacuolar membranes (41). There are two paths for PtdIns(3)P synthesis: the first one is the phosphoinositide 3-kinase (PI3K)-mediated phosphorylation of PI at the third position of the inositol ring; the other is via the dephosphorylation of PtdIns(3,4,5)P_3, mediated by 4- and 5-phosphatases (34). PtdIns(3)P-binding protein partners include “Fab1, YOTB, Vac1, EEA1” (FYVE), phox homology (PX) as well as pleckstrin homology (PH) domains, and such domain-containing proteins will be recruited to where PtdIns(3)P is located to participate in a series of signaling transduction pathways (35). Interestingly, Tyler and colleagues have found that PtdIns(3)P may also exist at the cellular plasma membrane, including plant and some animal cells, as well as human cells. They found that the presence of external PtdIns(3)P mediates the entry of effector proteins into host cells by specifically recognizing the N-terminal RxLR domain of the effector proteins (11). The PtdIns(3)P-binding sites of effector proteins does not share any similarity with reported specific PtdIns(3)P-binding

protein domains, such as PX and FYVE domains. However, the chemical presence of external PtdIns(3)P needs to be determined (11). Similarly, Haldar and colleagues have also found that the PtdIns(3)P present on endoplasmic reticulum also mediates the entry of the malarial effector protein into host cells via similar recognition mechanism (42). The detailed binding basis needs to be formulated in the future. In plants, PtdIns(3)P-involved signaling pathways are also of critical importance. Bae and colleagues have reported that PtdIns(3)P synthesis by activated PI3K plays a vital role in auxin signaling (43). Moreover, Hwang and colleagues have found that the endosome binding domain (EBD), which is a specific PtdIns(3)P-binding partner, plays a regulatory role in vesicle trafficking in *Arabidopsis* (22). Furthermore, according to Zhang and colleagues, AtVPS15, the PI3K in *Arabidopsis*, participates actively in pollen growth, including development and germination, by adjusting PtdIns(3)P level with accuracy, which suggests the regulatory role of PtdIns(3)P in the corresponding cellular processes (44). In addition, McCormick and colleagues have reported that PtdIns(3)P networking plays a key role in autophagic signaling in the pollen tube of *Arabidopsis* by its phosphatase PTEN (45).

Phosphatidylinositol 4-phosphate (PtdIns(4)P), the precursor of PtdIns(4,5)P_2, is the most abundant form of phosphoinositide in plant cells (46). It is localized in the plasma membrane as well as in the membranes of trans-Golgi networks (47). It is synthesized via phosphorylation at the fourth position of the inositol ring by several forms of phosphoinositide 4-kinases (PI4Ks), which include PI4K IIα, PI4K IIβ, PI4K IIIα, and PI4K IIIβ (48). The main generation place of PtdIns(4)P is the outer leaflet of the Golgi membranes, and in fact, PtdIns(4)P is considered as the subcellular marker for the Golgi complex (49). Dewald and colleagues have reported that PtdIns(4,5)P_2 plays a key role in the secretory pathway, linking Golgi to plasma membrane, by affecting the generation of secretory vesicles, which proposed that PtdIns(4,5)P_2 may have a direct role in cellular processes (50). Indeed, afterwards, many studies have supported their assumption. It seems that PtdIns(4)P not only functions inside

Golgi complex, but also participates actively outside the “trafficking/sorting machinery”. Recently, Francesco and colleagues have discovered that AL-9, belonging to one class of inhibitors of Hepatitus C virus, targets PI4K IIIα, one of the PI4Ks, by impacting the subcellular distribution of PtdIns(4)P, which indicates the potential role of PtdIns(4)P in future drug discovery (51). In plants, Luna and colleagues have found that proper dephosphorylation of PtdIns(4)P is crucial for normal root hair growth (52). In addition, it has been reported that PtdIns(4)P may play an essential role in cytoskeletal networking in plants (46). Furthermore, Clark and colleagues have reported that POL, a phosphatase recruited to the plasma membrane via acylation as well as the essential protein for stem cell maintenance in *Arabidopsis*, can be activated by PtdIns(4)P *in vitro*, which tentatively suggests the important role of this phosphoinositide, together with other phospholipids, in regulating important developmental pathways *in planta* (53). Moreover, according to Nielsen and colleagues, the PtdIns(4)P level, regulated by its phosphatase, which is encoded by *Root Hair Defective4* (*RHD4*), gets involved in the proper root hair development in *Arabidopsis* (54). Last but not least, Yang and colleagues have reported that PtdIns(4)P is no longer only a precursor of PtdIns(4,5)P_2, but also of importance in directly regulating cell signaling, such as clathrin-dependent endocytosis on the apex of pollen tubes in *Arabidopsis thaliana* as well as *Nicotiana tabacum* (55).

Phosphatidylinositol 5-phosphate (PtdIns(5)P) is still an enigmatic phosphoinositide, even it has been made public *in vivo* for fifteen years (56). In plants, PtdIns(5)P is generated either by the dephosphorylation of PtdIns(3,5)P_2 or PtdIns(4,5)P_2 (46). Just like other phosphoinositides, PtdIns(5)P also has its own subcellular locations. The majority of PtdIns(5)P is localized in the plasma membrane, while the minor part is in Golgi and Sarco/endoplasmic reticulum (SER) markers (57, 58). It has been suggested that PtdIns(5)P plays crucial roles in cellular signaling pathways, although the corresponding functional role needs to be well defined (46). In plants, a PtdIns(5)P-binding protein, called Patellin1, has been characterized by Luna

and colleagues in *Arabidopsis*. Patellin1 plays an important role in cell plate formation, which suggests the essential presence of PtdIns(5)P in its corresponding signaling pathway (52). Moreover, in *Arabidopsis*, ATX1, a protein of critical functional roles in varied regulatory pathways, including epigenetic regulations, is also a PtdIns(5)P receptor. Avramova and colleagues have found that ATX1 is negatively regulated by PtdIns(5)P, which suggests that PtdIns(5)P may be involved in epigenetic regulation (59). In addition, Tronchere and colleagues suggested that PtdIns(5)P play a role in oncogenesis, which related membrane trafficking, involved by PtdIns(5)P, to leads cancer (60). Intriguingly, it has been reported that PtdIns(5)P also exists in nucleus, and such nuclear PtdIns(5)P plays a crucial role in cellular response to external stress, such as ultraviolet exposure (61). Although there has not been any direct evidence relating PtdIns(5)P to human diseases, it has been reported that several PtdIns(5)P-binding proteins get involved in human diseases, e.g., ING2, a chromatin-associated protein involved in p53 acetylation, has been found to bind the nuclear PtdIns(5)P, which suggests the potential functional role of PtdIns(5)P in oncogenesis (62).

Phosphatidylinositol 3, 4-bisphosphate (PtdIns(3,4)P_2) is another species of less abundant phosphoinositide existing in cellular membranes. The major subcellular location of PtdIns(3,4)P_2 is plasma membrane, and it is also existing in endoplasmic reticulum as well as multivesicular endosomes (39, 63). In mammalian cells, the major PtdIns(3,4)P_2 synthesis is via PtdIns(3,4,5)P_3 5-phosphatase–mediated dephosphorylation of PtdIns(3,4,5)P_3 (64). In addition, it has been reported that there are other ways to synthesize PtdIns(3,4)P_2. According to Rittenhous and colleagues, PtdIns(3,4)P_2 may also be generated by the phosphorylation of PtdIns(3)P by PI4K in human platelets (65). Moreover, Downes and colleagues have noticed that the level of PtdIns(3,4)P_2 is increased under the circumstances of extracellular stimuli, such as osmotic stress as well as oxidative stress (66). It has been reported that PtdIns(3,4)P_2 recognizes several PH domains as well as the PX domain contained in $p47^{phox}$ (39). In addition,

PtdIns(3,4)P_2 also serves as a lipid second messenger, just like PtdIns(3,4,5)P_3 (39). More and more reports have indicated that PtdIns(4,5)P_2 is involved in human diseases. An exciting story is, in 2010, Sasaki and colleagues have found that INPP4A, a PtdIns(3,4)P_2 phosphatase, plays a key role in regulating the central neuronal signaling pathway by downregulating abnormal neurological activities, which indicates that proper PtdIns(3,4)P_2 metabolism is critical for normal central nervous signaling regulation (67). In 1992, Hanke and Brearley showed the first evidence that indicates the presence of PtdIns(3,4)P_2 in plants by using the aquatic plant *Spirodela polyrhiza* L. as a model organism (68), and furthermore, they also found that PI4K, which may activate the conversion of PtdIns(3)P to PtdIns(3,4)P_2, is also existing in the same organism, indicating the presence of PI4K in plant cells, other than in animal cells (69).

Since its first discovery *in vivo* at 1997, phosphatidylinositol 3, 5-bisphosphate (PtdIns(3,5)P_2) has not been paid as much attention as other PIPs are during the past years, although it plays indispensable roles in numerous cellular signaling pathways (70). PtdIns(3,5)P_2 is mainly localized on the yeast vacuole as well as the endolysosomes of higher eukaryotes (70). PtdIns(3,5)P_2 is synthesized via the PI5K-mediated phosphorylation at the fifth position of the inositol ring of PtdIns(3)P (71). At the first beginning, Michell and colleagues have found that PtdIns(3,5)P_2 level is adjusted by osmotic pressure in yeast, indicative of the role of this PIP in vesicular protein sorting (72). Moreover, Tavare and colleagues have demonstrated that PtdIns(3,5)P_2 level is adjusted by insulin, which gets involved in the membrane vesicle transporting (73). Furthermore, Li and colleagues have found that nerve cells are sensitive to even subtle change of PtdIns(3,5)P_2 level, which is adjusted by Fig4/PtdIns(3,5)P_2 signaling, indicating that PtdIns(3,5)P_2 is associated with neurodegenerative diseases (74). In plants, Sato and Hirano have postulated that FAB1A/B, a PtdIns(3,5)P_2 kinase in *Arabidopsis* and fission yeast, seems to participate in auxin signaling, which suggests the potential role of PtdIns(3,5)P_2 in endocytosis as well as vacuolar acidification (75). Last but not least, there has been evidence

showing that PtdIns(3,5)P_2 regulation plays an indispensable role in human diseases, such as myotubular myopathy and Charcot-Marie-Tooth type 4B1 (76).

Phosphatidylinositol 4, 5-bisphosphate (PtdIns(4,5)P_2) is the most well-studied phosphoinositide. It is localized in the cellular plasma membrane, accounting for the amount of around one to two percent of the total lipids (77), which is the most abundant form of phosphoinositide in animal cells (46). PtdIns(4,5)P_2 is synthesized via the phosphorylation of PtdIns(4)P at its fifth position of the inositol ring by PtdIns(4)P 5-kinase (PtdIns(4)P5K) (78). In living cells, it has been reported that the amount of PtdIns(4,5)P_2 may be varied via different ways. The first one is via its synthesis route stated above; the second one is by way of the phosphoinositide-specific phospholipase C (PI-PLC)-mediated hydrolysis of PtdIns(4,5)P_2 into inositol-1,4,5-trisphosphate (Ins(1,4,5)P_3) and diacylglycerol (DAG); the third way is via the phosphorylation of PtdIns(4,5)P_2 by PI3K to PtdIns(3,4,5)P_3; the last way is to adjust PtdIns(4,5)P_2 level by PtdIns(4,5)P_2-binding proteins (78). Intriguingly, Inoue and colleagues have recently reported that the level change of PtdIns(4,5)P_2 *in vivo* in different ways, and each of them has its own role in different regulatory pathways, such as endocytosis and cytoskeleton (77). Furthermore, PtdIns(4,5)P_2 also serves as the second messenger, participating in numerous cellular signaling pathways. In plants, it has been reported that PtdIns(4)P is critical for proper plant growth. Kost and colleagues have found that the presence of PtdIns(4,5)P_2 as well as one of its products, DAG, is required for the normal growth of pollen tube tip (79). Furthermore, Sun and colleagues have reported that PtdIns(4,5)P_2 gets involved in the thermotolerance of Arabidopsis. They found that the PI-PLC, which hydrolyzes PtdIns(4,5)P_2, plays a crucial role in regulating the overexpression level of several heat shock proteins in *Arabidopsis* (80). It has been reported that PtdIns(4,5)P_2 participates actively in actin dynamics. Particularly, PtdIns(4,5)P_2 plays a central role in actin polymerization by recruiting a large number of actin-binding proteins, which includes the corresponding inhibitors, such as cofilin

and profilin, and activators, such as WAVE and ERM (81, 82). At last, Drubin and colleagues have reported that PtdIns(4,5)P_2 is essential for actin-mediated endocytosis (82).

Phosphatidylinositol 3, 4, 5-trisphosphate (PtdIns(3,4,5)P_3) is a lipid second messenger in higher eukaryotes. It is synthesized via the phosphorylation of PtdIns(4,5)P_2 by activated PI3K, stimulated by interaction between p110 and activated Ras protein (83). PtdIns(3,4,5)P_3 is localized in the cellular plasma membrane (83). PH domain has been identified as a PtdIns(3,4,5)P_3-binding domain, and such recognition will recruit numerous PH domain-containing proteins to the plasma membrane in stimulated cells, which facilitates the interaction between these proteins, and such interaction impacts numerous cellular activities (39). Beauwens and colleagues have demonstrated that PtdIns(3,4,5)P_3 as well as PtdIns(3,4)P_2 play a crucial role in sodium channel regulation (84). Duronio and colleagues have reported that PtdIns(3,4,5)P_3, together with PtdIns(3,4)P_2, play a key role in the phosphorylation of Protein Kinase B (PKB), which is involved in the PI3K-PKB pathway (85). Interestingly, Schultz and colleagues have reported that they have synthesized PtdIns(3,4,5,6)P_4, an analog of PtdIns(3,4,5)P_3. They found that this analog can be used to activate a series of PI3K kinase pathways independent of growth factor stimuli, which suggests the potential role of such analog in studying PI metabolism involved in human diseases (86). Furthermore, Best et al. have reported that they have developed PtdIns(3,4,5)P_3 activity-based probes for the identification as well as characterization of PtdIns(3,4,5)P_3-binding proteins from cancer cell complex, which may facilitate lipid signaling studies in living organisms (87). In contrast to the multiple functional roles of PtdIns(3,4,5)P_3 in animal cells, currently, there is no experimental data demonstrating that PtdIns(3,4,5)P_3 is present in plant cells.

2. Research Proposal

I have taken strong interest to the recognition mechanism between Avr proteins and PtdIns(3)P. Avirulence homolog-5 (Avh5), secreted by *P. sojae*, has been the protein of interest in my project. It was shown by Tyler and colleagues that Avh5 binds PtdIns(3)P (11), and I have therefore investigated the structural basis of this interaction. Avh5 is a good representative of effector proteins secreted by *Phytophthora* pathogens. The virulence of Avh5 has been confirmed by Wang and colleagues (88), who found that Avh5 is able to enter the host plant cell to suppress the immune response of the host. Furthermore, the size of Avh5 is 13.87 kDa, which is suitable for protein structural studies using nuclear magnetic resonance (NMR) spectroscopy. Notably, Avh5 is soluble in the millimolar concentration range and is relatively stable. All of the properties stated above indicate that Avh5 is an ideal study target in this project. I have investigated the molecular mechanism of PtdIns(3)P recognition by Avh5 using the following specific aims:

i. Specific Aim 1: To map the PtdIns(3)P-binding site in Avh5

I have mapped the binding site in Avh5 involved in recognizing PtdIns(3)P using NMR spectroscopy. This aim helped me to identify potential PtdIns(3)P-binding regions in the protein. Two sub-aims are included under this aim. First, backbone resonances of Avh5 were obtained in collaboration with Dr. Hugo F. Azurmendi (Department of Chemistry, Virginia Tech). Secondly, the headgroup of PtdIns(3)P, Ins(1,3)P_2, has been employed as a ligand to titrate Avh5, the chemical shift perturbations caused accordingly has been used to map the PtdIns(3)P-binding site in Avh5.

NMR spectroscopy is one of the most powerful analytical tools in multiple disciplines, especially in chemistry and biology. Since the first protein structure was determined by using NMR spectroscopy in the early 1980s, NMR has become a valuable tool to be used to

determine protein structure, including the secondary and the tertiary, especially under physiological conditions (89), and moreover, NMR can be also employed to study the dynamic interaction of proteins with their ligands (90). Furthermore, NMR has been widely applied in clinical research, called magnetic resonance imaging (MRI), to help physicians diagnose potential disease regions in soft tissues, such as human brains (91). Furthermore, other than proteins, NMR may be also applied to study the dynamics of ribonucleic acid (RNA) (92), as well as the structure and conformational changes of carbohydrates (93).

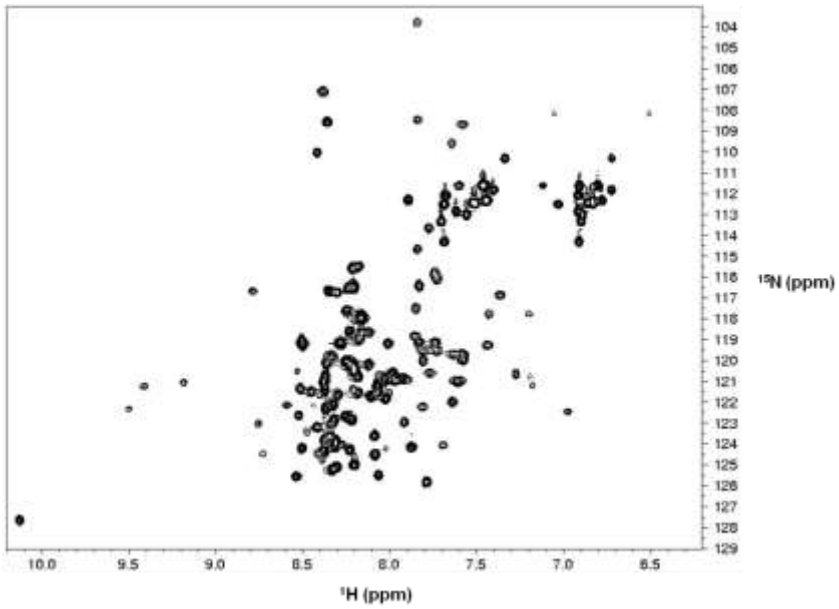

Figure 6. ^{15}N, ^{1}H-Heteronuclear single quantum coherence NMR spectra of Avh5. 75μM of uniformly ^{15}N-labeled Avh5 was dissolved in 90% H_2O/10% $^{2}H_2O$, and 20mM d_{11}-Tris-HCl (pH 5.8), 100mM NaCl, 1mM NaN_3. The spectrum was collected using Bruker Avance III 600 MHz spectrometer (Virginia Tech) equipped with an inverse detected TXI probe with z-axis pulse field gradients.

Every atom has its unique nuclei. Certain species of nuclei have magnetic properties, such as ^{1}H, ^{13}C, and ^{15}N (94). For those nuclei, they will absorb energy from the applied pulse in the magnetic field, and such adsorption will lead to signal to be detected by the detector (94). Every amino acid has its unique chemical environment, and therefore, it has its own chemical

shift, which is detected as a peak in the final spectra after Fourier transform. In ^{15}N-^{1}H heteronuclear single quantum coherence (HSQC) NMR experiments, the proton attached to the protein backbone amide will be directly detected, while the corresponding nitrogen will be indirectly detected (95, 96), and the final spectra should be well dispersed as long as the protein is well folded (97). In principle, every amino acid, except for proline, has its own unique peak. The first amino acid does not have its own backbone amide, and thus there is no signal detected. For asparagine and glutamine residues, there are also amine protons to be detected for each of their side chain amide, and therefore, there will be additional two signal peaks to be detected for each of them (96). For tryptophan residues, the side chain of which is detected as the aromatic NH, and then one more signal is to be detected. Just as what Figure 6 shows, each peak on the HSQC NMR spectra has its own chemical environment. When titrating the protein with its ligand, there may be chemical shift perturbations if there is interaction between the protein and its ligand. After the protein binds the ligand, there are two states of the amino acids involved in binding: free and bound. There could be three forms of the "free-bound" states: fast-exchange, intermediate-exchange, and slow-exchange (98). For fast-exchange, there is only one peak on the spectra after ligand titration, representing the population weighted average of the free- and bound-states of amino acids; for the intermediate exchange, there will be line broadening; for the slow exchange, the free state and bound state coexist, and therefore, there are two signal peaks to be detected for each of the involved amino acids (98). According to the extent to which the chemical shift perturbations occur, the potential ligand-binding site in the protein will be mapped. Furthermore, by analyzing the chemical shift of each amino acid, the protein secondary structure will be calculated, which might be useful for confirming the secondary structure predicted by other methods.

ii. Specific Aim 2: To identify the key Avh5 residues involved in PtdIns(3)P recognition

In the second aim, I have identified the key Avh5 residues involved in PtdIns(3)P recognition. I employed site-directed mutagenesis, protein-lipid overlay and liposome binding assays to accomplish this goal.

The protein-lipid overlay assay is a fast lipid-binding assay to identify lipid-binding proteins. Figure 7 briefly summarizes the key steps for this assay (99). This method allows to monitor protein-lipid interactions in a qualitative way (36). However, due to the lack of a biological membrane environment, this method sometimes leads to artifacts (36). Therefore, the protein-lipid overlay assay was only a good starting point. Further biological context-relevant assays have been employed to confirm and to investigate such interaction in a more quantitative way.

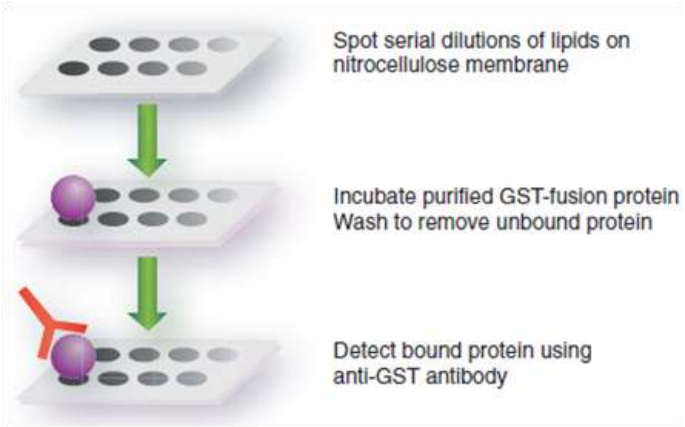

Figure 7. The key steps of the protein lipid overlay (PLO) assay. *From* [99]. *Reprinted with permission from AAAS.*

The liposome-binding assay is employed to monitor protein-lipid interactions in a biological membrane-related environment semi-quantitatively. Liposome is prepared by mixing different lipids at different ratios according to the membrane environment of the protein under investigation. Either tip-sonication or extrusion or both together helped me prepare small-unilamellar or large-unilamellar vesicles to mimic biological membrane environment (100-102).

In summary, I have identified the key amino acids of Avh5 involved in PtdIns(3)P recognition using the techniques stated above, which helped me map the PtdIns(3)P-binding site in Avh5.

iii. Specific Aim 3: To characterize the binding affinity of Avh5 for PtdIns(3)P

In this aim, I performed a kinetic study to quantify the binding affinity of Avh5 as well as its mutants with PtdIns(3)P in a biological membrane-related environment (*i.e.*, liposomes). In addition, I have also investigated the binding model between Avh5 proteins and PtdIns(3)P. Surface plasmon resonance (SPR) spectroscopy has been employed to accomplish this task since it is one of the widely used optical biosensors, serving as a valuable tool to monitor real-time interactions between varied bio-macromolecules, such as protein-protein, protein-DNA as

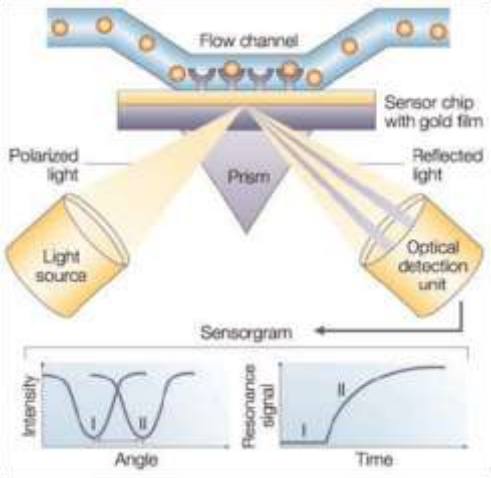

Figure 8. Typical set-up for an SPR biosensor. Surface plasmon resonance (SPR) detects changes in the refractive index in the immediate vicinity of the surface layer of a sensor chip. SPR is observed as a sharp shadow in the reflected light from the surface at an angle that is dependent on the mass of material at the surface. *Reprinted with permission from* [104].

well as protein-carbohydrates, without any molecular labeling, such as fluorescent labeling and radiolabelling (103).

The binding between the analyte and the ligand causes the change of refractive index on the medium close to the surface (104), which is monitored in real time (Figure 8). In fact, such change reflects the amount of analyte bound to the ligand, which is detected by the increase of the resonance signal (Figure 9). The corresponding association and dissociation is monitored with accuracy, respectively. In addition, the binding affinity can be calculated by using different potential binding models between the analyte and the ligand (104).

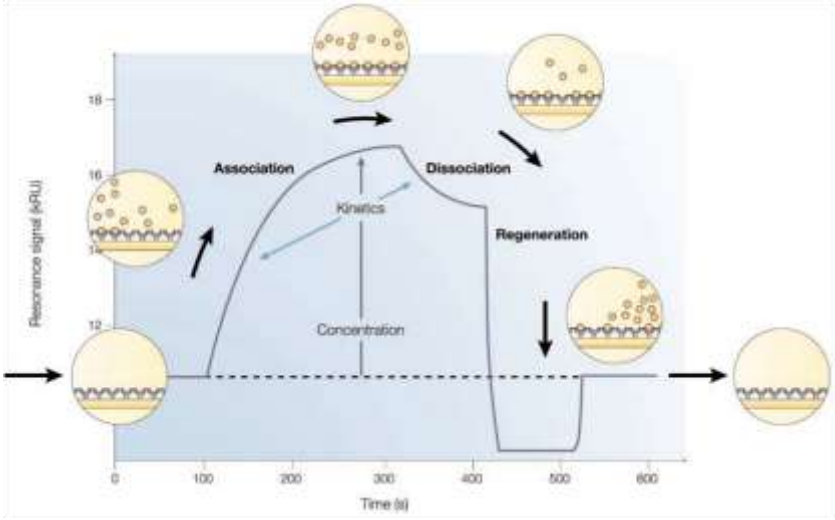

Figure 9. A typical binding cycle observed with an optical biosensor.
Reprinted with permission from [104].

iv. Specific Aim 4: To monitor conformational changes in Avh5 upon its interaction with PtdIns(3)P

In the last aim, since Avh5 is a membrane-binding protein, conformational changes may accompany membrane targeting. I have monitored the overall conformational changes of Avh5 accompanying its interaction with PtdIns(3)P. Circular Dichroism (CD) spectroscopy was the major tool I have employed to accomplish such task. In addition, I have also employed intrinsic

tryptophan fluorescence spectroscopy to monitor the local conformation of Avh5 upon Ins(1,3)P_2 binding.

CD spectroscopy is a powerful tool to help us quickly determine the protein secondary structure and to evaluate the integrity of protein tertiary structure (105). In addition, CD may be also employed to monitor the conformational changes of protein of interest upon ligand-binding or temperature change (105). The principle behind this critical technique is the absorption difference between the left-handed and right-handed circularly polarized light (106). As shown in Figure 10, if the absorption amount of left-handed light is bigger than the one of right-handed light, the corresponding CD signal will be positive; while if the absorption amount of right-handed light is bigger than the one of left-handed light, the corresponding CD signal will be negative, and if they are the same, there will be no CD signal (105).

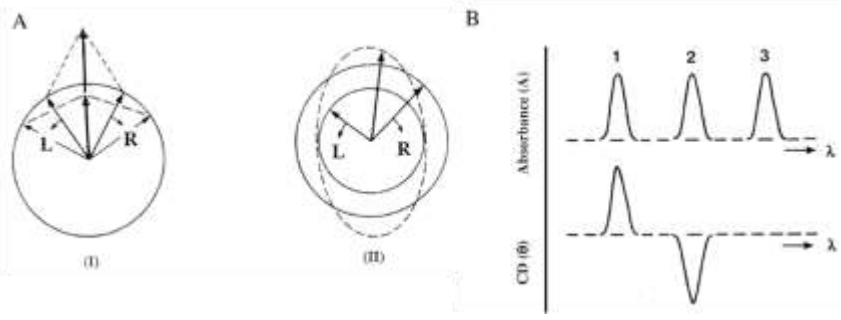

Figure 10. Origin of the CD effect. (A) The left (L) and right (R) circularly polarized components of plane polarized radiation: (I) the two components have the same amplitude and when combined generate plane polarized radiation; (II) the components are of different magnitude and the resultant (dashed line) is elliptically polarized. (B) The relationship between absorption and CD spectra. Band 1 has a positive CD spectrum with L absorbed more than R; band 2 has a negative CD spectrum with R absorbed more than L; band 3 is due to an achiral chromophore. *Reprinted with permission from* [105].

Secondary structure components can be quantitatively determined by CD spectroscopy. In far-UV region (190-250 nm), peptide bonds are the main chromophores (105). Distinct spectra represent different protein secondary structures. There are different kinds of protein secondary structures: α-helix, β-sheet, β-turn, and irregular structures, such as random coil. As

indicated in Figure 11, there are two minima at 208 and 222 nm, and a positive peak around 193 nm for helical proteins; there is one minimum at 218 nm and a positive peak around 200 nm for anti-parallel β-sheet proteins; there is a minimum at 190 nm and a positive peak around 210 nm for type I β-turn proteins; there is no positive peak, and the signal is flat for irregular proteins

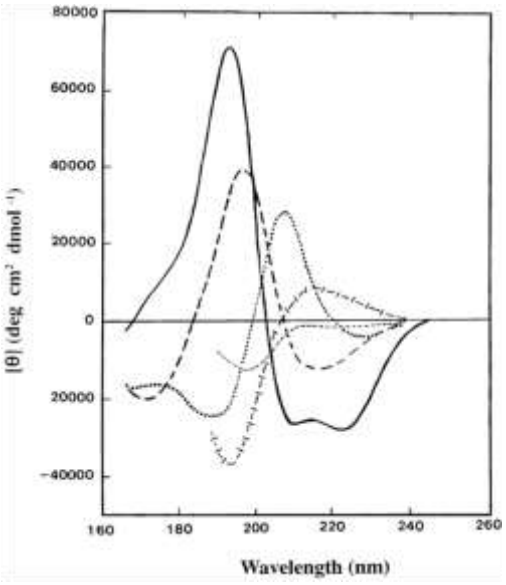

Figure 11. Far UV CD spectra associated with various types of secondary structure. Solid line, α-helix; long dashed line, anti-parallel β-sheet; dotted line, type I β-turn; cross dashed line, extended 3_1-helix or poly (Pro) II helix; short dashed line, irregular structure. *Reprinted with permission from* [105].

(105).

In the near-UV region (250-350 nm), the chromophore molecules of interest are the aromatic side chains of tryptophan, tyrosine, and phenylalanine, as well as disulfide bonds (105). Each of these amino acids has its unique spectra. For tryptophan residues, the distinct spectra are from 290 to 305 nm with a weak peak nearby 290 nm; for tyrosine residues, there is a distinct peak between 275 nm and 282 nm with a shoulder later; for phenylalanine residues, its spectra spans from 255 to 270 nm (105). In fact, the final shape as well as the intensity of the near-UV CD protein spectra relies upon many other factors, such as the total amount of each

aromatic amino acids present, as well as the physiological environment of those amino acids, such as hydrogen bonding (105).

Far-UV and near-UV CD spectra can help us to monitor the overall conformational change of protein upon ligand interaction. However, sometimes, the ligand binding can instead lead to local conformational changes. Tryptophan fluorescence has helped me to accomplish this hypothesis. The fluorescence of the indole group of tryptophan may be used as a natural fluorophore and the corresponding emission is quite sensitive to its microenvironment, thus tryptophan is able to probe the protein conformational change. Fortunately, Trp70 is the only and conserved tryptophan residue in Avh5 and this residue is quite close to the identified PtdIns(3)P-binding site (residues Lys62, Lys64 and Lys65; see below), and thus, it is an ideal reporter to be employed to monitor the local conformational changes of Avh5 in the presence of $Ins(1,3)P_2$.

v. Scientific Merit

Due to the economic importance as well as the ineffectiveness of conventional medicinal treatment, it is urgent to find novel therapeutic solutions to controlling oomycete infection (1). The detailed exploration of the recognition mechanism between effector proteins and phosphoinositides will provide insights into the entry mechanism of oomycete pathogens into host plants, which will propel our understanding towards the dynamic relationship between the pathogen invasion and the plant immunity. Actually, phosphoinositides may be only one of the receptors involved in mediating pathogen entry into host plant cells on the plant cell plasma membranes, and more efforts need to be made on further study, which will help us to explore other potential effector protein-receptor interaction mechanisms. This study will provide us with further understanding towards the molecular basis and the biological functions of eukaryotic

pathogen pathogenesis, and therefore, novel therapeutic solutions to pathogen effectors may be generated accordingly to control crop diseases.

vi. Broader Impact

To increase the food production in the world by curing crop diseases is always a dream for human beings, especially for people living in developing and undeveloped countries, in that, even in modern society, billions of people are still suffering from starvation. This project I have proposed will definitely help us move one step, bigger or smaller, towards alleviating this problem.

Chapter 2 MATERIALS AND METHODS

Chemicals

Following is a list of chemicals used and their suppliers: 1,2-dioleoyl-sn-glycero-3-phosphocholine (PtdCho), 1,2-dipalmitoyl-*sn*-glycero-3-phosphoethanolamine (PtdEth) (Avanti-Lipids); PtdIns(3)P, inositol (1,3)-bisphosphate (Ins(1,3)P_2) and inositol 1-phosphate (Ins(1)P) (Cayman Chemicals); restriction enzymes and other recombinant DNA reagents (New England Biolabs); isopropyl β-D-thiogalactopyranoside (IPTG) (Research Products International); pGEX6P1vector, prescission protease anti rabbit-horse radish peroxidase (HRP) (GE Healthcare); *Escherichia coli* (Rosetta; Stratagene); [^{15}N] ammonium chloride and [^{13}C] glucose (Cambridge Isotope Laboratory Inc.); Bis(Sulfosuccinimidyl) suberate and Supersignal West Pico chemiluminescent reagent (Pierce); fatty acid-free BSA (Sigma); rabbit anti-GST antibody (Santa Cruz Biotech); and N-octyl-β-D-glucopyranoside (Affymetrix). All other common chemicals were the highest analytical reagent grade.

Cloning, Expression, and Purification of Avh5 Constructs

P. sojae Avh5 cDNA was cloned into a pGEX6P1 vector (GE Healthcare). Site-directed mutagenesis of Avh5 was performed using QuikChange (Stratagene) and proteins were expressed in *Escherichia coli* (Rosetta; Stratagene). All of the plasmids containing Avh5 and its mutants encoding regions were sequenced in the Core Laboratory Facility at the Virginia Bioinformatics Institute. Figure 12 shows all of the relevant translated protein sequences in this project. Bacterial cells were grown in Luria-Bertani media at 37ºC until cells reached an optical density of 0.7-0.9. Induction of glutathione S-transferase (GST) fusion proteins resulted from the addition of 1 mM IPTG followed by 2-h incubation at 25ºC. ^{15}N- and ^{15}N,^{13}C-labeled proteins were produced in minimal media supplemented with [^{15}N] ammonium chloride and [^{13}C] glucose (Cambridge Isotope Laboratory Inc.) as the source of nitrogen and carbon, respectively.

Proteins were purified using glutathione beads as described (107). Purified fusion proteins were digested with *prescission protease* (GE Healthcare) overnight at 4°C to get rid of GST tag, and untagged proteins were then concentrated using 3 kDa-cut-off centrifugal filter units (Millipore). Proteins were further purified using an FPLC-driven Superdex 75 column (GE Healthcare) previously equilibrated with 50 mM Tris-HCl (pH 8) and 1 M NaCl. Fractions containing the purified protein were pooled and concentrated in 20 mM Tris-HCl (pH 5.8), 100 mM NaCl, and 1 mM NaN_3. Protein concentration was calculated using the UV-light absorbance method at 280 nm. Purity of proteins was over 95% as judged by SDS-PAGE and MALDI-TOF mass spectrometry (Tufts University, MA) analyses. The integrity of protein was verified by N-terminal sequencing (Tufts University, MA) analysis.

Wildtype:
GPLGSTRVPDDANLQSVNAPVQTVTRSRRFLRTADTDIVYEPKVHNPGKKQVFIEDKLQKALTDPKKNKKLYARWYNSGFTVKQVEGGLDQNENRELELTYKNLA
LGYAKYYQARRSQEAK
RFLR^{AAAA}:
GPLGSTRVPDDANLQSVNAPVQTVTRSRAAAATADTDIVYEPKVHNPGKKQVFIEDKLQKALTDPKKNKKLYARWYNSGFTVKQVEGGLDQNENRELELTYKNLA
LGYAKYYQARRSQEAK
QFLR:
GPLGSTRVPDDANLQSVNAPVQTVTRSRQFLRTADTDIVYEPKVHNPGKKQVFIEDKLQKALTDPKKNKKLYARWYNSGFTVKQVEGGLDQNENRELELTYKNLA
LGYAKYYQARRSQEAK
K52A:
GPLGSTRVPDDANLQSVNAPVQTVTRSRRFLRTADTDIVYEPKVHNPGKKQVFIEDALQKALTDPKKNKKLYARWYNSGFTVKQVEGGLDQNENRELELTYKNLA
LGYAKYYQARRSQEAK
K55A:
GPLGSTRVPDDANLQSVNAPVQTVTRSRRFLRTADTDIVYEPKVHNPGKKQVFIEDKLQAALTDPKKNKKLYARWYNSGFTVKQVEGGLDQNENRELELTYKNLA
LGYAKYYQARRSQEAK
K62A:
GPLGSTRVPDDANLQSVNAPVQTVTRSRRFLRTADTDIVYEPKVHNPGKKQVFIEDKLQKALTDPKANKKLYARWYNSGFTVKQVEGGLDQNENRELELTYKNLA
LGYAKYYQARRSQEAK
K64A:
GPLGSTRVPDDANLQSVNAPVQTVTRSRRFLRTADTDIVYEPKVHNPGKKQVFIEDKLQKALTDPKKNAKLYARWYNSGFTVKQVEGGLDQNENRELELTYKNLA
LGYAKYYQARRSQEAK
K65A:
GPLGSTRVPDDANLQSVNAPVQTVTRSRRFLRTADTDIVYEPKVHNPGKKQVFIEDKLQKALTDPKKNKALYARWYNSGFTVKQVEGGLDQNENRELELTYKNLA
LGYAKYYQARRSQEAK
L57A:
GPLGSTRVPDDANLQSVNAPVQTVTRSRRFLRTADTDIVYEPKVHNPGKKQVFIEDKLQKAATDPKKNKKLYARWYNSGFTVKQVEGGLDQNENRELELTYKNLA
LGYAKYYQARRSQEAK
T58A:
GPLGSTRVPDDANLQSVNAPVQTVTRSRRFLRTADTDIVYEPKVHNPGKKQVFIEDKLQKALADPKKNKKLYARWYNSGFTVKQVEGGLDQNENRELELTYKNLA
LGYAKYYQARRSQEAK
R90A:
GPLGSTRVPDDANLQSVNAPVQTVTRSRRFLRTADTDIVYEPKVHNPGKKQVFIEDKLQKALTDPKKNKKLYARWYNSGFTVKQVEGGLDQNENAELELTYKNLA
LGYAKYYQARRSQEAK
L57DT58V:
GPLGSTRVPDDANLQSVNAPVQTVTRSRRFLRTADTDIVYEPKVHNPGKKQVFIEDKLQKADVDPKKNKKLYARWYNSGFTVKQVEGGLDQNENRELELTYKNLA
LGYAKYYQARRSQEAK
K64AK65A:
GPLGSTRVPDDANLQSVNAPVQTVTRSRRFLRTADTDIVYEPKVHNPGKKQVFIEDKLQKALTDPKKNAALYARWYNSGFTVKQVEGGLDQNENRELELTYKNLA
LGYAKYYQARRSQEAK
K62AK64AK65A:
GPLGSTRVPDDANLQSVNAPVQTVTRSRRFLRTADTDIVYEPKVHNPGKKQVFIEDKLQKALTDPKANAALYARWYNSGFTVKQVEGGLDQNENRELELTYKNLA
LGYAKYYQARRSQEAK

Figure 12. Protein sequences of Avh5 and its mutants. The first five residues (glycine, proline, leucine, glycine, and serine) are from the vector.

Chemical Cross-Linking

Ten μg of purified Avh5 was incubated with 0.25, 0.5, and 1 mM of Bis(Sulfosuccinimidyl) suberate (BS^3; Pierce) in 20 mM HEPES (pH 7.5) for 30 min. To quench the reaction, Tris-HCl (pH 6.8) was added at a final concentration of 40 mM, followed by 15-min incubation. Proteins were subject to SDS-PAGE analysis.

Liposome-Binding Assay

Stocks of phospholipids were prepared in organic solvents per manufacturer instructions. Liposomes were prepared by a weight ratio of 1:1 PtdCho:PtdEth and 10 % of PtdIns(3)P. Controls were prepared by adjusting the ratios with PtdCho and PtdEth. Lipid films were generated by drying the lipid mixture with nitrogen gas for 30 min followed by lyophilization overnight at room temperature. Lipid films were hydrated in 20 mM Tris-HCl (pH 6.8), 100 mM NaCl, and 1 mM NaN_3 to 1 mg/mL at 67ºC for 1 h and freeze-thawed three times. Liposomes were sonicated, pelleted, and suspended at 5 mg/mL in 20 mM Tris-HCl (pH 5.8), 50 mM NaCl, and 1 mM NaN_3. Ten μg of protein was incubated with 200 μg of total lipid for 30 min at room temperature. Liposome-bound and free-protein fractions were separated by centrifugation and analyzed by SDS-PAGE. Protein bands were quantified using the AlphaEase FC software. Differences among conditions were evaluated using the t-test analysis.

Protein-Lipid Overlay Assay

Lipid strips were prepared by spotting 1 μL of the indicated amounts of PtdIns(3)P, dissolved in chloroform:methanol:water (65:35:8), onto Hybond-C extra membranes (GE Healthcare) and dried for 2 h at room temperature. Lipid strips were blocked with 3% fatty acid-free BSA (Sigma) for 1 h and then incubated with 1 μg/mL of the indicated GST fusion proteins in 20 mM Tris-HCl (pH 8.0), 150 mM NaCl, 0.1% Tween-20, and 3% fatty acid-free BSA overnight at 4°C. Following four washes with the same buffer, bound proteins were probed with

rabbit anti-GST antibody (Santa Cruz Biotech) and donkey anti rabbit-horse radish peroxidase (HRP) (GE Healthcare). Protein binding was detected using Supersignal West Pico chemiluminescent reagent (Pierce).

NMR Spectroscopy

Resonance assignments of Avh5 were obtained from NMR samples containing 1 mM of uniformly ^{15}N, ^{13}C-labeled Avh5 in 90% H_2O/10% ^2H_2O, and 20 mM d_{11}-Tris-HCl (pH 5.8), 100 mM NaCl, and 1 mM NaN_3 (NMR buffer). Triple-resonance experiments were acquired at 25°C on a Bruker Avance 800 MHz spectrometer equipped with a cryoprobe at the University of Virginia. ^1H chemical shifts were referenced using sodium 4,4-dimethyl-4-silapentane-1-sulfonate (50 µM) as an internal reference. Sequential assignments of the backbone ^1H, ^{13}C, and ^{15}N resonances were made from ^1H, ^{15}N-HSQC, CBCA(CO)NNH, HNCACB, and HNCO experiments (108, 109). All spectra were processed using NMRpipe (110), and ^1H, ^{15}N, and ^{13}C resonance assignments were determined using the CCPNMR package (111). The resonance assignments of Avh5 have been deposited in the Biological Magnetic Resonance Bank under accession number 18157. The secondary structure of the protein was derived from the backbone dihedral angles ϕ and ψ predicted using the DANGLE algorithm (112). Ins(1,3)P_2 and Ins(1)P titrations were carried out on a Bruker Avance III 600 MHz spectrometer (Virginia Tech) equipped with an inverse detected TXI probe with z-axis pulse field gradients. Lipid head group binding was monitored by comparing ^1H, ^{15}N HSQC spectra of 75 µM ^{15}N-labeled Avh5 in NMR buffer. Spectra were processed with NMRPipe (110) and analyzed using nmrDraw (113). Chemical shift perturbations were calculated according to the following formula (114):

$$\Delta\delta(^1H,^{15}N)=[(\Delta\delta^1H)^2 + (\Delta\delta^{15}N)^2/6]^{0.5}$$

Circular Dichroism Spectroscopy

Far-UV circular dichroism (CD) spectra were generated using purified Avh5 proteins (10 μM) in 5 mM Tris-citrate (pH 6.8) and 100 mM KF on a Jasco J-815 spectropolarimeter equipped with a Jasco PFD-425 S temperature control unit. Spectra were collected in a 1-mm path length quartz cell at 25°C. Spectra were obtained from five accumulated scans from 250 to 190 nm using a bandwidth of 1-nm and a response time of 1 s at a scan speed of 20 nm/min. Buffer backgrounds were used to subtract from the protein spectra. Secondary structure fractions of the proteins were estimated using the CDSSTR algorithm available on the CDPro software package (115). Ten accumulated near-UV CD spectra of Avh5 (40 μM) were collected using a 1-mm path length at 20 nm/min between 350 and 250 nm with a response time of 1 s and a data pitch of 0.5 nm. In both far- and near-UV CD experiments, protein spectra were obtained in the absence and presence of 0.8 mg/mL of PtdIns(3)P-free and PtdIns(3)P-containing liposomes prepared as described above. The thermal denaturation of Avh5 (10 μM) was studied in the range of 4-90 °C following the temperature-induced changes in ellipticity at 222 nm, where the temperature was increased 1 °C/min, using a 1.5-nm bandwidth, an averaging time of 30 s, and an equilibration time of 2 min.

Fluorescence Spectroscopy

Intrinsic tryptophan fluorescence spectra of purified Avh5 (1 μM) in 5 mM Tris-citrate (pH 6.8) and 100 mM KF were generated on a J-815 Jasco spectropolarimeter at 25 °C in a 1-cm path length cuvette. Three accumulated fluorescence spectra were collected from 310 nm to 410 nm with an excitation wavelength of 295 nm. Buffer backgrounds were used to subtract from the protein spectra.

Homology Modeling

Predicted Avh5 tertiary structure was obtained by homology modeling using Av3a4 as a template (PDB# 2LC2) and using the ALT2TS server

(http://proteinmodel.org/AS2TS/AL2TS/al2ts.html). Avh5 sequence was aligned with the corresponding to that of Avr3a4 using CLUSTALW (Figure 13) and this alignment was used as an input. The corresponding predicted atomic coordinates of Avh5 were visualized using PyMol.

Figure 13. Sequence alignment of the following oomycete Avr proteins. *P. capsici* AVR3a4 (PDB accession 2LC2_A) and *P. sojae* Avh5 (Genbank accession AEK80452).

Surface Plasmon Resonance

All SPR measurements were carried out on a BIAcore X100 instrument (GE Healthcare) at room temperature in 20 mM HEPES (pH 6.8), 100 mM NaCl, and 1 mM NaN_3. Liposomes, with or without 5% PtdIns(3)P, were prepared by sonication followed by extrusion using 200-nm membranes (Avanti Polar Lipids). The surface of an L1 sensor chip (GE Healthcare) was preconditioned by injecting 40 mM N-octyl-β-D-glucopyranoside at a flow rate of 5 μL/min. The first flow cell of the sensor chip was used as a control surface, whereas the second flow cell was employed as the active surface. Approximately 6,000 response units (RU) of 1 mg/mL each of the liposomes tested were immobilized on the surface of the preconditioned L1 sensor chip. After liposome immobilization, 30 μL of 10 mM NaOH at a flow rate of 30 μL/min was used to wash away any unbound liposome. Nonspecific binding sites at the sensor chip surface were then blocked with the injection of 250 μL of 0.1 mg/mL of fatty acid-free BSA at a flow rate of 5 μL/min. A range of concentrations of protein analytes was prepared in the same buffer and injected on both flow cell surfaces at a flow rate of 30 μL/min. Sensorgrams were obtained from

eight different concentrations of each of the tested proteins. Association and dissociation times for each protein injection were set at 120 and 600 s, respectively. The remaining bound protein was washed away by the injection of 30 μL of 10 mM NaOH. The sensor chip surface was regenerated using 40 mM N-octyl-β-D-glucopyranoside and recoated with fresh liposomes for the next protein titration. To estimate the kinetic parameters, sensorgrams were fitted to a two-state (conformational change) binding model using BIAcore X100 evaluation software (version 2.0).

Human Epithelial Cell Uptake Assay

Human A549 airway epithelial cells were cultured in a 96-well plate (~50,000 cells per well) in 90 μL of Dulbecco's Modified Eagle Medium containing 0.1% fetal bovine serum in the presence of 5% CO_2 at 37°C. GFP-fusion protein was added to 12-well plate per experiment at a final concentration of 0.2 mg/mL for approximately 10 minutes and then washed twice with 100 μL PBS. GFP fluorescence was quantitated using a microplate spectrofluorometer with 20 scans per sample. A two-tailed, heteroscedastic student's t-test was used to determine statistical significance for the amount of internalized protein between the various GFP-fusion proteins. GFP-fusion protein cell entry was visualized using a Zeiss Laser Scanning Microscope (LSM) 510. Blocking experiments were performed as described above but in the presence of Ins(1,3)P_2 (500 μM) or Hrs 2xFYVE domain (0.4 mg/mL).

Fluorophore Conjugation

Proteins (1 mg) were buffer exchanged into PBS (pH 6.8) and incubated at room temperature in the presence of 20 μg of DyLight 488 sulfhydryl-reactive dye (added from 10 μg/μL in dimethylformamide; Pierce) overnight in the dark. A C-terminal reduced cystein residue, created by the attB2 site (Protein-TQLS***C***TKWSLEHHHHHH) was the site of alkylation to the reactive maleimide moiety on DyLight 488 forming a stable thioether bond. Proteins were

washed three times with PBS using a centrifugal filter device (3-kDa cut-off; Millipore) to remove the unconjugated fluorophore.

Soybean Root Uptake Assay

Soybean seeds were grown at 25°C in vermiculite for ~4 days. Five root tips of ~2 cm in length were incubated in 200 µL of effector protein-fluorophore conjugates (0.4 mg/mL in PBS, pH 7.2) for 2 h. Cells were washed for 30 min with PBS (pH 7.2) and imaged by visualized using a Zeiss LSM 510.

Confocal Laser Scanning Microscopy

GFP fusion proteins and DyLight 488 conjugated proteins were excited at 488 nm and their emissions were captured using a 505-530 nm broad pass filter. The detector gain measurements were between 700-740 (GFP) and 600-640 (DyLight 488) with an amplifier offset ranging from -0.1 to 0. Propidium iodide was excited at 543 nm and the emission was captured using a 580-615 nm broad pass filter. The detector gain measurements were between 550-600 with an amplifier offset ranging from -0.1 to 0. All images are representative of at least 8 scans.

Chapter 3 RESULTS AND DISCUSSION

Dr. Hugo F. Azurmendi assigned the backbone amide resonances of Avh5.

Dr. Shiv D. Kale performed all of the host cell entry experiments.

I. Results

1. Integrity of Avh5

Initially, the Avh5 PtdIns(3)P-binding activity could not be detected (Figure 14). With careful analysis, I found that there was potential secondary thrombin digestion site at the N-terminus of Avh5, which may explain the fact that there were two products of quite similar size after thrombin digestion (Figure 15). In fact, the N-terminal sequencing result (Figure 16) for the protein generated using this construct suggested the compromised integrity of the Avh5 protein. Since prescission protease digestion is more specific, I finally decided to sub-clone Avh5 cDNA into pGEX6P1 vector, which contains a prescission protease cleavage site. At the end, there was a single band with correct size on 10% SDS-PAGE (Figure 17). In addition, the N-terminal sequencing (Figure 16) and MALDI-TOF Mass Spectrometry (Figure 18) analyses together verified the integrity and purity of the protein.

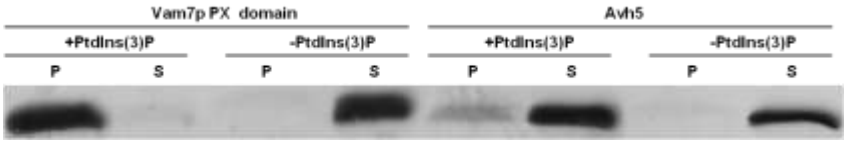

Figure 14. Liposome-binding assay of Vam7p PX domain and Avh5 with liposomes with or without PtdIns(3)P. Liposomal pellet and supernatant fractions were obtained after centrifugation, which correspond to the unbound and bound fractions, respectively. Samples were analyzed by SDS-PAGE and Coomassie Blue staining.

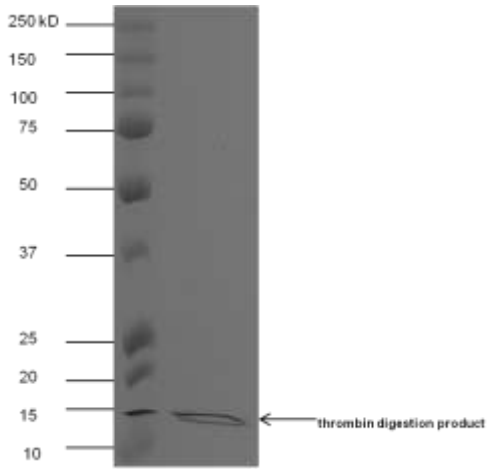

Figure 15. Thrombin digestion result of Avh5. After purified using glutathione beads, the GST fusion Avh5 was digested with thrombin overnight at 4°C. A small aliquot of the digested product was subject to SDS-PAGE analysis.

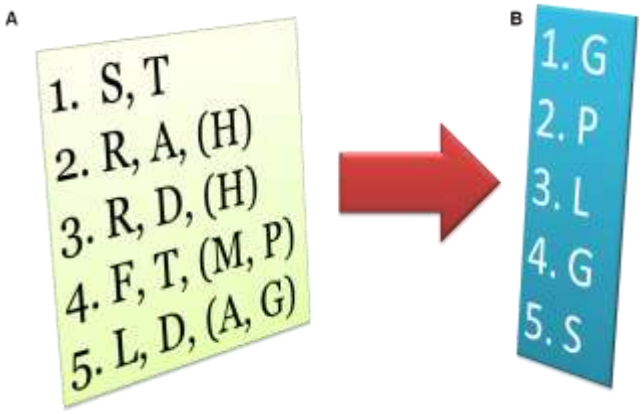

Figure 16. N-terminal sequencing of Avh5. The first five residues of Avh5 were sequenced. (A) N-terminal sequencing result for Avh5 digested by thrombin. (B) N-terminal sequencing result for Avh5 digested by prescission protease.

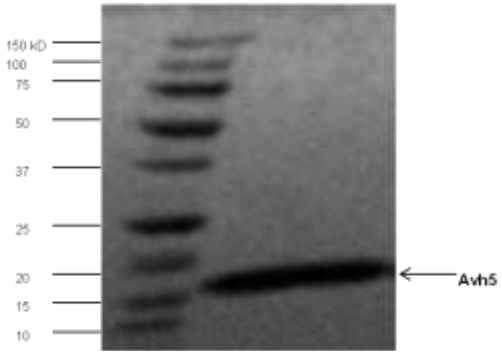

Figure 17. Purified Avh5 on SDS-PAGE. The molecular weight of Avh5 is 13.87 kDa. After purification, Avh5 (10 μg) shows one band on SDS-PAGE.

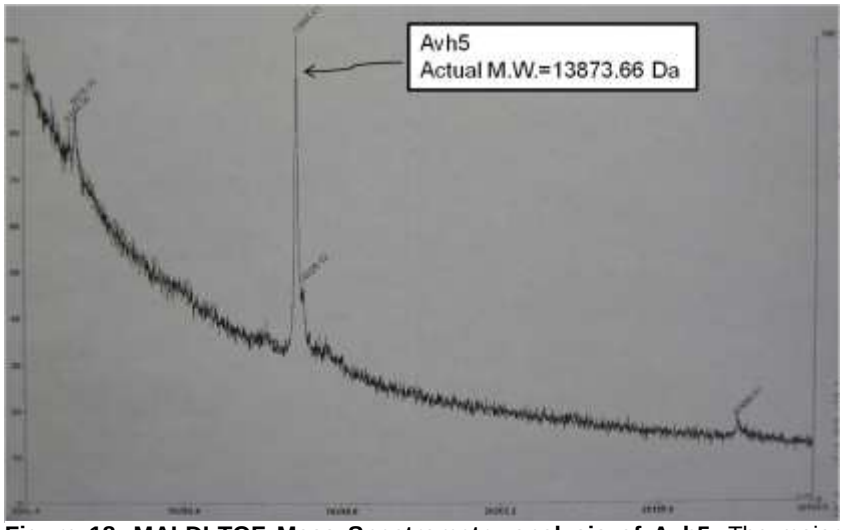

Figure 18. MALDI-TOF Mass Spectrometry analysis of Avh5. The major peak with 13844.01Da indicates that the purified Avh5 is integral.

2. Oligomeric state exploration of Avh5

The actual molecular weight of the Avh5 protein is 13.9 kDa. However, the calculated molecular weight is 28.7kDa from size-exclusion chromatography (Figure 19). There are two possible explanations for this result. On the one hand, the long N-terminal disordered region makes the Avh5 protein quite non-globular, which may result in the shifted chromatogram after size-exclusion purification. On the other hand, Avh5 may adopt a dimeric form. To verify such hypothesis, I performed chemical cross-linking by using a homobifunctional cross-linker, called Bis(Sulfosuccinimidyl) suberate (BS^3). BS^3 may react with any primary amine-containing

molecule, such as lysines, within certain distance (11Å) to form stable amide bonds. If the protein adopts an oligomeric state, which suggests that each subunit is close enough to each other to be covalently cross-linked, then it will show the corresponding size of the oligomer on SDS-PAGE. Figure 20 demonstrates that Avh5 adopted a monomeric state in the presence of BS^3. However, derived from this experiment, I cannot draw a conclusion that Avh5 is a dimer if the lysine residues in Avh5 are not close enough to facilitate the BS^3 linker insertion. Definitely, the use of a native gel or sedimentation ultracentrifugation provides alternative methods to confirm the oligomeric state of Avh5, which will be explored in the near future.

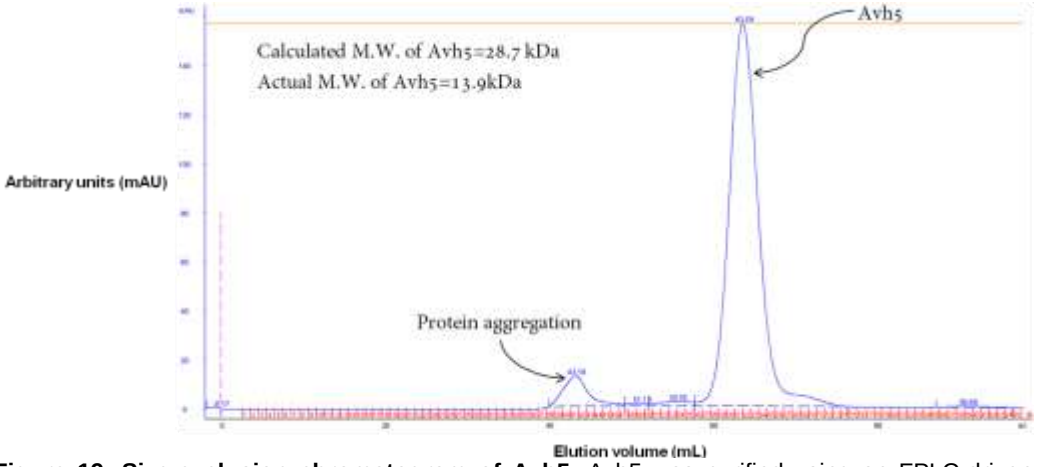

Figure 19. Size-exclusion chromatogram of Avh5. Avh5 was purified using an FPLC-driven Superdex 75 column previously equilibrated with 50 mM Tris-HCl (pH 8.0) and 1 M NaCl.

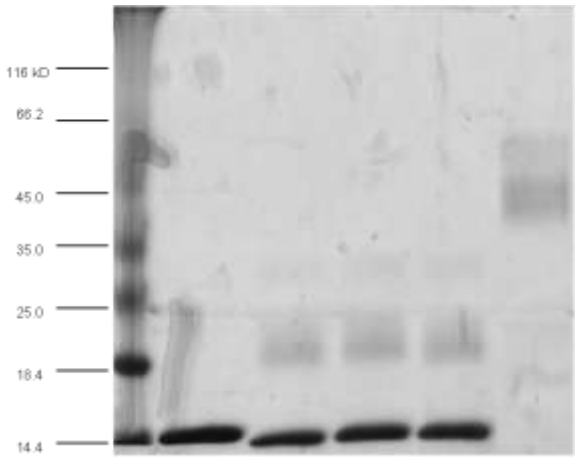

Figure 20. Chemical cross-linking analysis of Avh5 with BS^3. Ten µg of purified Avh5 was incubated with 0.25, 0.5, and 1 mM of BS^3 in 20 mM HEPES (pH 7.5) for 30 min. To quench the reaction, Tris-HCl (pH 6.8) was added at a final concentration of 40 mM, followed by 15-min incubation. Proteins were subject to SDS-PAGE analysis. From left to right: protein marker, Avh5, Avh5+0.25 mM BS^3, Avh5+0.5 mM BS^3, Avh5+1 mM BS^3, GST (10µg).

3. Structural properties of Avh5

To precisely characterize Avh5 structurally and functionally, I collected the ^{1}H, ^{15}N HSQC spectrum of the full-length protein (Figure 21). The spectrum exhibited good NH signal dispersion but with a number of chemical shifts clustered in the center (between 8 and 8.5 ppm). This pattern can be explained by the presence of structured and unstructured regions in the protein. Backbone resonance assignments of the protein were determined based on three-dimensional HNCO, HN(CO)CA, HNCACB and HN(CO)CACB NMR experiments. Ninety-one percent of ^{1}HN and ^{15}N resonances of the backbone amide of the protein (excluding the five proline residues) were assigned. Furthermore, 88% of carbonyls, 89% of Cα, and 87% of Cβ resonances of Avh5 were assigned. Four helical elements were mapped in the second half of the protein based on the protein resonance assignments, spanning to residues Lys52-Leu57 (helix-1), Pro60-Asn72 (helix-2), Val77-Gly82 (helix-3), and Asn89-Glu114 (helix-4) (Figure 22). These calculations are in agreement with the secondary structure content of Avh5 estimated from the far-UV circular dichroism spectrum of the protein (Figure 23A and Table 2). The near-UV CD spectrum of Avh5 showed a strong minimum at ~278 nm, indicating that Tyr aromatic side chains contribute to the tertiary structure of the protein (Figure 23B).

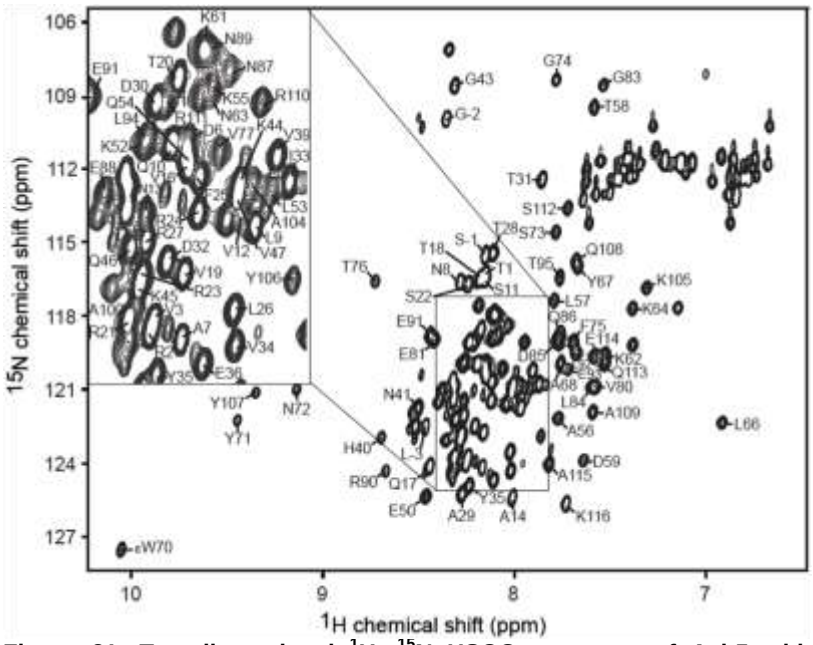

Figure 21. Two-dimensional ^{1}H, ^{15}N HSQC spectrum of Avh5 with assigned resonances labeled. The crowded region of the spectrum is zoomed in the inset.

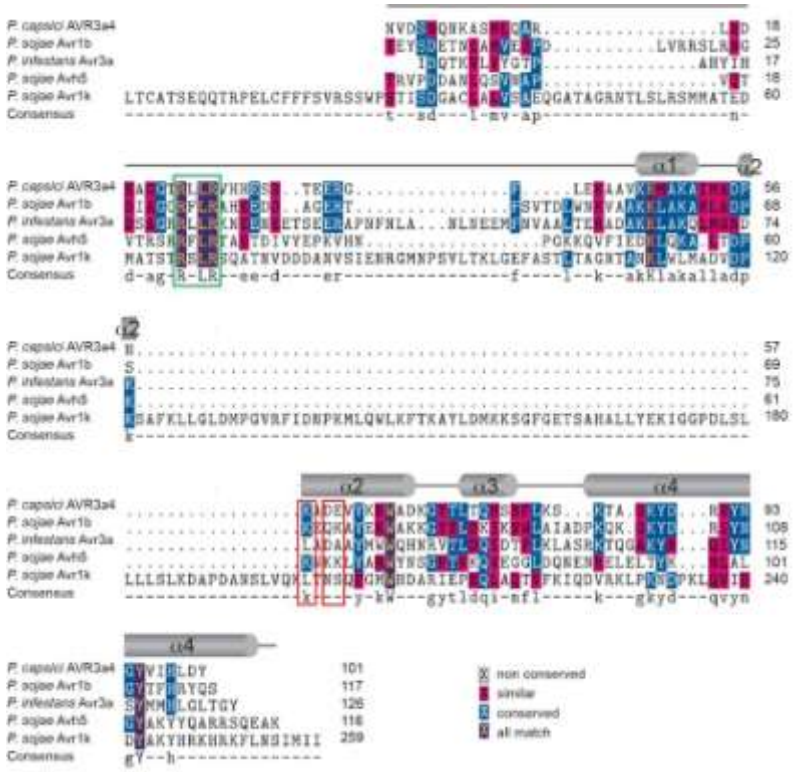

Figure 22. Sequence alignment of the following oomycete Avr proteins. *P. capsici* AVR3a4 (PDB accession 2LC2_A), *P. sojae* Avr1b (Genbank accession AAM20935), *P. infestans* Avr3a (Genbank accession ADC96696), *P. sojae* Avh5 (Genbank accession AEK80452), and *P. sojae* Avr1k (Genbank accession ABZ10806). Secondary structure elements of Avh5 are shown on top of the alignment. Lysine residues of Avh5 engaged in PtdIns(3)P binding are boxed in red, whereas the conserved RxLR motifs are boxed in green.

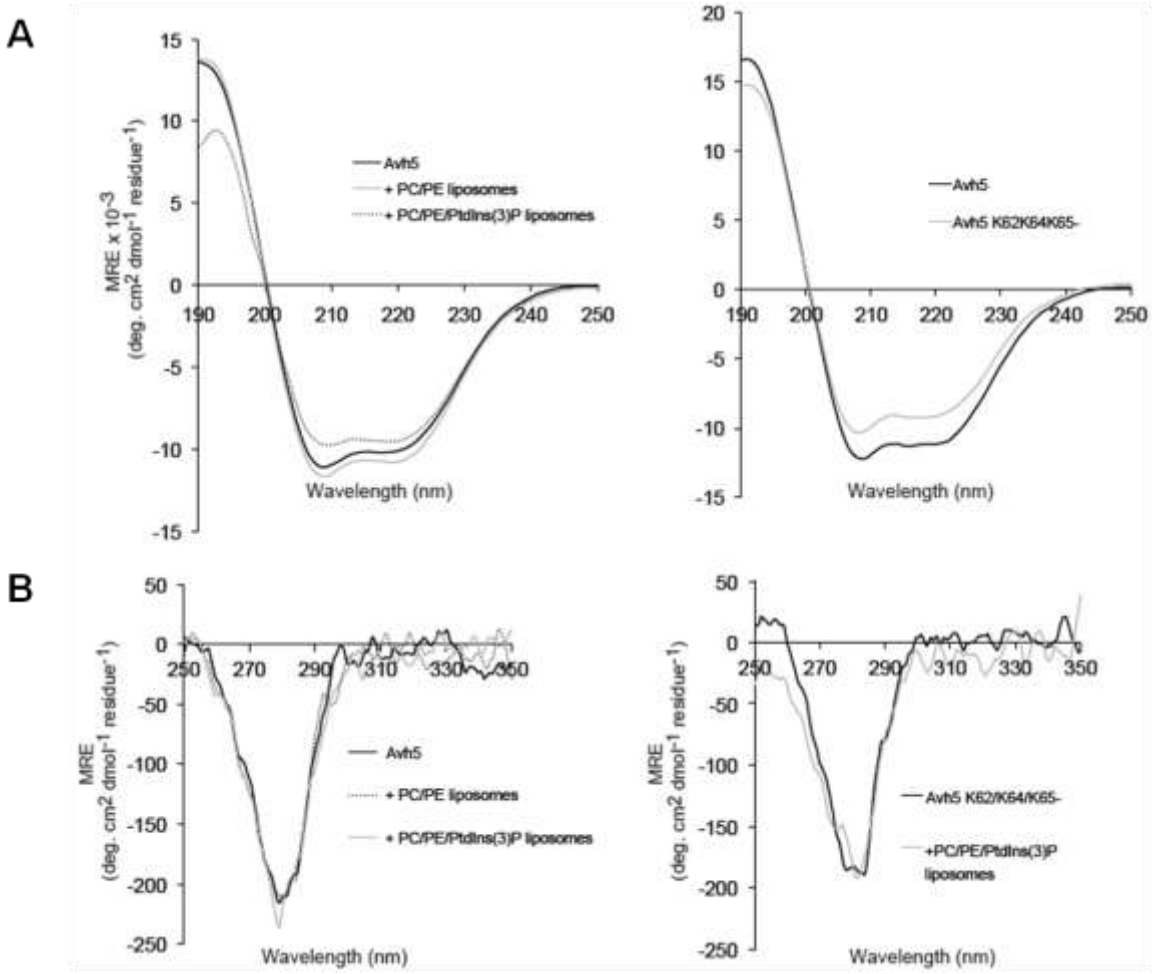

Figure 23. Structural properties of Avh5. (A) left, far-UV CD spectra of Avh5 in the absence (solid black) and presence of PtdCho/PtdEth liposomes (solid gray) or PtdCho/PtdEth/PtdIns(3)P liposomes (dotted black); right, far-UV CD spectrum of Avh5 wild-type (black) and K62A/K64A/K65A (gray). (B) left, near-UV CD spectra of Avh5 in the absence (solid black) and presence of PtdCho/PtdEth liposomes (solid gray) or PtdCho/PtdEth/PtdIns(3)P liposomes (dotted black); right, near-UV CD spectra of Avh5 K62A/K64A/K65A in the absence (black) and presence of PtdCho/PtdEth/PtdIns(3)P liposomes (solid gray).

Table 2. Predicted secondary structure content of wild-type Avh5 and mutants.

Avh5	αR	αD	βR	βD	Turns	Unordered
Wild-type	35.0	17.4	7.5	4.8	14.1	21.3
K62A/K64A/K65A	35.6	17.1	7.1	4.8	14.4	21.8
RFLR^{AAAA} K62A/K64A/K65A	35.7	17.2	6.5	4.6	14.4	22.1

The secondary structural elements content of the proteins are in %. R and D represent predicted regular and distorted secondary structure elements, respectively. Predictions were generated using CDPro and deconvoluted using the CDSSTR algorithm.

4. Mapping the PtdIns(3)P-binding site in Avh5 using NMR spectroscopy

I initially titrated ^{1}H, ^{15}N Avh5 with dioctanoyl-PtdIns(3)P and collected HSQC spectra for each of the titration points. The protein exhibited reduced solubility in the presence of PtdIns(3)P at the NMR scale. I therefore used the PtdIns(3)P head group, inositol 1,3-bisphosphate (Ins(1,3)P_2) as a ligand. Avh5 bound to Ins(1,3)P_2 in a fast exchange regime manner (Figure 24). The HSQC spectrum of ^{1}H, ^{15}N Avh5 showed no perturbations upon addition of Ins(1)P, demonstrating that phosphorylation of the third position at the inositol ring is critical for lipid head group binding (Figure 25). Most prominent Ins(1,3)P_2-induced chemical shift changes were clustered in residues Lys52, Gln54, Leu57, Thr58, and Lys62 located around the 1 and 2 helices and Gln86, Glu88, and Arg90 residues located at the beginning of the long 4 helical element (Figure 26). Interestingly, weak chemical shift perturbations were observed in the RFLR disordered region as well as in other basic residues such as Lys55 and Lys64 (Figure 26). To identify the Ins(1,3)P_2 binding surface, a homology model of *P. sojae* Avh5 was generated based on the structure of the oomycete homolog Avr3a4 (116) using the AL2TS server (http://proteinmodel.org/AS2TS/AL2TS/al2ts.html). The homology model was consistent with the NMR data. Mapping of the NMR chemical shift changes onto the Avh5 structure displayed two Ins(1,3)P_2-interacting regions at the surface of the protein (Figure 27).

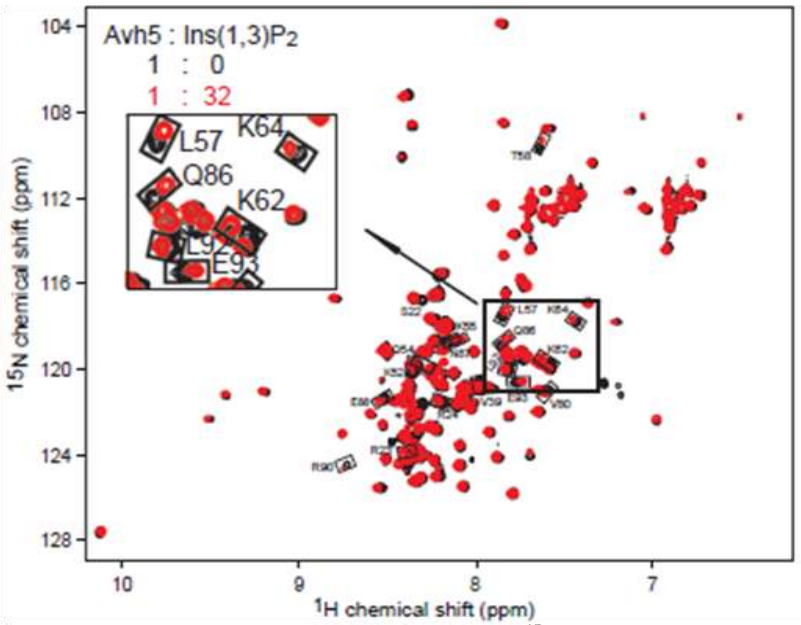

Figure 24. Titrated Avh5 by Ins(1,3)P_2. The ^{15}N-labeled Avh5 (black) was subjected to ^{1}H,^{15}N-HSQC analysis following titration with PtdIns(3)P head group, Ins (1,3)P_2 (red).

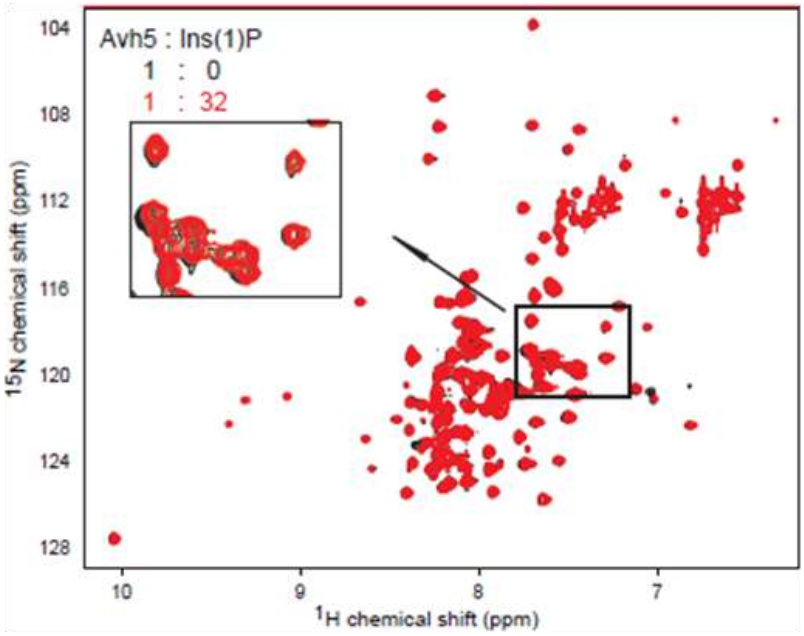

Figure 25. Titrated Avh5 by Ins(1)P. The ^{15}N-labeled Avh5 (black) was subjected to ^{1}H,^{15}N-HSQC analysis following titration with PI head group, Ins(1)P (red).

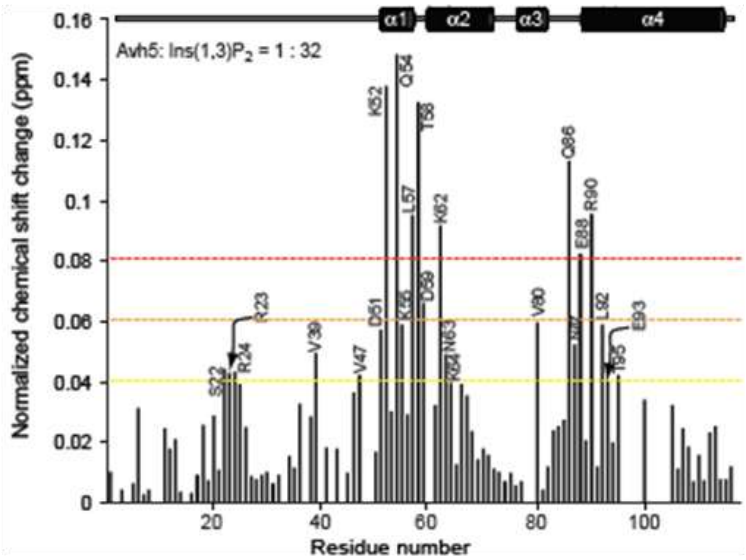

Figure 26. Normalized chemical shift perturbations of Avh5 upon Ins(1,3)P_2 titration. The histogram shows normalized chemical shift perturbations in the backbone amides of Avh5 induced by Ins(1,3)P_2. The colored dashed lines represent significant changes, based on the magnitude of their associated chemical shifts changes: red ($\Delta\delta_{average}$ + 2.5 x standard deviation) > orange ($\Delta\delta_{average}$ + 2 x standard deviation) > yellow ($\Delta\delta_{average}$ + 1.5 x standard deviation).

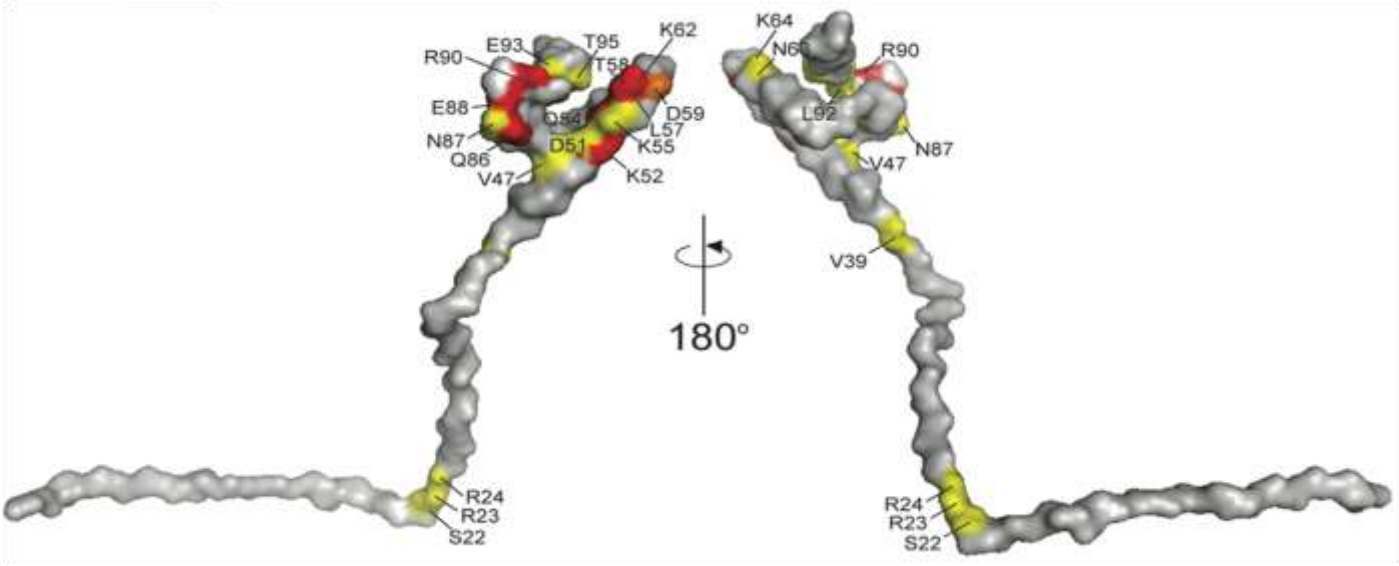

Figure 27. Homology modeling of Avh5. Residues that exhibit significant chemical shift perturbations in Figure 23 are labeled on the modeled Avh5 surface and color-coded according to the scale defined in Figure 25.

5. Identification of key PtdIns(3)P-binding residues of Avh5

As indicated by the NMR data above, the PtdIns(3)P-binding site maps to a region that predominantly includes the first, second, and fourth helices of the protein. Since Ins(1,3)P_2-induced chemical shift changes in the Avh5 NMR spectrum can be associated to residues that are directly in contact with the ligand and/or conformational changes of the protein, I collected CD spectra of the protein in the presence of PtdIns(3)P-free and -enriched liposomes. Negligible conformational changes of Avh5 upon addition of PtdIns(3)P liposomes were observed upon analysis of the far- and near-UV CD spectra of the protein (Figure 23A and B), which indicates that there is no overall conformational change accompanying PtdIns(3)P binding. However, I was curious whether or not there may be local conformational changes in the protein upon interaction with PtdIns(3)P. In the presence of Ins(1,3)P_2, the fluorescence intensity of tryptophan decreased with the increase of Ins(1,3)P_2 concentration (Figure 28), which indicates that Trp70 is moving from a hydrophobic environment to a hydrophilic one, suggesting that local conformation changes in Avh5 are induced by the PtdIns(3)P head group. Next, I carried out site-directed mutagenesis of Avh5 at the Ins(1,3)P_2-perturbed residues. Alanine single mutations in the Lys52, Lys55, Leu57, Thr58, and Arg90 residues did not affect lipid binding when monitored using liposome-binding assays (Figure 29). Minor reduction in PtdIns(3)P binding was observed for alanine single mutations in the Lys62, Lys64, and Lys65 residues of the second helix (Figure 29), suggesting that this basic-rich region is involved in PtdIns(3)P binding. Glutamine mutation in Arg24, which was previously described to be critical for lipid recognition in certain protein effectors (11), and alanine mutations in Leu57/Thr58 did not obviously alter PtdIns(3)P binding under the experimental conditions of our liposome binding assay (Figure 30). A ~30% reduction of lipid binding was observed when the entire RFLR motif was mutated to alanine ($RFLR^{AAAA}$), consistent with the detected minor NMR chemical shift perturbations of this region in the presence of Ins(1,3)P_2 (Figure 26, 30 and 31). Furthermore,

the N-terminal region of Avh5 (as a GFP fusion) containing the RFLR motif (residues 1-44; N-term) also bound to PtdIns(3)P liposomes and the RFLR^{AAAA} mutation reduced binding of this domain to the lipid (Figure 32). Double alanine mutations in the Lys64 and Lys65 (K64A/K65A) residues reduced lipid binding by ~50% while an additional alanine mutation in Lys62 (K62A/K64A/K65A) further reduced it (Figure 30 and 31). CD analysis was then used to address differences in the secondary structure of Avh5 and its PtdIns(3)P-binding mutant. The structural integrity of Avh5 upon mutation in residues Lys62, Lys64, and Lys65 was preserved based on a strong overlap on all CD traces (Figure 23A and B), and secondary structure content remained unchanged (Table 2). Thus, the Lys62, Lys64, and Lys65 mutations appear to directly affect PtdIns(3)P binding.

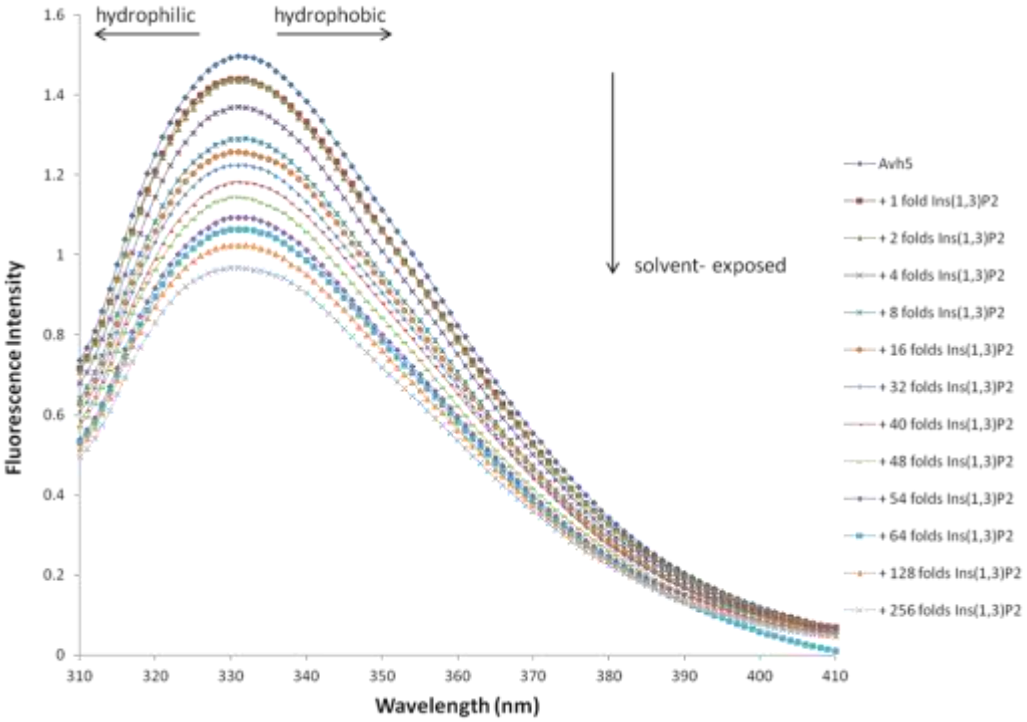

Figure 28. Intrinsic tryptophan quenching of Avh5 in the presence of PtdIns(3)P head group. 1µM of purified Avh5 was quenched in the presence of 1-256 folds of Ins(1,3)P_2, respectively.

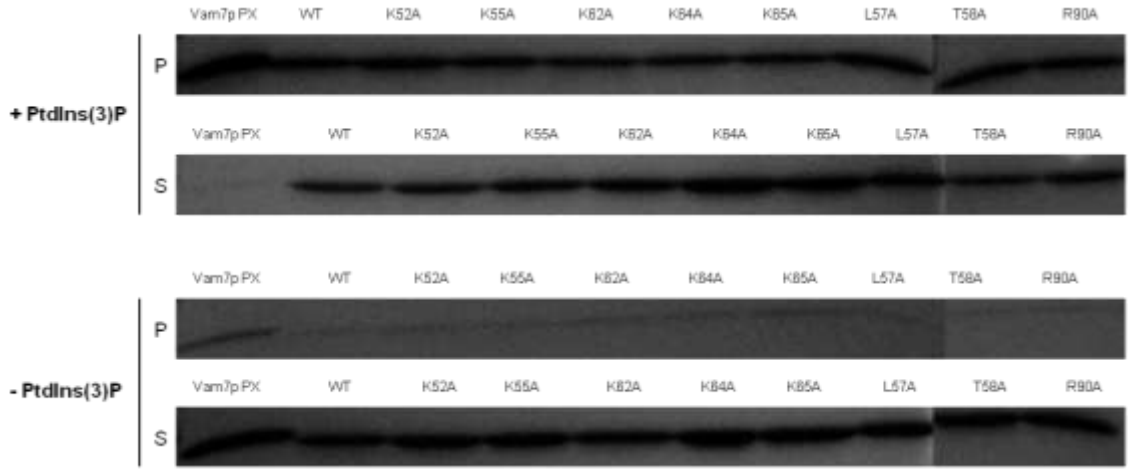

Figure 29. Liposome-binding assay of Vam7p PX domain, wild-type Avh5 and the indicated Avh5 mutants with liposomes without or with PtdIns(3)P. Liposomal pellet and supernatant fractions were obtained after centrifugation, which correspond to the unbound and bound fractions, respectively. Samples were analyzed by SDS-PAGE and Coomassie Blue staining.

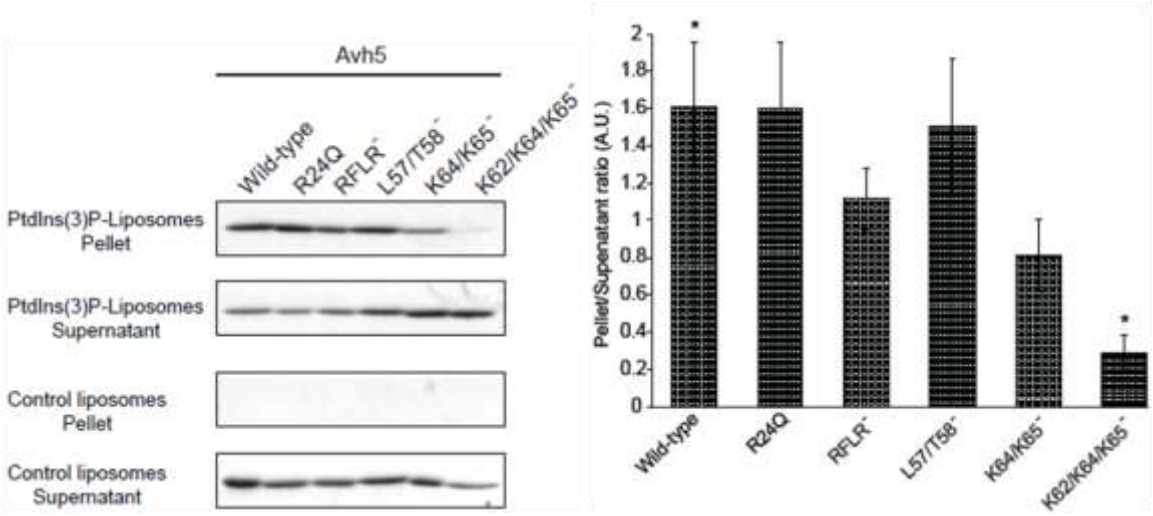

Figure 30. Liposome-binding assay of wild-type Avh5 and the indicated mutants with liposomes without or with PtdIns(3)P. Liposomal pellet and supernatant fractions were obtained after centrifugation, which correspond to the unbound and bound fractions, respectively. Samples were analyzed by SDS-PAGE and Coomassie Blue staining (left panels) and quantified by densitometry (right panel). *, *P*<0.04. The ratios represent averages of three independent assays. Error bars represent standard deviations of the averages

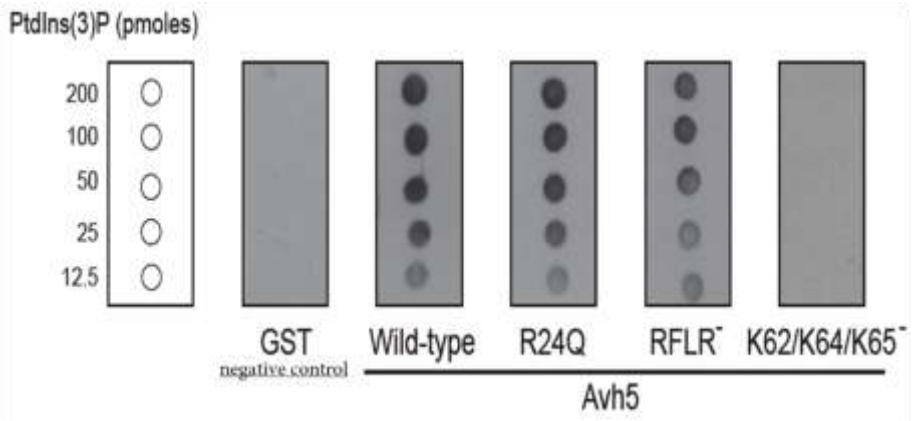

Figure 31. Lipid-protein overlay assay of Avh5 and the indicated mutants as GST fusion proteins were examined for PtdIns(3)P binding. Each spot in the lipid strip contains from 12.5 to 200 pmoles of PtdIns(3)P. GST was employed as a negative control.

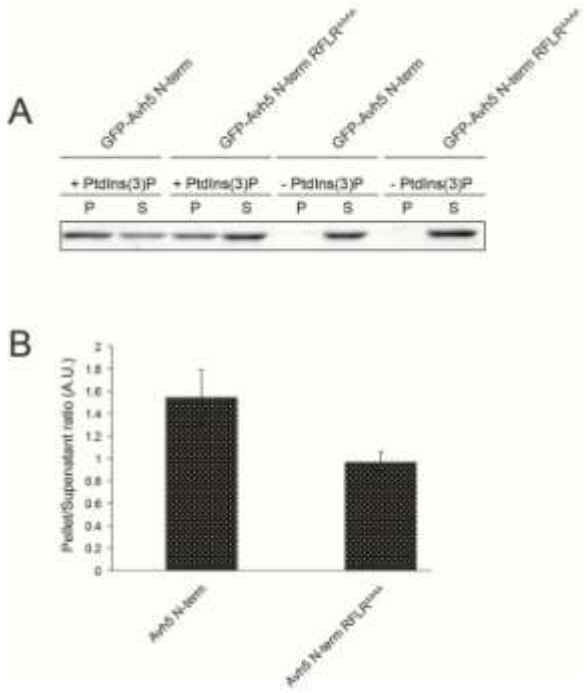

Figure 32. The N-terminal region of Avh5 (residues 1-44) binds PtdIns(3)P liposomes. (A) The indicated GFP fusion proteins were incubated with PtdIns(3)P-free or -enriched liposomes. Liposomal pellet (P) and supernatant (S) fractions were obtained after centrifugation, subjected to SDS-PAGE, and stained with Coomassie Blue. (B) SDS-PAGE bands were quantified by densitometry.

6. PtdIns(3)P binding of Avh5 increases thermostability

It has previously been suggested that PtdIns(3)P binding by Avr3a stabilizes the protein within the host cytoplasm (14). Similarly, external PtdIns(3)P could potentially stabilize effector proteins, such as Avr3a and Avh5, against degradation in the apoplast during the delivery process by oomycetes into plant cells (11). We therefore investigated the thermal stability of Avh5 in the presence or absence of PtdIns(3)P. We gradually increased the temperature while monitoring the protein CD signal at 222 nm. Avh5 showed an apparent melting temperature (T_m) of 42.3 ± 0.5 °C (χ^2=0.21) (Figure 33). Interestingly, addition of PtdIns(3)P-enriched liposomes increased the T_m value of the protein to 46.9 ± 0.5 °C (χ^2=0.19), a shift not observed when PtdIns(3)P-free liposomes were evaluated (T_m= 42.8 ± 0.5 °C; χ^2=0.22) (Figure 33). This shift in T_m by ~4°C suggests that PtdIns(3)P promotes Avh5 stability.

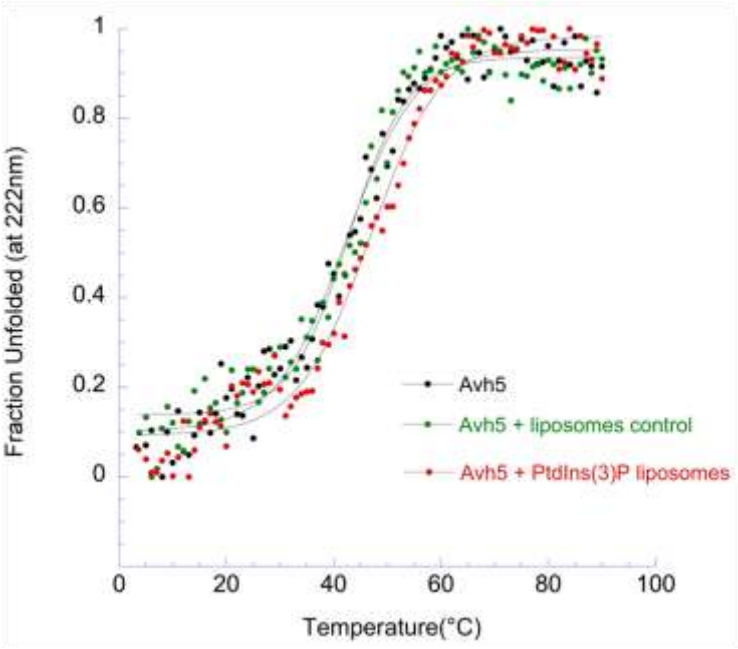

Figure 33. Thermal stability of Avh5 in the presence of PtdIns(3)P ligand. CD monitoring of the thermal unfolding of Avh5 (at 222 nm) in the absence (black) and presence of PtdCho/PtdEth (green), or PtdCho/PtdEth/PtdIns(3)P (red).

7. Kinetic properties of Avh5-PtdIns(3)P association

To obtain a quantitative measure of binding, I carried out SPR experiments by immobilizing PtdIns(3)P-free or PtdIns(3)P-enriched liposomes on an L1 sensor chip and using wild-type Avh5, or mutants $RFLR^{AAAA}$, K62A/K64A/K65A, or $RFLR^{AAAA}$ K62A/K64A/K65A as analytes. When these proteins were passed over the sensor chip, binding was observed in a concentration-dependent manner in all cases and exhibited rapid association and dissociation rates (Figure 34). Avh5 sensorgrams best fitted with a two-state conformational change model and resulted in a dissociation constant (K_D) of 2.3 µM (Table 1). Mutations in the RFLR motif of Avh5 slightly reduced PtdIns(3)P binding, giving a K_D of 3.5 µM (Figure 34B). Consistent with the data shown in Figure 30 and 31, the Avh5 K62A/K64A/K65A mutant showed a substantial reduction in binding, with a 44-fold reduction in affinity (Figure 34C), while mutations in both RxLR motif and the basic-rich region together almost abolished PtdIns(3)P binding (Figure 34D) without affecting the overall structure of the protein (Figure 35). The differences between Avh5 and its mutants for PtdIns(3)P in affinity are evident when plotting the maximum response units against protein concentration (Figure 34E). In all titrations, PtdIns(3)P binding exhibited a saturable binding isotherm that is indicative of specific binding.

Table 1. Dissociation constants (K_D) and association (k_a) and dissociation (k_d) rate constants of PtdIns(3)P binding of Avh5.

Avh5	k_{a1} (M^{-1} s^{-1})	k_{d1} (s^{-1})	k_{a2} (s^{-1})	k_{d2} (s^{-1})	K_D (M)	Fit (χ^2)
Wild-type	2.12×10^{4}	8.54×10^{-2}	5.13×10^{-3}	7.07×10^{-3}	2.33×10^{-6}	5.2
$RFLR^{AAAA}$	4.78×10^{4}	4.73×10^{-2}	6.87×10^{-3}	3.85×10^{-3}	3.55×10^{-6}	7.9
K62A/K64A/K65A	3.39×10^{2}	6.44×10^{-2}	6.82×10^{-3}	7.88×10^{-3}	1.02×10^{-4}	5.5

The association rate constant k_a refers to the rate of protein-PtdIns(3)P liposome complex formation per second in a one molar solution of ligand (PtdIns(3)P liposomes) and analyte (Avh5 or mutants), while the dissociation rate constant k_d defines the stability of the complex in the same experimental condition. The affinity of an interaction is the equilibrium dissociation rate constant (K_D), which equals k_d/k_a. Since data best fitted with the two-state conformational model, the reaction is accompanied with two sets of rates. Data are representative of three independent experiments with at least seven different protein concentrations.

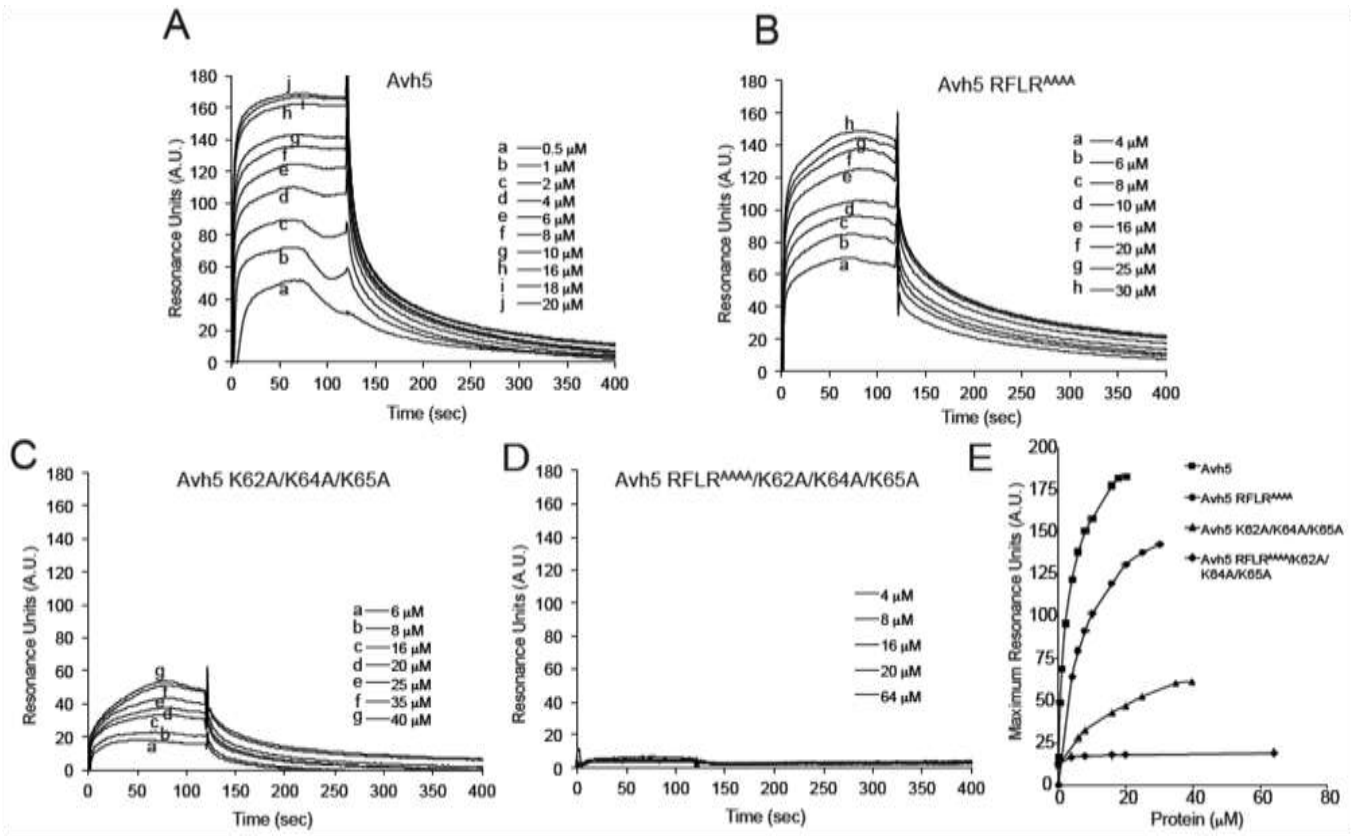

Figure 34. Kinetic analysis of Avh5 proteins with PtdIns(3)P. SPR sensorgrams for the binding of wild-type Avh5 (A), and mutants RFLR^{AAAA} (B), K62A/K64A/K65A (C), and RFLR^{AAAA} K62A/K64A/K65A (D) with immobilized PtdIns(3)P liposomes. The indicated protein concentration range for each of the constructs was flowed over the liposomes attached on an L1 sensor chip. *A.U.*, arbitrary units. (E) Strength of the associations is represented in the plot in which the maximum of resonance units for each protein concentration is indicated.

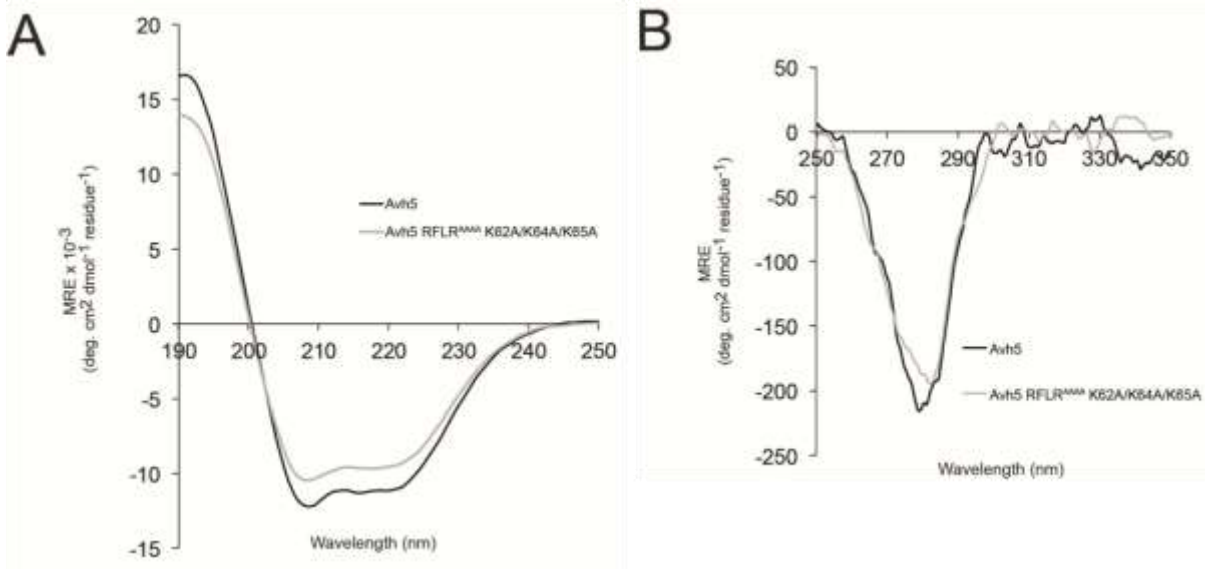

Figure 35. Mutations in both RFLR motif and basic region do not alter Avh5 structure. CD far-UV (A) and near UV (B) of Avh5 RFLR^{AAAA} K62A/K64A/K65A. The spectra are compared with those corresponding to the wild-type Avh5.

8. Avh5 requires intact RFLR and lysine-rich regions to be efficiently translocated into host cells and depends on external PtdIns(3)P

To define what region of Avh5 is important for cell entry, proteins were fused to GFP and the fusion proteins were incubated with human airway epithelial cells (Figure 36A and B). The entry of RxLR effectors, including Avh5, into the human cells can be accurately quantified compared with soybean root cells, which exhibit high background for quantification purposes. Consistent with previous observations (11), wild-type Avh5 accumulated intracellularly, whereas the $RFLR^{AAAA}$ mutant was reduced in cell entry by about 4-fold. Interestingly, the C-terminal region of Avh5, lacking the RxLR domain but containing the basic-rich PtdIns(3)P-interacting region (residues 33-116), exhibited ~35% reduction in cell entry compared to the wild-type protein. The contribution of the C-terminal PtdIns(3)P-interacting residues of Avh5 to cell entry was confirmed by the ~50% reduction in uptake of the N-terminal RxLR domain of the protein (residues 1-44) compared to the wild-type, but the N-terminal domain nevertheless retains substantial (~50%) entry activity. Mutation in the RFLR motif drastically reduced entry of this N-terminal domain into the epithelial cells, showing that the entry activity of this domain depended on the RFLR motif. Consistent with the lipid-binding assays, mutations in the PtdIns(3)P-interacting residues Lys62, Lys64, and Lys65 substantially reduced Avh5 entry into epithelial cells indicating that these three residues are critical for the cell entry activity of the C-terminal domain. Lys61, which is not critical for lipid binding (Figure 24), appeared not to contribute to Avh5 entry into epithelial cells (Figure 36A). To validate the human cell entry data in a more physiologically relevant context, and to avoid any potential artifacts introduced by the use of GFP fusions, fluorophore-conjugated Avh5 proteins were incubated with soybean root cells. Full-length wild-type Avh5 protein efficiently entered the root cells within 2 h, whereas mutations in the RFLR motif or the key basic C-terminal residues drastically reduced cell entry (Figure 37 and 38). Importantly, the N-terminal domain was still able to enter root cells, whereas a mutation in its RFLR motif abrogated protein entry (Figure 37), indicating that this motif mediates Avh5

uptake. Uptake of the C-terminal domain alone by the soybean root cells was weaker than uptake of the N-terminal domain, and could not be clearly detected until 4 h (Figure 37).

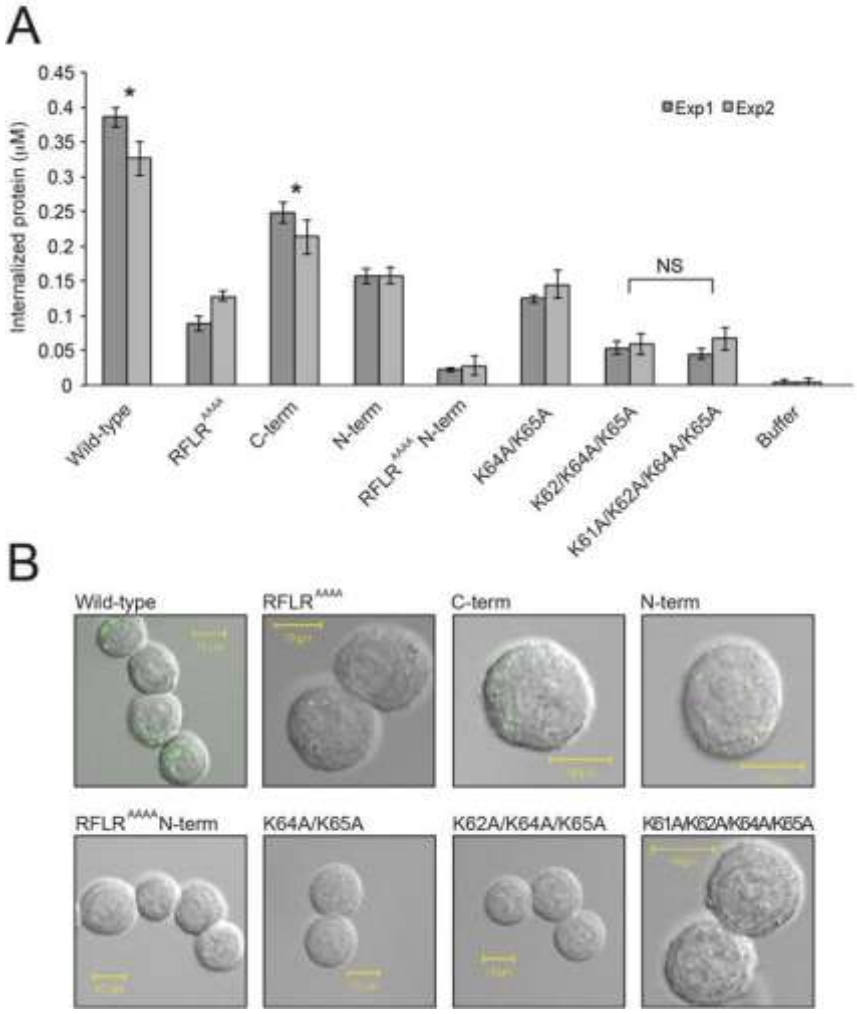

Figure 36. The role of the RFLR motif and the basic-rich region of Avh5 in human cell entry. (A), Cell entry of the following Avh5 GFP fusion proteins (from left): wild-type, $RFLR^{AAAA}$ (RFLR motif mutated to AAAA), C-term (residues 33-116), N-term (residues 1-44), $RFLR^{AAAA}$ N-term (residues 1-44 with a RFLR mutation to AAAA), K64A/K65A (residues Lys64 and Lys65 mutated to alanine), K62A/K64A/K65A (residues Lys62, Lys64, and Lys65 mutated to alanine), K61A/K62A/K64A/K65A (residues Lys61, Lys62, Lys64, and Lys65 mutated to alanine). Each of the experiments has been statistically pairwise compared. All values are displayed as mean ± standard error, n=12. * $P<0.05$. NS, not significant. (B) A549 human epithelial cells were incubated for 10 min at 37°C with the GFP fusions indicated in (A) and then washed to remove the excess of extracellular protein. Light micrographs are overlaid with the fluorescence images.

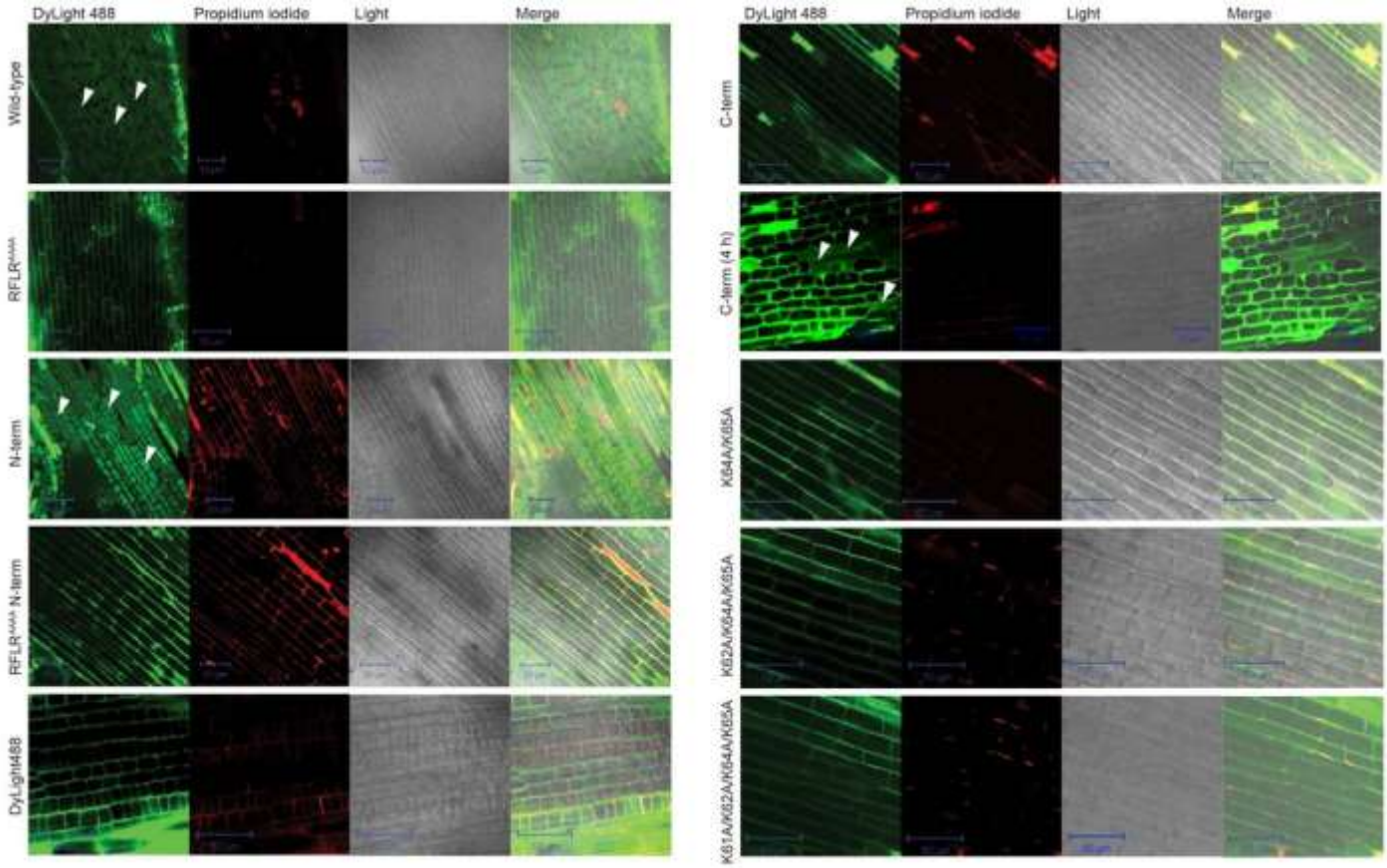

Figure 37. *P. sojae* Avh5 RFLR motif and C-terminal basic residues are both critical for root cell uptake. Soybean root cell entry of the following DyLight 488-conjugated Avh5 proteins (from top to the bottom): wild-type, $RFLR^{AAAA}$ (RFLR motif mutated to AAAA), N-term (residues 1-44), $RFLR^{AAAA}$ N-term (residues 1-44 with a RFLR mutation to AAAA), and DyLight488 (unconjugated DyLight 488) (left panels); C-term (residues 33-116), C-term (residues 33-116; 4 h incubation), K64A/K65A (residues Lys64 and Lys65 mutated to alanine), K62A/K64A/K65A (residues Lys62, Lys64, and Lys65 mutated to alanine) and K61A/K62A/K64A/K65A (residues Lys61, Lys62, Lys64, and Lys65 mutated to alanine) (right panels). Roots were incubated in 0.4 µg/µL protein solution for ~2 h, washed for 30 min, and stained for 5-10 min in the presence of propidium iodide to detect dead or dying cells. Left panels indicate fluorescence micrograph of effector protein distribution, followed by propidium iodide detection, light micrographs, and the merge between effector protein and propidium iodide images over light micrographs.

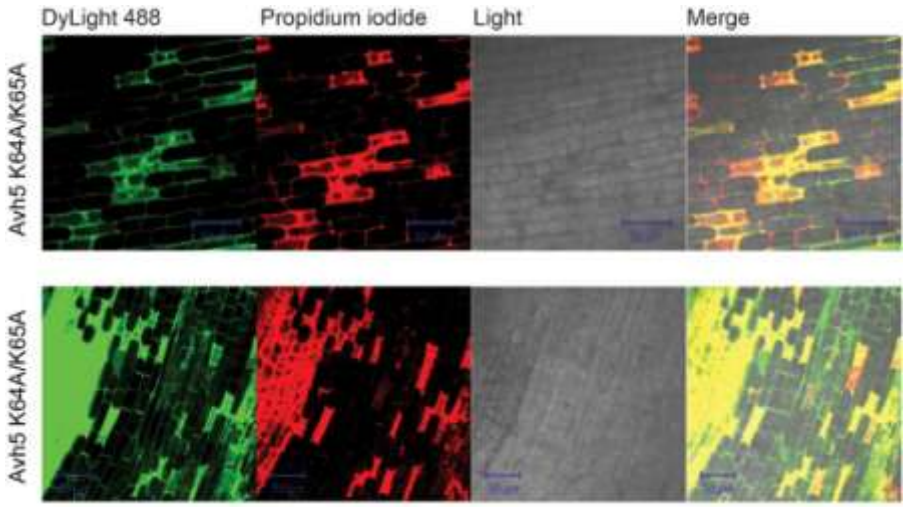

Figure 38. Soybean root cells undergoing cell death internalize protein in a nonspecific manner. Soybean root cells undergoing cell death are brightly stained with propidium iodide and rapidly internalize proteins (in this case fluorophore-labeled Avh5 K64A/K65A) in a nonspecific manner. Root damage primarily occurs from inappropriate growth conditions, and contaminants in the protein solutions, especially imidazole. Roots with multiple patches of cell death were discarded, due to the significant degree of nonspecific internalization.

Since entry of Avh5 depends on both an intact RFLR and the basic residues located at the C-terminal region of the protein, we asked whether uptake of Avh5 and its isolated domains depends on the presence of extracellular PtdIns(3)P. Therefore, GFP-Avh5 (or its mutants) was pre-incubated with Ins(1,3)P_2, and then protein entry into human epithelial cells was quantified using fluorescence spectroscopy (Figure 39A). In all cases, including both the isolated N-terminal and C-terminal domains, protein uptake was reduced by the PtdIns(3)P head group. These data suggest that the cell entry activities of the truncated or mutated proteins, due to either an intact RFLR or a basic-rich region, were dependent of their remaining PtdIns(3)P-binding activities. Accordingly, protein entry into both human and soybean root cells was also drastically reduced by the presence, respectively, of Hrs 2xFYVE domain (Figure 39A) or PEPP1 PH domain (Figure 39B), which are PtdIns(3)P-binding domains that can bind tightly to and occlude cell surface PtdIns(3)P. Overall, these results indicate that Avh5 cell entry depends on the binding of both its N-terminal and C-terminal domains to external PtdIns(3)P.

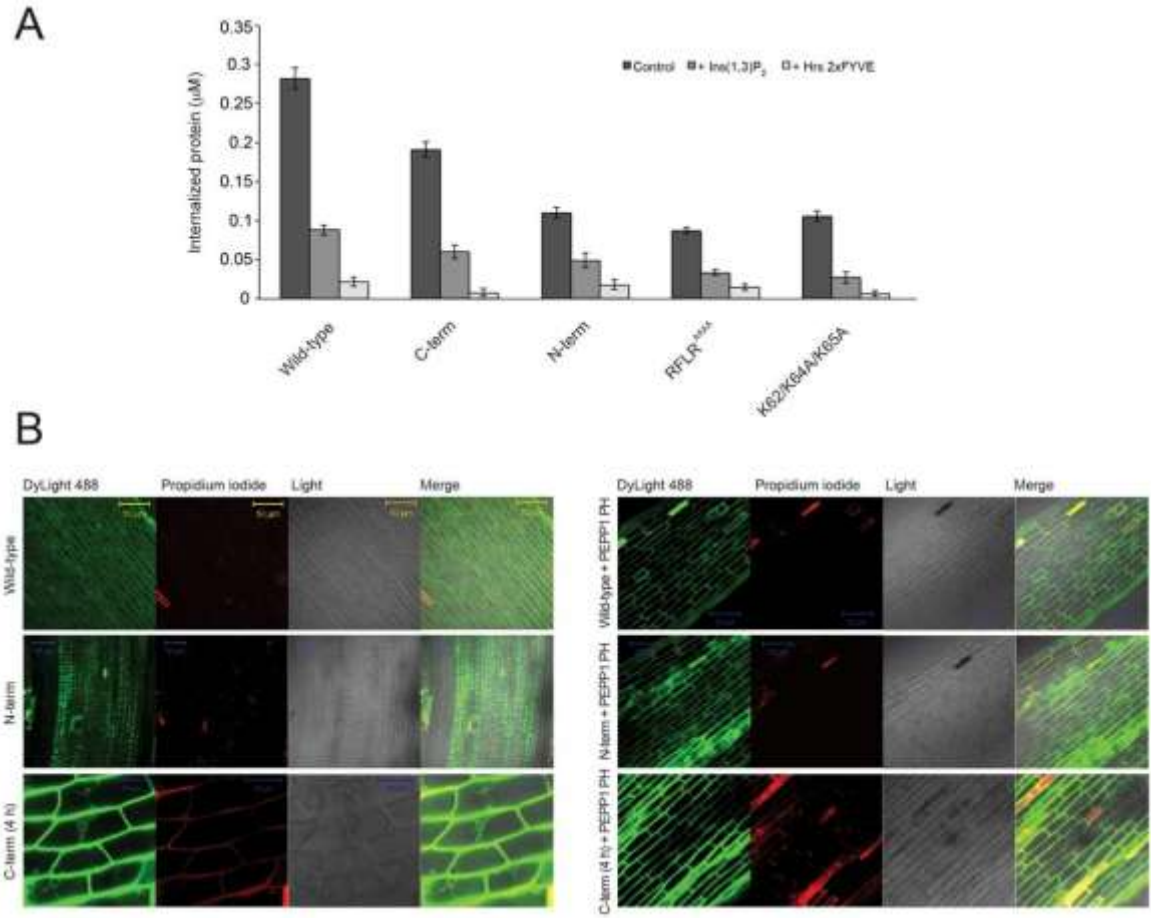

Figure 39. Inhibition of Avh5 entry by Ins(1,3)P_2 and PtdIns(3)P-binding proteins. (A) Human A549 airway epithelial cells were incubated with GFP-Avh5 or the indicated mutants in the absence and presence of either Ins(1,3)P_2 or the Hrs 2xFYVE domain. Experimental conditions are the same as described in Figure 5. (B) Soybean root cells were incubated with DyLight 488-conjugated Avh5 or the indicated truncated proteins in the absence and presence of PEPP1 PH domain. Experimental conditions are the same as described in Figure 30.

II. DISCUSSION

Effector proteins are secreted by oomycete and fungal plant pathogens to manipulate the host's physiology to promote infection, including debilitation of the immune system. A large class of oomycete effector proteins is characterized by the presence of conserved RxLR-dEER motifs at their N-termini, which are necessary to facilitate the entry of effector proteins into the plant cell (5, 8). Intriguingly, this finding correlates with the observation that numerous RxLR

motifs are present in plant proteins that are associated with membrane trafficking (117), suggesting that oomycetes (and perhaps fungi) may be utilizing plant cell endocytic pathways during invasion. Furthermore, several oomycete and fungal effector proteins bind PIPs, primarily PtdIns(3)P, PtdIns(4)P, and PtdIns(5)P (11, 14, 118). However, recent reports differ regarding the PIP-binding site in these proteins (11, 14, 118). These differences are difficult to resolve in the absence of any biophysical or structural data to clearly identify key PIP interacting residues (15). In this study, we used a combination of NMR, SPR, CD, liposome-binding, protein-lipid overlay assays, and site-directed mutagenesis to determine the PtdIns(3)P-binding sites in Avh5 and their individual contributions to cell entry activity. The lysine-rich region, corresponding to helix 2, is the major contributor to PIP recognition, in agreement with the report by Yaeno and colleagues for lipid interactions by Avr3a and Avr1b (14). Our previous studies suggested that the RxLR motif is necessary and sufficient for Avh5 to recognize PtdIns(3)P (11). Our current results confirm that the N-terminal domain can indeed bind PtdIns(3)P, and that binding by this domain requires the RxLR motif; however binding by this domain alone is weak compared with binding by the C-terminus alone. Furthermore, in the intact protein, the contributions of the C-terminus are most relevant. The previous lipid-binding assays were carried out with the GST- and GFP-fusion versions of the protein in a full-length state as well as the N-terminal RxLR region; this may account for the differences with our previous findings. Considering the secondary structure analysis of Avh5 reported in this study, the N-terminal region of the protein is anticipated to be disordered, as reported for Avr3a4 (116) and therefore presumably adopts a conformation that can bind to PIPs. In either case, and in agreement with previous hypotheses that effector proteins present additional requirements for cell entry (5, 11, 42), we demonstrate that Avh5 presents a basic region located in the second helix of the protein as a major contributor for PtdIns(3)P recognition with the RFLR motif playing a more minor role. Therefore, these studies represent the functional-structural characterization of the interaction of PtdIns(3)P

with an RxLR effector protein and provide further insight into the molecular mechanisms involved in the PIP recognition by this subfamily of RxLR effectors.

PIPs represent a minor constituent of the total lipids in all eukaryotic cells. To date, six different phosphorylated states of the lipid are found in plants: PtdIns(3)P, PtdIns(4)P, PtdIns(5)P, PtdIns(3,4)P_2, PtdIns(3,5)P_2, and PtdIns(4,5)P_2 (38). PtdIns(3)P represents 2-15% of the total monophosphate PIPs (38). Using a chimeric YFP fused with a tandem dimer of the PtdIns(3)P-binding FYVE domain from the growth factor–regulated tyrosine kinase substrate, it has been demonstrated that PtdIns(3)P localizes in both endosomal/pre-vacuolar vesicles and vacuolar membranes (119). Indeed, PtdIns(3)P has been shown to participate in vacuolar trafficking in *Arabidopsis* (22) and *Nicotiana* (120). This function is also extended to endosomes, in which PtdIns(3)P controls the movement of these organelles in root hairs (121). In addition, extracellular PIPs, such as PtdIns(4)P, have been reported in tomato cell suspensions (122). In animal cells, PtdIns(3)P also localizes to early endosomes, where it is required for protein trafficking. More recently, it has been reported that PtdIns(3)P associates with the plasma cell membrane during responses to insulin (123) and that plasma membrane-associated PtdIns(3)P is required for both glucose transporter 4 protein translocation to the plasma membrane (123) and neurosecretory granule release (124). PtdIns(3)P is generally found on the cytoplasmic leaflet of internal membranes. However, in *Plasmodium* parasites, PtdIns(3)P has been reported inside the endoplasmic reticulum (42), a location expected if PtdIns(3)P were to be secreted to the outer leaflet of the plasma membrane.

A major current question is to understand the biological consequences of PIP recognition by RxLR effector proteins. External PtdIns(3)P has been proposed to mediate RxLR effector protein entry into plant cells, based on the observation that exogenous PtdIns(3)P-binding proteins abolish effector entry into plant and human cells (11, 118). In addition, PIP binding by the Avr1b and Avr3a basic-rich region has been proposed as necessary to enhance

their intracellular virulence activity (14). However, the role of the basic-rich region of effector proteins in cell entry was not previously tested (5, 8, 11, 14, 118). Oomycete RxLR effectors are characterized by their low sequence identity, particularly in the effector domain, a region that is key to the activity of this class of proteins (125), though recognizable levels of similarity can be observed within certain sub-families, such as the 1b3a sub-family. The crystal structures of the C-terminal effector domains of *P. capsici* Avr3a11 and *P. infestans* PexRD2, and the NMR structure of *P. capsici* Avr3a4 share a common α-helical fold despite displaying a very low degree of sequence identity (14, 116, 126). This helical bundle is also anticipated to be present in Avh5 based on the NMR data and homology modeling analyses (Figure 24-27). The helical domain of 1b3a sub-family proteins contains conserved sequence motifs named K-, W-, and Y-motifs (127). As a member of this sub-family, Avh5 bears all these motifs, with the K-motif spanning the 1 to the 2 elements, the W-motif (that includes conserved leucine residues) comprising 2 and 3, and the Y-motif found at the C-terminal 4 element (Figure 22). The conserved residue Trp96 in Avr3a11 (equivalent to Trp70 in Avh5) is buried in the tertiary structure of the protein and exhibits interactions with the conserved Tyr125 residue (equivalent to Tyr103 in Avh5), which in turn, forms a hydrogen bond with the carbonyl oxygen of Leu103 (equivalent to Val107 in Avh5), making a stable structural core (116). Since mutations in the W- and Y-motifs lead to protein destabilization (127, 128), Banfield and colleagues defined this core folded region as the WY-domain (116). According to their bioinformatic analysis, the WY-domain is predicted to be present in 44% of *Phytophthora* RxLR-containing effectors, but not in non-RxLR effector proteins (116). A model was proposed, in which the helical fold of these proteins is conserved despite a series of insertions and deletions in helical connecting loops, extensions in their N- and C-termini, substitutions in key surface residues, domain duplications, and oligomerization (such as PexRD2), all of which are changes associated with rapid adaptive diversification of these proteins (116, 126). Since fungal RxLR-like effectors have presumably evolved independently of oomycete RxLR effectors, it would not be surprising if they had

completely different structures. Indeed, the structure of two proteins from *M. lini* that have RxLR-like motifs, AvrL567-A and AvrL567-D, show a β-sandwich fold (129) and a patch of basic residues can be identified upstream of the 6 strand element to the three-residue 3_{10} helix in these proteins, which may represent a PIP-binding site.

Several groups have demonstrated that RxLR effector proteins bind PIPs (11, 14, 118). Using site-directed mutagenesis and semi-quantitative binding assays, two different outcomes have been reported, in which either the RxLR domain or the K motif, but not both, are responsible for PIP binding (11, 14). Here, we were able to precisely define the lipid-binding site by a combination of biophysical assays. We observe that both the Avh5 RFLR motif and the lysine-rich region (within the K motif) are perturbed by the lipid head group (Figure 26). A surface basic-rich interacting region has been described in both the early endosome antigen 1 (EEA1) FYVE and the Vam7p PX domains, which interact with endosomal membranes by association with PtdIns(3)P and in coordination with their hydrophobic membrane interaction loops (MILs) and electrostatic interactions with phosphatidylserine (130). The MIL region is represented by EEA1 FYVE domain residues Val1366, Thr1367, and Val1368 (131) and by the Vam7p PX domain residues Val70, Leu71, and Trp75 (132), respectively. Intriguingly, Avh5 (and other 1b3a family proteins) may harbor a MIL, with two hydrophobic regions located before and after helix 1 and surrounded by the PtdIns(3)P-interacting basic residues (Figure 22). Two different possible roles have been proposed for PIP binding by effector proteins: that cell surface PIPs may mediate protein effector binding and entry into plant cells (11) and that intracellular PIPs may enhance the contribution of the effector to virulence (14). Mutation of Avr3a in Lys85, a critical residue for PIP binding, reduces the stability of the protein and its intracellular accumulation *in planta* (14). A stabilizing effect of PIP binding has been reported for other membrane-bound proteins, including the Disabled-2 N-PTB module (96) and the prokaryotic potassium channel KcsA protein (133). Our CD temperature-dependence analysis of

Avh5 shows similarly shaped temperature-dependent traces in the absence and presence of liposomes, but a shift towards increased stability is observed in the presence of PtdIns(3)P by a magnitude of 4°C (Figure 33). Together, these data suggest that PtdIns(3)P increases the stability of the protein *in vitro*, but whether this increased protein stability occurs extra- or intracellularly, or both, remains to be elucidated.

Our SPR data indicate that the basic-rich region of Avh5, rather than the RFLR motif, contributes predominantly to PtdIns(3)P recognition in liposomes (Figure 34). Recognition of the lipid by Avh5 appears to be reversible and fits best with the two-state reaction model, in which the protein binds PtdIns(3)P followed by a conformational change. Analysis of the near-UV CD data suggests that minor changes in the tertiary structure of the protein are observed around aromatic side chain residues (Figure 23B) and when the lysine-rich region of the protein is mutated to alanine (Figure 23B). The latter can be explained by the fact that the RFLR motif is present and may contribute to PtdIns(3)P binding as observed in the NMR, liposome-binding and SPR assays (Figure 24-27, Figure 30 and 34B). Nonetheless, changes in conformation of the protein upon lipid binding are suggested from HSQC titrations and liposome binding analyses, in which mutations in severely perturbed resonances from residues such as Leu57 and Thr58 do not alter PtdIns(3)P recognition (Figure 24-27 and 30). SPR analysis of the association of Avh5 with PtdIns(3)P-containing liposomes allowed us to estimate the K_D of Avh5 for PtdIns(3)P to be 2.3 µM. This value is within the range of other PtdIns(3)P-binding protein domains such as the EEA1 FYVE and the Vam7p PX domains (131, 132), but is 3-10-fold higher to that estimated for Avr1b and AvrL567 using effector binding to cells and liposome binding assays (11); this higher affinity value may be explained by the presence of additional tags in the proteins tested in these assays that may contribute to the binding (134). Nonetheless, a modest affinity of a protein to phosphoinositides, such as Avh5, may be required for its further release from intracellular membranes to target other subcellular compartments (135).

The RxLR and dEER motifs were initially proposed to have a major role in the entry of a protein effector to a cell due to their conservation among this class of proteins (136). More importantly, the RxLR motif has been demonstrated to be required for cell entry without the presence of the pathogen by both oomycete and fungal effectors (11, 118, 137-139), emphasizing its major role in this mechanism. Indeed, we observe that loss of an intact RFLR motif in Avh5 impairs internalization of the protein in human epithelial and soybean root cell entry assays (Figure 36A, B, and 37). Interestingly, the C-terminal basic region of Avh5 that lacks the RFLR motif and the N-terminal region of the protein that lacks the basic-rich region both showed measurable, albeit reduced, internalization, confirming the idea that both regions contribute to cell entry via binding to PtdIns(3)P. This hypothesis is strengthened by the observed inhibition of cell uptake of Avh5 mutants with a functional PtdIns(3)P-interacting region (either RFLR or Lys62/Lys64/Lys65) by either Ins(1,3)P_2 or by the Hrs 2xFYVE or PEPP PH domains (Figure 39) and consistent with the reported PtdIns(3)P-dependent cell entry of Avh5 (11).

The precise mechanism by which each domain interacts with PtdIns(3)P to facilitate cell entry is not yet clear. It is noteworthy that the N-terminal RxLR domain of Avh5 exhibits stronger cell entry activity than the C-terminal domain relative to its PtdIns(3)P-binding affinity, especially in the soybean root cell assays (Figure 37). Nonetheless, entry by the N-terminal domain can be blocked by PtdIns(3)P binding proteins or by Ins(1,3)P_2. The SPR results suggest a two-state binding process, in which Avh5 binds to membrane-embedded PtdIns(3)P, followed by a conformational change of the protein. The association of Avh5 with PtdIns(3)P could follow a model in which the two domains would bind two different molecules of PtdIns(3)P with different affinities. Another possible model is that the C-terminal domain is responsible for initial binding to PtdIns(3)P, followed by a shift in which the RxLR domain contacts PtdIns(3)P in order to initiate the cell entry process. Alternatively, it is possible that the RFLR region of Avh5 might

interact with additional surface molecules such as a protein receptor or other acidic lipids, which strengthen the association of the protein to the cell surface for delivery. Indeed, it has been brought to attention that it is difficult to associate with membrane just due to phosphoinositide recognition for PIP-binding proteins. Some other factors may involve (35, 37, 40, 140), e.g., protein oligomerization (141). Currently, we are investigating these possibilities and work is in progress.

The strong relationship between PtdIns(3)P binding and cell entry by both the N-terminal and C-terminal domains of Avh5 supports the hypothesis that PtdIns(3)P binding is an important step in cell entry by RxLR effectors. The K motif, which contains the C-terminal PtdIns(3)P binding site in the 1b3a family, is not found in most other RxLR effectors, including Avh331 which was validated to bind PtdIns(3)P, and to enter plant and animal cells via a PtdIns(3)P-dependent mechanism (11). Furthermore, the isolated RxLR domain of the *P. infestans* effector Nuk10 bound PtdIns(3)P with high affinity (42).

This suggests that in some RxLR effectors the RxLR domain may be solely responsible for PtdIns(3)P binding and for cell entry, or whether those other effectors contain different kinds of C-terminal binding sites. The fact that the K motif is present in only a minority of RxLR effectors suggests that it is a relatively recent evolutionary innovation, perhaps to increase the affinity of the 1b3a family for PtdIns(3)P and the efficiency of entry.

In summary, the functional and structural properties of Avh5 reported in this study, including the identification of the PtdIns(3)P-binding site, provides an improved and updated model of how RxLR effector proteins recognize phosphoinositides and of the contributions of the RxLR motif and basic residue-rich C-terminal regions to the internalization process.

Chapter 4 SUMMARY AND PERSPECTIVES

My work has proposed an updated PtdIns(3)P-binding model of Avh5, which is a good representative of effector proteins secreted by oomycete species. This model has suggested that the C-terminal positively charged region play a much more important role than the conserved N-terminal RxLR (RFLR) domain does concerned with PtdIns(3)P recognition, which modifies the previously proposed mechanism by Tyler and colleagues. Interestingly, from the cell entry assays provided by our collaborators, we may draw a conclusion that the N-terminal RxLR domain also plays a critical role in effector cell entry into host plant and human cells, respectively, indicative of the indispensable role of the N-terminal portion in promoting the pathogen virulence. Therefore, an interesting question comes out: how does the C-terminal basic residue-rich portion of Avh5 collaborate with the N-terminal RxLR domain to enter the host cells? That may be a general question to be answered in the future for all of the oomycete (as well as fungal, probably) pathogens. A potential possibility is that there may be other effector protein-receptor(s) or other molecular ligand(s) on the host plant cell plasma membrane, which has binding preference to the RxLR domain over the C-terminal portion, and such recognition will cooperate with PtdIns(3)P-recognition, which is mainly contributed by the C-terminal positively charged portion, to facilitate the effector protein entry into host cells.

To explore the oomycete pathogen entry mechanism in detail has great significance. Due to their economic importance and the ineffectiveness of conventional medicinal treatment, it is urgent to find novel therapeutic solutions to controlling oomycete infection. Ins(1,3)P_2 blocking assay just provides a potentially wanted solution to tackle this problem. However, whether or not such method can be applied widely in agriculture has not been drawn a conclusion. In addition, due to the huge cost of large amount of Ins(1,3)P_2 to be used, searching for its substitute by producing analogs with lower cost may be in need in the near future.

REFERENCES

1. Tyler BM. Phytophthora sojae: root rot pathogen of soybean and model oomycete. Molecular Plant Pathology 2007;8(1):1-8.

2. Sogin ML, Silberman JD. Evolution of the protists and protistan parasites from the perspective of molecular systematics. International Journal for Parasitology 1998;28(1):11-20.

3. Förster H, Coffey MD, Elwood H, Sogin ML. Sequence Analysis of the Small Subunit Ribosomal RNAs of Three Zoosporic Fungi and Implications for Fungal Evolution. Mycologia 1990;82(3):306-312.

4. SHAW D. Phytophthora Diseases Worldwide by D. C. Erwin & O. K. Ribeiro, xii+562 pp. St Paul, Minnesota: The American Phytopathological Society (1996). The Journal of Agricultural Science 1998;131(02):245-249.

5. Dou D, Kale SD, Wang X, Jiang RHY, Bruce NA, Arredondo FD, Zhang X, Tyler BM. RXLR-Mediated Entry of Phytophthora sojae Effector Avr1b into Soybean Cells Does Not Require Pathogen-Encoded Machinery. The Plant Cell Online 2008;20(7):1930-1947.

6. Chen Y, Liu Z, Halterman DA. Molecular Determinants of Resistance Activation and Suppression by *Phytophthora infestans* Effector IPI-O. PLoS Pathogens 2012;8(3):e1002595.

7. Grünwald NJ, Garbelotto M, Goss EM, Heungens K, Prospero S. Emergence of the sudden oak death pathogen Phytophthora ramorum. Trends in Microbiology 2012;20(3):131-138.

8. Whisson SC, Boevink PC, Moleleki L, Avrova AO, Morales JG, Gilroy EM, Armstrong MR, Grouffaud S, van West P, Chapman S, Hein I, Toth IK, Pritchard L, Birch PRJ. A translocation signal for delivery of oomycete effector proteins into host plant cells. Nature 2007;450(7166):115-118.

9. Allen RL, Bittner-Eddy PD, Grenvitte-Briggs LJ, Meitz JC, Rehmany AP, Rose LE, Beynon JL. Host-parasite coevolutionary conflict between Arabidopsis and downy mildew. Science 2004;306(5703):1957-1960.

10. Alfano JR, Collmer A. Type III Secretion System Effector Proteins: Double Agents in Bacterial Disease and Plant Defense. Annual Review of Phytopathology 2004;42(1):385-414.

11. Kale SD, Gu B, Capelluto DGS, Dou D, Feldman E, Rumore A, Arredondo FD, Hanlon R, Fudal I, Rouxel T, Lawrence CB, Shan W, Tyler BM. External Lipid PI3P Mediates Entry of Eukaryotic Pathogen Effectors into Plant and Animal Host Cells. Cell 2010;142(2):284-295.

12. Tyler BM. Entering and breaking: virulence effector proteins of oomycete plant pathogens. Cellular Microbiology 2009;11(1):13-20.

13. Armstrong MR, Whisson SC, Pritchard L, Bos JIB, Venter E, Avrova AO, Rehmany AP, Bohme U, Brooks K, Cherevach I, Hamlin N, White B, Fraser A, Lord A, Quail MA, Churcher C, Hall N, Berriman M, Huang S, Kamoun S, Beynon JL and Birch PRJ. An ancestral oomycete locus contains late blight avirulence gene Avr3a, encoding a protein that is recognized in the host cytoplasm. Proceedings of the National Academy of Sciences of the United States of America 2005;102(21):7766-7771.

14. Yaeno T, Li H, Chaparro-Garcia A, Schornack S, Koshiba S, Watanabe S, Kigawa T, Kamoun S, Shirasu K. Phosphatidylinositol monophosphate-binding interface in the oomycete RXLR effector AVR3a is required for its stability in host cells to modulate plant immunity. Proceedings of the National Academy of Sciences 2011;108(35):14682-14687.

15. Ellis JG, Dodds PN. Showdown at the RXLR motif: Serious differences of opinion in how effector proteins from filamentous eukaryotic pathogens enter plant cells. Proceedings of the National Academy of Sciences 2011;108(35):14381-14382.

16. Jones JDG, Dangl JL. The plant immune system. Nature 2006;444(7117):323-329.

17. Spoel SH, Dong X. How do plants achieve immunity? Defence without specialized immune cells. Nature Reviews Immunology 2012;12(2):89-100.

18. Flor HH. Current Status of the Gene-For-Gene Concept. Annual Review of Phytopathology 1971;9(1):275-296.

19. Dangl JL, Jones JDG. Plant pathogens and integrated defence responses to infection. Nature 2001;411(6839):826-833.

20. Van Der Biezen EA, Jones JDG. Plant disease-resistance proteins and the gene-for-gene concept. Trends in Biochemical Sciences 1998;23(12):454-456.

21. Mackey D, Holt Iii BF, Wiig A, Dangl JL. RIN4 Interacts with Pseudomonas syringae Type III Effector Molecules and Is Required for RPM1-Mediated Resistance in Arabidopsis. Cell 2002;108(6):743-754.

22. Kim DH, Eu Y-J, Yoo CM, Kim Y-W, Pih KT, Jin JB, Kim SJ, Stenmark H, Hwang I. Trafficking of Phosphatidylinositol 3-Phosphate from the trans-Golgi Network to the Lumen of the Central Vacuole in Plant Cells. The Plant Cell Online 2001;13(2):287-301.

23. Yu J, Hu S, Wang J, Wong GK-S, Li S, Liu B, Deng Y, Dai L, Zhou Y, Zhang X, Cao M, Liu J, Sun J, Tang J, Chen Y, Huang X, Lin W, Ye C, Tong W, Cong L, Geng J, Han Y, Li L, Li W, Hu G, Huang X, Li W, Li J, Liu Z, Li L, Liu J, Qi Q, Liu J, Li L, Li T, Wang X, Lu H, Wu T, Zhu M, Ni P, Han H, Dong W, Ren X, Feng X, Cui P, Li X, Wang H, Xu X, Zhai W, Xu Z, Zhang J, He S, Zhang J, Xu J, Zhang K, Zheng X, Dong J, Zeng W, Tao L, Ye J, Tan J, Ren X, Chen X, He J, Liu D, Tian W, Tian C, Xia H, Bao Q, Li G, Gao H, Cao T, Wang J, Zhao W, Li P, Chen W, Wang X, Zhang Y, Hu J, Wang J, Liu S, Yang J, Zhang G, Xiong Y, Li Z, Mao L, Zhou C, Zhu Z, Chen R, Hao B, Zheng W, Chen S, Guo W, Li G, Liu S, Tao M, Wang J, Zhu L, Yuan L and Yang H. A Draft Sequence of the Rice Genome (Oryza sativa L. ssp. indica). Science 2002;296(5565):79-92.

24. Meyers BC, Kozik A, Griego A, Kuang H, Michelmore RW. Genome-Wide Analysis of NBS-LRR–Encoding Genes in Arabidopsis. The Plant Cell Online 2003;15(4):809-834.

25. Chen S-J, Chao Y-L, Chen C-Y, Chang C-M, Wu EC-H, Wu C-S, Yeh H-H, Chen C-H, Tsai H-J. Prevalence of autoimmune diseases in in-patients with schizophrenia: nationwide population-based study. The British Journal of Psychiatry 2012.

26. Tu H, Li Q, Xiang S, Jiang H, Mao Y, Shou Z, Chen J. Dual effects of statins therapy in systemic lupus erythematosus and SLE-related atherosclerosis: The potential role for regulatory T cells. Atherosclerosis (0).

27. Bomblies K, Lempe J, Epple P, Warthmann N, Lanz C, Dangl JL, Weigel D. Autoimmune Response as a Mechanism for a Dobzhansky-Muller-Type Incompatibility Syndrome in Plants. PLoS Biology 2007;5(9):e236.

28. Stokes TL, Kunkel BN, Richards EJ. Epigenetic variation in Arabidopsis disease resistance. Genes & Development 2002;16(2):171-182.

29. Li Y, Li S, Bi D, Cheng YT, Li X, Zhang Y. SRFR1 Negatively Regulates Plant NB-LRR Resistance Protein Accumulation to Prevent Autoimmunity. PLoS Pathogens 2010;6(9):e1001111.

30. Netea Mihai G, Quintin J, van der Meer Jos WM. Trained Immunity: A Memory for Innate Host Defense. Cell Host & Microbe 2011;9(5):355-361.

31. Beckers GJM, Jaskiewicz M, Liu Y, Underwood WR, He SY, Zhang S, Conrath U. Mitogen-Activated Protein Kinases 3 and 6 Are Required for Full Priming of Stress Responses in Arabidopsis thaliana. The Plant Cell Online 2009;21(3):944-953.

32. Jaskiewicz M, Conrath U, Peterhansel C. Chromatin modification acts as a memory for systemic acquired resistance in the plant stress response. EMBO Reports 2011;12(1):50-55.

33. Molinier J, Ries G, Zipfel C, Hohn B. Transgeneration memory of stress in plants. Nature 2006;442(7106):1046-1049.

34. Misra S, Miller GJ, Hurley JH. Recognizing Phosphatidylinositol 3-Phosphate. Cell 2001;107(5):559-562.

35. Lemmon MA. Membrane recognition by phospholipid-binding domains. Nature Reviews Molecular Cell Biology 2008;9(2):99-111.

36. Rusten TE, Stenmark H. Analyzing phosphoinositides and their interacting proteins. Nature Methods 2006;3(4):251-258.

37. Cullen PJ. Phosphoinositides and the regulation of tubular-based endosomal sorting. Biochemical Society Transactions 2011;39:839-850.

38. Furt F, Simon-Plas F, Mongrand S. Lipids of the Plant Plasma Membrane

The Plant Plasma Membrane. 2011;19:3-30.

39. Lemmon MA. Phosphoinositide Recognition Domains. Traffic 2003;4(4):201-213.

40. Di Paolo G, De Camilli P. Phosphoinositides in cell regulation and membrane dynamics. Nature 2006;443(7112):651-657.

41. Gillooly DJ, Morrow IC, Lindsay M, Gould R, Bryant NJ, Gaullier J-M, Parton RG, Stenmark H. Localization of phosphatidylinositol 3-phosphate in yeast and mammalian cells. EMBO Journal 2000;19(17):4577-4588.

42. Bhattacharjee S, Stahelin Robert V, Speicher Kaye D, Speicher David W, Haldar K. Endoplasmic Reticulum PI(3)P Lipid Binding Targets Malaria Proteins to the Host Cell. Cell 2012;148(1–2):201-212.

43. Joo JH, Yoo HJ, Hwang I, Lee JS, Nam KH, Bae YS. Auxin-induced reactive oxygen species production requires the activation of phosphatidylinositol 3-kinase. FEBS Letters 2005;579(5):1243-1248.

44. Xu N, Gao X-Q, Zhao X, Zhu D, Zhou L, Zhang X. *Arabidopsis* AtVPS15 is essential for pollen development and germination through modulating phosphatidylinositol 3-phosphate formation. Plant Molecular Biology 2011;77(3):251-260.

45. Zhang Y, Li S, Zhou L-Z, Fox E, Pao J, Sun W, Zhou C, McCormick S. Overexpression of Arabidopsis thaliana PTEN caused accumulation of autophagic bodies in pollen tubes by disrupting phosphatidylinositol 3-phosphate dynamics. The Plant Journal 2011;68(6):1081-1092.

46. Boss WF, Im YJ. Phosphoinositide Signaling. Annual Review of Plant Biology 2012;63(1):null.

47. He J, Gajewiak J, Scott Jordan L, Gong D, Ali M, Best Michael D, Prestwich Glenn D, Stahelin Robert V, Kutateladze Tatiana G. Metabolically Stabilized Derivatives of Phosphatidylinositol 4-Phosphate: Synthesis and Applications. Chemistry & Biology 2011;18(10):1312-1319.

48. D'Angelo G, Vicinanza M, Di Campli A, De Matteis MA. The multiple roles of PtdIns(4)P – not just the precursor of PtdIns(4,5)P2. Journal of Cell Science 2008;121(12):1955-1963.

49. D'Angelo G, Vicinanza M, Wilson C, De Matteis MA. Phosphoinositides in Golgi Complex Function

Phosphoinositides II: The Diverse Biological Functions. 2012;59:255-270.

50. Hama H, Schnieders EA, Thorner J, Takemoto JY, DeWald DB. Direct Involvement of Phosphatidylinositol 4-Phosphate in Secretion in the Yeast Saccharomyces cerevisiae. Journal of Biological Chemistry 1999;274(48):34294-34300.

51. Bianco A, Reghellin V, Donnici L, Fenu S, Alvarez R, Baruffa C, Peri F, Pagani M, Abrignani S, Neddermann P, De Francesco R. Metabolism of Phosphatidylinositol 4-Kinase III α -Dependent PI4P Is Subverted by HCV and Is Targeted by a 4-Anilino Quinazoline with Antiviral Activity. PLoS Pathogens 2012;8(3):e1002576.

52. Peterman TK, Ohol YM, McReynolds LJ, Luna EJ. Patellin1, a Novel Sec14-Like Protein, Localizes to the Cell Plate and Binds Phosphoinositides. Plant Physiology 2004;136(2):3080-3094.

53. Gagne JM, Clark SE. The Arabidopsis Stem Cell Factor POLTERGEIST is Membrane Localized and Phospholipid Stimulated. The Plant Cell Online 2010;22(3):729-743.

54. Thole JM, Vermeer JEM, Zhang Y, Gadella TWJ, Nielsen E. ROOT HAIR DEFECTIVE4 Encodes a Phosphatidylinositol-4-Phosphate Phosphatase Required for Proper Root Hair Development in Arabidopsis thaliana. The Plant Cell Online 2008;20(2):381-395.

55. Zhao Y, Yan A, Feijó JA, Furutani M, Takenawa T, Hwang I, Fu Y, Yang Z. Phosphoinositides Regulate Clathrin-Dependent Endocytosis at the Tip of Pollen Tubes in Arabidopsis and Tobacco. The Plant Cell Online 2010;22(12):4031-4044.

56. Rameh LE, Tolias KF, Duckworth BC, Cantley LC. A new pathway for synthesis of phosphatidylinositol-4,5-bisphosphate. Nature 1997;390(6656):192-196.

57. Grainger DL, Tavelis C, Ryan AJ, Hinchliffe KA. The emerging role of PtdIns5P: another signalling phosphoinositide takes its place. Biochemical Society Transactions 2012;40:257-261.

58. Sarkes D, Rameh LE. A novel HPLC-based approach makes possible the spatial characterization of cellular PtdIns5P and other phosphoinositides. Biochemical Journal 2010;428:375-384.

59. Alvarez-Venegas R, Sadder M, Hlavacka A, Baluška F, Xia Y, Lu G, Firsov A, Sarath G, Moriyama H, Dubrovsky JG, Avramova Z. The Arabidopsis homolog of trithorax, ATX1, binds phosphatidylinositol 5-phosphate, and the two regulate a common set of target genes. Proceedings of the National Academy of Sciences 2006;103(15):6049-6054.

60. Coronas S, Lagarrigue F, Ramel D, Chicanne G, Delsol G, Payrastre B, Tronchère H. Elevated levels of PtdIns5P in NPM-ALK transformed cells: Implication of PIKfyve. Biochemical and Biophysical Research Communications 2008;372(2):351-355.

61. Jones DR, Bultsma Y, Keune W-J, Halstead JR, Elouarrat D, Mohammed S, Heck AJ, D'Santos Clive S, Divecha N. Nuclear PtdIns5P as a Transducer of Stress Signaling: An In Vivo Role for PIP4Kbeta. Molecular Cell 2006;23(5):685-695.

62. Gozani O, Karuman P, Jones DR, Ivanov D, Cha J, Lugovskoy AA, Baird CL, Zhu H, Field SJ, Lessnick SL, Villasenor J, Mehrotra B, Chen J, Rao VR, Brugge JS, Ferguson CG, Payrastre B, Myszka DG, Cantley LC, Wagner G, Divecha N, Prestwich GD and Yuan J. The PHD Finger of the Chromatin-Associated Protein ING2 Functions as a Nuclear Phosphoinositide Receptor. Cell 2003;114(1):99-111.

63. Swan L. An Unnatural PIP Simulates Growth Factor Signaling. Chemistry & Biology 2009;16(11):1127-1128.

64. Stephens LR, Jackson TR, Hawkins PT. Agonist-stimulated synthesis of phosphatidylinositol(3,4,5)-trisphosphate: A new intracellular signalling system? Biochimica et Biophysica Acta (BBA) - Molecular Cell Research 1993;1179(1):27-75.

65. Banfić H, Tang X-w, Batty IH, Downes CP, Chen C-s, Rittenhouse SE. A Novel Integrin-activated Pathway Forms PKB/Akt- stimulatory Phosphatidylinositol 3,4-Bisphosphate via Phosphatidylinositol 3-Phosphate in Platelets. Journal of Biological Chemistry 1998;273(1):13-16.

66. Van der Kaay J, Beck M, Gray A, Downes CP. Distinct Phosphatidylinositol 3-Kinase Lipid Products Accumulate upon Oxidative and Osmotic Stress and Lead to Different Cellular Responses. Journal of Biological Chemistry 1999;274(50):35963-35968.

67. Sasaki J, Kofuji S, Itoh R, Momiyama T, Takayama K, Murakami H, Chida S, Tsuya Y, Takasuga S, Eguchi S, Asanuma K, Horie Y, Miura K, Davies EM, Mitchell C, Yamazaki M, Hirai H, Takenama T, Suzuki A and Sasaki T. The PtdIns(3,4)P2 phosphatase INPP4A is a suppressor of excitotoxic neuronal death. Nature 2010;465(7297):497-501.

68. Brearley CA, Hanke DE. 3-Phosphorylated and 4-Phosphorylated Phosphatidylinositols in the aquatic plant Spirodela-polyrhiza L. Biochemical Journal 1992;283:255-260.

69. Brearley CA, Hanke DE. Pathway of Synthesis of 3,4-Phosphorylated and 4,5-Phosphorylated Phosphatidylinositols in the duckweed Spirodela-polyrhiza L. Biochemical Journal 1993;290:145-150.

70. Ho CY, Alghamdi TA, Botelho RJ. Phosphatidylinositol-3,5-Bisphosphate: No Longer the Poor PIP2. Traffic 2012;13(1):1-8.

71. Whiteford CC, Brearley CA, Ulug ET. Phosphatidylinositol 3,5-bisphosphate defines a novel PI 3-kinase pathway in resting mouse fibroblasts. Biochemical Journal 1997;323:597-601.

72. Dove SK, Cooke FT, Douglas MR, Sayers LG, Parker PJ, Michell RH. Osmotic stress activates phosphatidylinositol-3,5-bisphosphate synthesis. Nature 1997;390(6656):187-192.

73. Berwick DC, Dell GC, Welsh GI, Heesom KJ, Hers I, Fletcher LM, Cooke FT, Tavaré JM. Protein kinase B phosphorylation of PIKfyve regulates the trafficking of GLUT4 vesicles. Journal of Cell Science 2004;117(25):5985-5993.

74. Yan Q, Guo J, Zhang X, Bai Y, Wang L, Li J. Trauma does not accelerate neuronal degeneration in Fig4 insufficient mice. Journal of the Neurological Sciences 2012;312(1–2):102-107.

75. Hirano T, Sato MH. Arabidopsis FAB1A/B is possibly involved in the recycling of auxin transporters. Plant Signaling & Behavior 2011;6(4):583-585.

76. Bolino A, Muglia M, Conforti FL, LeGuern E, Salih MAM, Georgiou D-M, Christodoulou K, Hausmanowa-Petrusewicz I, Mandich P, Schenone A, Gambardella A, Bono F, Quattrone A, Devoto M, Monaco AP. Charcot-Marie-Tooth type 4B is caused by mutations in the gene encoding myotubularin-related protein-2. Nature Genetics 2000;25(1):17-19.

77. Ueno T, Falkenburger BH, Pohlmeyer C, Inoue T. Triggering Actin Comets Versus Membrane Ruffles: Distinctive Effects of Phosphoinositides on Actin Reorganization. Science Signaling 2011;4(203):ra87-.

78. McLaughlin S, Wang J, Gambhir A, Murray D. PIP2 and Proteins: Interactions, Organization, and Information Flow. Annual Review of Biophysics and Biomolecular Structure 2002;31(1):151-175.

79. Helling D, Possart A, Cottier S, Klahre U, Kost B. Pollen Tube Tip Growth Depends on Plasma Membrane Polarization Mediated by Tobacco PLC3 Activity and Endocytic Membrane Recycling. The Plant Cell Online 2006;18(12):3519-3534.

80. Zheng S-Z, Liu Y-L, Li B, Shang Z-l, Zhou R-G, Sun D-Y. Phosphoinositide-specific phospholipase C9 is involved in the thermotolerance of Arabidopsis. The Plant Journal 2012;69(4):689-700.

81. Saarikangas J, Zhao H, Lappalainen P. Regulation of the Actin Cytoskeleton-Plasma Membrane Interplay by Phosphoinositides. Physiological Reviews 2010;90(1):259-289.

82. Sun Y, Kaksonen M, Madden DT, Schekman R, Drubin DG. Interaction of Sla2p's ANTH Domain with PtdIns(4,5)P2 Is Important for Actin-dependent Endocytic Internalization. Molecular Biology of the Cell 2005;16(2):717-730.

83. Cantley LC. The Phosphoinositide 3-Kinase Pathway. Science 2002;296(5573):1655-1657.

84. Markadieu N, Blero D, Boom A, Erneux C, Beauwens R. Phosphatidylinositol 3,4,5-trisphosphate: an early mediator of insulin-stimulated sodium transport in A6 cells. American Journal of Physiology - Renal Physiology 2004;287(2):F319-F328.

85. Ma K, Cheung SM, Marshall AJ, Duronio V. PI(3,4,5)P3 and PI(3,4)P2 levels correlate with PKB/akt phosphorylation at Thr308 and Ser473, respectively; PI(3,4)P2 levels determine PKB activity. Cellular Signalling 2008;20(4):684-694.

86. Laketa V, Zarbakhsh S, Morbier E, Subramanian D, Dinkel C, Brumbaugh J, Zimmermann P, Pepperkok R, Schultz C. Membrane-Permeant Phosphoinositide Derivatives as Modulators of Growth Factor Signaling and Neurite Outgrowth. Chemistry & Biology 2009;16(11):1190-1196.

87. Rowland MM, Bostic HE, Gong D, Speers AE, Lucas N, Cho W, Cravatt BF, Best MD. Phosphatidylinositol 3,4,5-Trisphosphate Activity Probes for the Labeling and Proteomic Characterization of Protein Binding Partners. Biochemistry 2011;50(51):11143-11161.

88. Wang Q, Han C, Ferreira AO, Yu X, Ye W, Tripathy S, Kale SD, Gu B, Sheng Y, Sui Y, Wang X, Zhang Z, Cheng B, Dong S, Shan W, Zheng X, Dou D, Tyler BM and Wang Y. Transcriptional Programming and Functional Interactions within the Phytophthora sojae RXLR Effector Repertoire. The Plant Cell Online 2011.

89. Wüthrich K. Protein structure determination in solution by NMR spectroscopy. Journal of Biological Chemistry 1990;265(36):22059-22062.

90. Zech SG, Olejniczak E, Hajduk P, Mack J, McDermott AE. Characterization of Protein−Ligand Interactions by High-Resolution Solid-State NMR Spectroscopy. Journal of the American Chemical Society 2004;126(43):13948-13953.

91. Frahm J, Bruhn H, Gyngell ML, Merboldt KD, Hänicke W, Sauter R. Localized proton NMR spectroscopy in different regions of the human brain in vivo. Relaxation times and concentrations of cerebral metabolites. Magnetic Resonance in Medicine 1989;11(1):47-63.

92. Bothe JR, Nikolova EN, Eichhorn CD, Chugh J, Hansen AL, Al-Hashimi HM. Characterizing RNA dynamics at atomic resolution using solution-state NMR spectroscopy. Nature Methods 2011;8(11):919-931.

93. Wormald MR, Petrescu AJ, Pao Y-L, Glithero A, Elliott T, Dwek RA. Conformational Studies of Oligosaccharides and Glycopeptides: Complementarity of NMR, X-ray Crystallography, and Molecular Modelling. Chemical Reviews 2002;102(2):371-386.

94. Cavanagh J, Fairbrother WJ, Palmer Iii AG, Rance M, Skelton NJ. Chapter 2 - Theoretical description of NMR spectroscopy. Protein NMR Spectroscopy (Second Edition). Burlington: Academic Press; 2007. p. 29-113.

95. Cavanagh J, Fairbrother WJ, Palmer Iii AG, Rance M, Skelton NJ. Chapter 7 - Heteronuclear NMR experiments. Protein NMR Spectroscopy (Second Edition). Burlington: Academic Press; 2007. p. 533-678.

96. Alajlouni R, Drahos KE, Finkielstein CV, Capelluto DGS. Lipid-mediated membrane binding properties of Disabled-2. Biochimica et Biophysica Acta (BBA) - Biomembranes 2011;1808(11):2734-2744.

97. Montelione GT, Zheng D, Huang YJ, Gunsalus KC, Szyperski T. Protein NMR spectroscopy in structural genomics. Nature Structural & Molecular Biology.

98. Fukui L, Chen Y. NvMap: automated analysis of NMR chemical shift perturbation data. Bioinformatics 2007;23(3):378-380.

99. Dowler S, Kular G, Alessi DR. Protein Lipid Overlay Assay. Science Signaling: Signal Transduction Knowledge Environment 2002;2002(129):pl6-.

100. Saunders L, Perrin J, Gammack D. Ultrasonic Irradiation of some Phospholipid Sols. Journal of Pharmacy and Pharmacology 1962;14(1):567-572.

101. Huang C-H. Phosphatidylcholine vesicles. Formation and physical characteristics. Biochemistry 1969;8(1):344-352.

102. Hauser H, Gains N. Spontaneous vesiculation of phospholipids: a simple and quick method of forming unilamellar vesicles. Proceedings of the National Academy of Sciences 1982;79(6):1683-1687.

103. Arima Y, Toda M, Iwata H. Surface plasmon resonance in monitoring of complement activation on biomaterials. Advanced Drug Delivery Reviews 2011;63(12):988-999.

104. Cooper MA. Optical biosensors in drug discovery. Nature Reviews Drug Discovery 2002;1(7):515-528.

105. Kelly SM, Jess TJ, Price NC. How to study proteins by circular dichroism. Biochimica et Biophysica Acta (BBA) - Proteins & Proteomics 2005;1751(2):119-139.

106. Greenfield NJ. Using circular dichroism spectra to estimate protein secondary structure. Nature Protocols 2007;1(6):2876-2890.

107. Capelluto DGS, Kutateladze TG, Habas R, Finkielstein CV, He X, Overduin M. The DIX domain targets dishevelled to actin stress fibres and vesicular membranes. Nature 2002;419(6908):726-729.

108. Löhr F, Rüterjans H. Correlation of Backbone Amide and Side-Chain 13C Resonances in Perdeuterated Proteins. Journal of Magnetic Resonance 2002;156(1):10-18.

109. Muhandiram DR, Kay LE. Gradient-Enhanced Triple-Resonance Three-Dimensional NMR Experiments with Improved Sensitivity. Journal of Magnetic Resonance, Series B 1994;103(3):203-216.

110. Delaglio F, Grzesiek S, Vuister GW, Zhu G, Pfeifer J, Bax A. NMRPipe: A multidimensional spectral processing system based on UNIX pipes. Journal of Biomolecular NMR 1995;6(3):277-293.

111. Vranken WF, Boucher W, Stevens TJ, Fogh RH, Pajon A, Llinas M, Ulrich EL, Markley JL, Ionides J, Laue ED. The CCPN data model for NMR spectroscopy: Development of a software pipeline. Proteins: Structure, Function, and Bioinformatics 2005;59(4):687-696.

112. Cheung M-S, Maguire ML, Stevens TJ, Broadhurst RW. DANGLE: A Bayesian inferential method for predicting protein backbone dihedral angles and secondary structure. Journal of Magnetic Resonance 2010;202(2):223-233.

113. Garrett DS, Powers R, Gronenborn AM, Clore GM. A common sense approach to peak picking in two-, three-, and four-dimensional spectra using automatic computer analysis of contour diagrams. Journal of Magnetic Resonance 2011;213(2):357-363.

114. Gautier A, Mott HR, Bostock MJ, Kirkpatrick JP, Nietlispach D. Structure determination of the seven-helix transmembrane receptor sensory rhodopsin II by solution NMR spectroscopy. Nature Structural & Molecular Biololgy 2010;17(6):768-774.

115. Sreerama N, Woody RW. Computation and Analysis of Protein Circular Dichroism Spectra. In: Ludwig B, Michael LJ, editors. Methods in Enzymology: Academic Press; 2004. p. 318-351.

116. Boutemy LS, King SRF, Win J, Hughes RK, Clarke TA, Blumenschein TMA, Kamoun S, Banfield MJ. Structures of Phytophthora RXLR Effector Proteins. Journal of Biological Chemistry 2011;286(41):35834-35842.

117. Birch PRJ, Boevink PC, Gilroy EM, Hein I, Pritchard L, Whisson SC. Oomycete RXLR effectors: delivery, functional redundancy and durable disease resistance. Current Opinion in Plant Biology 2008;11(4):373-379.

118. Plett Jonathan M, Kemppainen M, Kale Shiv D, Kohler A, Legué V, Brun A, Tyler Brett M, Pardo Alejandro G, Martin F. A Secreted Effector Protein of Laccaria bicolor Is Required for Symbiosis Development. Current Biology 2011;21(14):1197-1203.

119. Vermeer JEM, Van Leeuwen W, Tobeña-Santamaria R, Laxalt AM, Jones DR, Divecha N, Gadella TWJ, Munnik T. Visualization of PtdIns3P dynamics in living plant cells. The Plant Journal 2006;47(5):687-700.

120. Matsuoka K, Bassham DC, Raikhel NV, Nakamura K. Different sensitivity to wortmannin of two vacuolar sorting signals indicates the presence of distinct sorting machineries in tobacco cells. The Journal of Cell Biology 1995;130(6):1307-1318.

121. Voigt B, Timmers ACJ, Samaj J, Hlavacka A, Ueda T, Preuss M, Nielsen E, Mathur J, Emans N, Stenmark H, Nakano A, Baluska F, Menzel D. Actin-based motility of endosomes is linked to the polar tip growth of root hairs. European Journal of Cell Biology 2005;84(6):609-621.

122. Gonorazky G, Laxalt AM, Testerink C, Munnik T, De La Canal L. Phosphatidylinositol 4-phosphate accumulates extracellularly upon xylanase treatment in tomato cell suspensions. Plant, Cell & Environment 2008;31(8):1051-1062.

123. Falasca M, Hughes WE, Dominguez V, Sala G, Fostira F, Fang MQ, Cazzolli R, Shepherd PR, James DE, Maffucci T. The Role of Phosphoinositide 3-Kinase C2α in Insulin Signaling. Journal of Biological Chemistry 2007;282(38):28226-28236.

124. Wen PJ, Osborne SL, Morrow IC, Parton RG, Domin J, Meunier FA. Ca2+-regulated Pool of Phosphatidylinositol-3-phosphate Produced by Phosphatidylinositol 3-Kinase C2α on Neurosecretory Vesicles. Molecular Biology of the Cell 2008;19(12):5593-5603.

125. Schornack S, Huitema E, Cano LM, Bozkurt TO, Oliva R, Van Damme M, Schwizer S, Raffaele S, Chaparro-Garcia A, Farrer R, Segretin ME, Bos J, Haas BJ, Zody MC, Nusbaum C, Win J, Thines M and Kamoun S. Ten things to know about oomycete effectors. Molecular Plant Pathology 2009;10(6):795-803.

126. Win J, Krasileva KV, Kamoun S, Shirasu K, Staskawicz BJ, Banfield MJ. Sequence Divergent RXLR Effectors Share a Structural Fold Conserved across Plant Pathogenic Oomycete Species. PLoS Pathogens 2012;8(1):e1002400.

127. Dou D, Kale SD, Wang X, Chen Y, Wang Q, Wang X, Jiang RHY, Arredondo FD, Anderson RG, Thakur PB, McDowell JM, Wang Y, Tyler BM. Conserved C-Terminal Motifs Required for Avirulence and Suppression of Cell Death by Phytophthora sojae effector Avr1b. The Plant Cell Online 2008;20(4):1118-1133.

128. Bos JIB, Chaparro-Garcia A, Quesada-Ocampo LM, Gardener BBM, Kamoun S. Distinct Amino Acids of the Phytophthora infestans Effector AVR3a Condition Activation of R3a Hypersensitivity and Suppression of Cell Death. Molecular Plant-Microbe Interactions 2009;22(3):269-281.

129. Wang C-IA, Guncar G, Forwood JK, Teh T, Catanzariti A-M, Lawrence GJ, Loughlin FE, Mackay JP, Schirra HJ, Anderson PA, Ellis JG, Dodds PN, Kobe B. Crystal Structures of Flax Rust Avirulence Proteins AvrL567-A and -D Reveal Details of the Structural Basis for Flax Disease Resistance Specificity. The Plant Cell Online 2007;19(9):2898-2912.

130. Kutateladze TG. Mechanistic similarities in docking of the FYVE and PX domains to phosphatidylinositol 3-phosphate containing membranes. Progress in Lipid Research 2007;46(6):315-327.

131. Kutateladze TG, Capelluto DGS, Ferguson CG, Cheever ML, Kutateladze AG, Prestwich GD, Overduin M. Multivalent Mechanism of Membrane Insertion by the FYVE Domain. Journal of Biological Chemistry 2004;279(4):3050-3057.

132. Lee SA, Kovacs J, Stahelin RV, Cheever ML, Overduin M, Setty TG, Burd CG, Cho W, Kutateladze TG. Molecular Mechanism of Membrane Docking by the Vam7p PX Domain. Journal of Biological Chemistry 2006;281(48):37091-37101.

133. Triano I, Barrera FN, Renart ML, Molina ML, Fernández-Ballester G, Poveda JA, Fernández AM, Encinar JA, Ferrer-Montiel AV, Otzen D, González-Ros JM. Occupancy of Nonannular Lipid Binding Sites on KcsA Greatly Increases the Stability of the Tetrameric Protein. Biochemistry 2010;49(25):5397-5404.

134. Narayan K, Lemmon MA. Determining selectivity of phosphoinositide-binding domains. Methods 2006;39(2):122-133.

135. Blatner NR, Stahelin RV, Diraviyam K, Hawkins PT, Hong W, Murray D, Cho W. The Molecular Basis of the Differential Subcellular Localization of FYVE Domains. Journal of Biological Chemistry 2004;279(51):53818-53827.

136. Kale SD, Tyler BM. Entry of oomycete and fungal effectors into plant and animal host cells. Cellular Microbiology 2011;13(12):1839-1848.

137. Gu B, Kale SD, Wang Q, Wang D, Pan Q, Cao H, Meng Y, Kang Z, Tyler BM, Shan W. Rust Secreted Protein Ps87 Is Conserved in Diverse Fungal Pathogens and Contains a RXLR-like Motif Sufficient for Translocation into Plant Cells. PLoS ONE 2011;6(11):e27217.

138. Rafiqi M, Gan PHP, Ravensdale M, Lawrence GJ, Ellis JG, Jones DA, Hardham AR, Dodds PN. Internalization of Flax Rust Avirulence Proteins into Flax and Tobacco Cells Can Occur in the Absence of the Pathogen. The Plant Cell Online 2010;22(6):2017-2032.

139. Dou D, Kale SD, Liu T, Tang Q, Wang X, Arredondo FD, Basnayake S, Whisson S, Drenth A, Maclean D, Tyler BM. Different Domains of Phytophthora sojae Effector Avr4/6 Are

Recognized by Soybean Resistance Genes Rps4 and Rps6. Molecular Plant-Microbe Interactions 2010;23(4):425-435.

140. Carlton JG, Cullen PJ. Coincidence detection in phosphoinositide signaling. Trends in Cell Biology 2005;15(10):540-547.

141. Lemmon MA. Pleckstrin homology (PH) domains and phosphoinositides. In: Wakelam MJO, editor. Cell Biology of Inositol Lipids and Phosphates; 2007. p. 81-93.

APPENDIX

Biochem J. 2011 May 1; 435(3):597-608.

The C2 domain of Tollip, a Toll-like receptor signalling regulator, exhibits broad preference for phosphoinositides.

Ankem G, Mitra S, ***Sun F***, Moreno AC, Chutvirasakul B, Azurmendi HF, Li L, Capelluto DG.

Source

Protein Signaling Domains Laboratory, Department of Biological Sciences, Virginia Tech, Blacksburg, VA 24061, USA.

Abstract

TLRs (Toll-like receptors) provide a mechanism for host defence immune responses. Activated TLRs lead to the recruitment of adaptor proteins to their cytosolic tails, which in turn promote the activation of IRAKs (interleukin-1 receptor-associated kinases). IRAKs act upon their transcription factor targets to influence the expression of genes involved in the immune response. Tollip (Toll-interacting protein) modulates IRAK function in the TLR signalling pathway. Tollip is multimodular, with a conserved C2 domain of unknown function. We found that the Tollip C2 domain preferentially interacts with phosphoinositides, most notably with PtdIns3P (phosphatidylinositol 3-phosphate) and PtdIns(4,5)P_2 (phosphatidylinositol 4,5-bisphosphate), in a Ca^{2+}-independent manner. However, NMR analysis demonstrates that the Tollip C2 domain binds Ca^{2+}, which may be required to target the membrane interface. NMR and lipid-protein overlay analyses suggest that PtdIns3P and PtdIns(4,5)P_2 share interacting residues in the protein. Kinetic studies reveal that the C2 domain reversibly binds PtdIns3P and PtdIns(4,5)P_2, with affinity values in the low micromolar range. Mutational analysis identifies key PtdIns3P- and PtdIns(4,5)P_2-binding conserved basic residues in the protein. Our findings suggest that basic residues of the C2 domain mediate membrane targeting of Tollip by interaction with phosphoinositides, which contribute to the observed partition of the protein in different subcellular compartments.

BJ www.biochemj.org

BJ Structure

Biochem. J. (2011) **435**, 597–608 (Printed in Great Britain) doi:10.1042/BJ20102160

online data

The C2 domain of Tollip, a Toll-like receptor signalling regulator, exhibits broad preference for phosphoinositides

Gayatri ANKEM*[1], Sharmistha MITRA*[1], Furong SUN*, Anna C. MORENO*, Boonta CHUTVIRASAKUL*[2], Hugo F. AZURMENDI‡, Liwu LI† and Daniel G. S. CAPELLUTO*[3]

*Protein Signaling Domains Laboratory, Department of Biological Sciences, Virginia Tech, Blacksburg, VA 24061, U.S.A., †Laboratory of Innate Immunity and Inflammation, Department of Biological Sciences, Virginia Tech, Blacksburg, VA 24061, U.S.A., and ‡Department of Chemistry, Virginia Tech, Blacksburg, VA 24061, U.S.A.

TLRs (Toll-like receptors) provide a mechanism for host defence immune responses. Activated TLRs lead to the recruitment of adaptor proteins to their cytosolic tails, which in turn promote the activation of IRAKs (interleukin-1 receptor-associated kinases). IRAKs act upon their transcription factor targets to influence the expression of genes involved in the immune response. Tollip (Toll-interacting protein) modulates IRAK function in the TLR signalling pathway. Tollip is multimodular, with a conserved C2 domain of unknown function. We found that the Tollip C2 domain preferentially interacts with phosphoinositides, most notably with PtdIns3*P* (phosphatidylinositol 3-phosphate) and PtdIns(4,5)P_2 (phosphatidylinositol 4,5-bisphosphate), in a Ca^{2+}-independent manner. However, NMR analysis demonstrates that the Tollip C2 domain binds Ca^{2+}, which may be required to target the membrane interface. NMR and lipid–protein overlay analyses suggest that PtdIns3*P* and PtdIns(4,5)P_2 share interacting residues in the protein. Kinetic studies reveal that the C2 domain reversibly binds PtdIns3*P* and PtdIns(4,5)P_2, with affinity values in the low micromolar range. Mutational analysis identifies key PtdIns3*P*- and PtdIns(4,5)P_2-binding conserved basic residues in the protein. Our findings suggest that basic residues of the C2 domain mediate membrane targeting of Tollip by interaction with phosphoinositides, which contribute to the observed partition of the protein in different subcellular compartments.

Key words: C2 domain, calcium, nuclear magnetic resonance (NMR), phosphoinositide, Toll-interacting protein (Tollip), Toll-like receptor (TLR).

INTRODUCTION

Both TLRs (Toll-like receptors) and IL-1Rs (interleukin-1 receptors) provide a mechanism for host defence responses by activating the innate and adaptive immune responses [1]. These receptors are single-transmembrane proteins with ecto-domains composed largely of leucine-rich repeats and with a conserved cytosolic TIR (Toll/interleukin-1 receptor) domain, which facilitates the recruitment of adaptor proteins [2]. TLRs are broadly distributed on cells of the immune system and are the best-studied immune sensors of invading pathogens. There are at least eleven human TLRs (TLR1–TLR11) [3] that use the adaptor protein MyD88 (myeloid differentiation factor 88) to signal, with the exception of TLR3 and TLR4 [4]. TLR types 1, 2, 4, 5, and 6 are expressed on the cell surface and are involved in recognizing lipopeptides and proteins. On the other hand, the antiviral TLR types 3, 7, 8, and 9 are localized in endosomes [4]. Upon activation (i.e. by microbial products), TLRs are believed to either homo- or hetero-dimerize, followed by MyD88 binding to the cytosolic TIR domain of the TLR (for a review, see [1]). This, in turn, promotes the activation of stress-activated protein kinases, including the IRAKs (IL-1R-associated kinases) 1, 2, M and 4. These kinases bind to MyD88 by their death domains, facilitating the activation of the tumour-necrosis factor-receptor-associated factor 6, which forms a protein complex with two ubiquitin-conjugating enzymes, the ubiquitin-conjugating enzyme variant 1A and ubiquitin-conjugating enzyme 13. Activation of other kinases by TLRs, including IκB [inhibitor of NF-κB (nuclear factor κB)] kinases, leads to the release of the transcription factor NF-κB from IκB and subsequent phosphorylation and ubiquitin-dependent degradation of IκB. NF-κB translocates to the nucleus, which promotes pro-inflammatory responses by mediating cytokine gene expression [5].

Tollip (Toll-interacting protein) controls IRAK function in both TLR and IL-1R signalling pathways [6–8]. In resting cells, Tollip regulates these pathways on two different levels. First, Tollip associates with IL-1R, TLR2 and TLR4 after lipopolysaccharide activation, inhibiting TLR-mediated cell activation [7]. Secondly, Tollip binds directly to IRAK, inhibiting IRAK autophosphorylation [6,7]. Indeed, overexpression of Tollip leads to inhibition of TLR-mediated NF-κB activation [6,7]. Following TLR signalling stimulation, the Tollip–IRAK complex associates with the cytosolic tails of IL-1R and TLR. IRAK autophosphorylates and phosphorylates Tollip [7], thus

Abbreviations used: C2 domain, conserved 2 domain; CBR, Ca^{2+}-binding region; CUE, coupling of ubiquitin to endoplasmic reticulum degradation; DTT, dithiothreitol; GST, glutathione transferase; HSQC, heteronuclear single quantum coherence; IκB, inhibitor of nuclear factor κB; IL-1R, interleukin-1 receptor; Ins(1,3)P_2, inositol (1,3)-bisphosphate; Ins(1,4,5)P_3, inositol (1,4,5)-trisphosphate; IPTG, isopropyl β-D-thiogalactopyranoside; IRAK, IL-1 receptor-associated kinase; MyD88, myeloid differentiation factor 88; NF-κB, nuclear factor κB; PA, 1,2-dioleoyl-*sn*-glycero-3-phosphate; PC 1,2-dioleoyl-*sn*-glycero-3-phosphocholine; PE, 1,2-dipalmitoyl-*sn*-glycero-3-phosphoethanolamine; PG, 1,2-dipalmitoyl-*sn*-glycero-3-phospho-(1′-*rac*-glycerol); PH, pleckstrin homology; PI, phosphatidylinositol; PKC, protein kinase C; PtdIns3*P*, phosphatidylinositol 3-phosphate; PtdIns(4,5)P_2, phosphatidylinositol (4,5)-bisphosphate; PtdIns(3,4,5)P_3, phosphatidylinositol (3,4,5)-trisphosphate; PS, 1,2-dioleoyl-*sn*-glycero-3-phospho-L-serine; SPR, surface plasmon resonance; TBD, Tom1-binding domain; TIR, Toll/interleukin-1 receptor; TLR, Toll-like receptor; Tollip, Toll-interacting protein.

[1] These authors contributed equally to this work.
[2] Present address: Department of Pharmaceutical Chemistry and Pharmacognosy, Srinakharinwirot University, Nakornnayok 26120, Thailand.
[3] To whom correspondence should be addressed (email capellut@vt.edu).

initiating downstream signalling [6]. In addition, Tollip is involved in protein sorting by its association with Tom1 (target of Myb1), ubiquitin, and clathrin [9]. Tollip is localized on early endosomes, where it is required for both degradation of ubiquitin-conjugated proteins [8] and sorting of IL-1R on late endosomes [10]. Recently, Tollip has been shown to be SUMOylated and to mediate IL-1R SUMOylation [11]. This novel function makes Tollip a putative regulator of nuclear and cytoplasmic protein trafficking.

Tollip is a modular protein containing an N-terminal TBD (Tom1-binding domain), a central C2 (conserved 2) domain and a C-terminal CUE (coupling of ubiquitin to endoplasmic reticulum degradation) domain [6]. Using a lipid–protein overlay assay, Tollip was found to bind to both PtdIns3*P* (phosphatidylinositol 3-phosphate) and PtdIns(3,4,5)P_3 [phosphatidylinositol (3,4,5)-trisphosphate] [12]. A lysine to glutamic acid mutation located within the C2 domain (K150E) abrogates phosphoinositide binding [12], suggesting that the Tollip C2 domain is engaged in lipid binding. The CUE domain is a ubiquitin-binding module [13] that has been shown to bind to, and be phosphorylated by, IRAK proteins [7]. The tertiary structure of the CUE domain from two yeast proteins reveals a helical conformation with the Vps9p CUE domain being a dimer [14], whereas the CUE domain of Cue2 protein is a monomer [15]. Two-hybrid studies show that rat Tollip interacts with itself, suggesting that the protein forms oligomers [11]. In agreement, we have recently shown that the human Tollip CUE domain forms tight dimers that can contribute to Tollip oligomerization and ligand recognition [16].

There are at least 200 C2 domains and, after the PH (pleckstrin homology) domain, they represent the second most common lipid-binding domain [17]. Numerous C2 domains mediate signalling in a Ca^{2+}-dependent membrane-binding manner, as is the case for the conventional protein kinase C and synaptotagmin I, in which ion binding occurs via three loops known as CBRs (Ca^{2+}-binding regions) (for a review, see [18]). Binding of Ca^{2+} potentiates C2 domain recognition to acidic phospholipid membranes by changing the overall electrostatic potential at the C2 domain surface [19]. However, the C2 domain of the cytosolic phospholipase A2 binds to neutral membranes in a Ca^{2+}-bound state [19]. A minor group of C2 domains shows weak membrane affinity and is usually engaged in protein–protein interactions or exhibits a structural function. A third group of C2 domains does not bind Ca^{2+} at all, but binds to membranes or participates in protein–protein interactions [20–22]. The Tollip C2 domain lacks two aspartic acid residues necessary for Ca^{2+} binding [6]. However, recent studies of the C2 domain of synaptotagmin IV indicate that Ca^{2+} binding cannot always be predicted from sequence-based analysis [23].

The structure of C2 domains typically presents eight-stranded antiparallel β-sandwiches consisting of two sets of four-stranded β-sheets [18]. The C2 domain surface loops connect β-strands in two different topologies. The majority of the C2 domains present a cationic patch in the interior of the β-sandwich, which is known as the β-groove. Owing to the cationic nature of the β-groove and the Ca^{2+}-binding loops, both are proposed to be two different lipid-binding sites [18]. The C2 domains are known to bind a wide spectrum of phospholipids without a well-defined lipid-binding site [18]. A possible explanation is that, in the absence of Ca^{2+}, the cationic β-groove provides lipid recognition, necessary for the vesicle fusion activity of host proteins [24].

In the present study, we demonstrate that the C2 domain region is responsible for phosphoinositide recognition in Tollip. Remarkably, our findings support a broad range of specificity in which the phosphoinositide moiety is a common theme. Moreover, our results indicate that two of the most preferred ligands, PtdIns3*P* and PtdIns(4,5)P_2 [phosphatidylinositol (4,5)-bisphosphate], interact with basic residues in the Tollip C2 domain with affinities in the low-micromolar range and that binding of Ca^{2+} to the C2 domain is dispensable for phosphoinositide recognition. Overall, our findings might provide an explanation for the underlying mechanism responsible for Tollip's partition into different subcellular membrane compartments.

EXPERIMENTAL

Chemicals

A list of chemicals used and their suppliers follows: PC (1,2-dioleoyl-*sn*-glycero-3-phosphocholine), PS (1,2-dioleoyl-*sn*-glycero-3-phospho-L-serine), PA (1,2-dioleoyl-*sn*-glycero-3-phosphate), PE (1,2-dipalmitoyl-*sn*-glycero-3-phosphoethanolamine), PG [1,2-dipalmitoyl-*sn*-glycero-3-phospho-(1′-*rac*-glycerol)] and PI (phosphatidylinositol) (Avanti Polar Lipids); PtdIns3*P*, PtdIns4*P*, PtdIns5*P*, PtdIns(3,4)P_2, PtdIns(3,5)P_2, PtdIns(4,5)P_2, and PtdIns(3,4,5)P_3 (Cayman Chemicals); Ins1*P* (inositol 1-phosphate), Ins(1,3)P_2 (inositol 1,3-bisphosphate) and Ins(1,4,5)P_3 (inositol 1,4,5-trisphosphate) (Echelon); and IPTG (isopropyl β-D-thiogalactopyranoside) (Research Products International). All other chemicals were analytical reagent grade.

Cloning, expression and purification of the Tollip constructs

The human full-length Tollip, its isolated C2 domain (residues 54–182), and the *Saccharomyces cerevisiae* Vam7p PX domain (residues 2–134) cDNAs were cloned into a pGEX4T3 vector (GE Healthcare) and expressed in *Escherichia coli* (Rosetta; Stratagene). Briefly, bacterial cells were grown in Luria–Bertani medium at 37 °C until they reached a D_{600} of ~0.8. Induction of GST (glutathione transferase)-fusion proteins resulted from the addition of 0.1 mM IPTG followed by a 4 h incubation at 25 °C. Cell pellets were suspended in ice-cold buffer containing 50 mM Tris/HCl (pH 7.3), 500 mM NaCl, 500 mM benzamidine, 0.1 mg/ml lysozyme, 5 mM DTT (dithiothreitol) and 0.1 % Triton X-100. Suspensions were further processed by sonication (using a Branson sonifier 250 with a duty cycle of 30 % and eight pulses of 30 s each), centrifuged (1940 ***g***, 30 min, 4 °C) and the resultant supernatants loaded on to a glutathione–Sepharose 4B (GE Healthcare) column. In some cases, fusion proteins were eluted off the beads by addition of 20 mM Tris/HCl (pH 7), 500 mM NaCl and 100 mM reduced glutathione. In other purifications, the GST tag was removed by incubation of the fusion protein with thrombin (EMD Biosciences) overnight at 4 °C. Proteins were recovered in a buffer containing 20 mM Tris/HCl (pH 8) and 500 mM NaCl, concentrated using a 3-kDa-cut-off concentrator device (Millipore) and further purified by an ÄKTA FPLC system using a size-exclusion chromatography column (Superdex 75; GE Healthcare) equilibrated with 50 mM Tris/HCl (pH 8), 1 M NaCl and 1 mM DTT. Protein peak fractions were pooled, exchanged in the corresponding buffer, and further concentrated for functional and structural analysis.

Liposome-binding assay

Stocks of phospholipids were prepared in organic solvents as described in the manufacturer's instructions. Liposomes were prepared by a weight ratio of 1:1 PC/PE, and 5 % of the phospholipid under investigation was used. Controls were prepared by adjusting ratios with both PC and PE. Lipid films were generated by freeze-drying and hydrated in 50 mM Hepes (pH 6) and 100 mM NaCl to 1 mg/ml at 67 °C for 30 min and freeze–thawed three times. Liposomes were sonicated (using a

Branson sonifier 250 with a duty cycle of 30 % and eight pulses of 30 s each), pelleted (15000 ***g***, 20 min, 22 °C), and suspended at 5 mg/ml in the same buffer. A 10 μg portion of protein was incubated with 200 μg of total lipid for 30 min at room temperature (22 °C). Liposome-bound and free-protein fractions were obtained by centrifugation and analysed by SDS/PAGE (10 % gels). Protein bands were quantified using AlphaEase FC software.

NMR spectroscopy

NMR protein samples contained 150 μM Tollip C2 domain, 90 % H_2O/10 % ^2H_2O, 20 mM $^2H_{11}$ Tris/HCl (pH 6.8), 150 mM KCl, 5 mM $^2H_{10}$ DTT and 1 mM NaN_3. Two-dimensional NMR experiments were acquired at 25 °C using a Bruker Avance III 600 MHz spectrometer (Virginia Tech) equipped with an inverse TXI probe with *z*-axis pulsed-field gradients. Additional NMR experiments were performed on a Bruker Avance 800 MHz spectrometer equipped with a cryoprobe at the University of Virginia. Phospholipid head group and $CaCl_2$ titrations into the ^{15}N-labelled C2 domain were analysed by ^{1}H-^{15}N HSQC (heteronuclear single quantum coherence) experiments. Spectra were processed with NMRPipe [25] and analysed using nmrDraw [26].

CD spectroscopy

Far-UV CD spectra were generated using purified proteins (10 μM) in 5 mM Tris/HCl (pH 6.8), 100 mM KF and 0.1 mM DTT on a Jasco J-815 spectropolarimeter equipped with a Jasco PFD-425 S temperature control unit. Spectra were collected in a 1-mm-pathlength quartz cell at 25 °C. Spectra were obtained from five accumulated scans from 240 to 190 nm using a bandwidth of 1 nm and a response time of 1 s at a scan speed of 20 nm/min. Buffer backgrounds were used to subtract from the protein spectra. Secondary structure content of the proteins was estimated with the online server DICHROWEB [27] using the CDSSTR algorithm [28]. Near-UV CD spectra were collected using a 0.1-cm pathlength at 20 nm/min between 340 and 250 nm with a response time of 1 s and data pitch of 0.5 nm. Owing to the weak molar absorptivity of aromatic amino acids, 100 μM protein was employed for the near-UV CD experiments. Thermal denaturation of the proteins (10 μM) was investigated in the range 4–90 °C following temperature-induced changes in ellipticity at 218 nm, where the temperature was increased 1 °C/min, using 1.5-nm bandwidth, an averaging time of 30 s and an equilibration time of 2 min.

Fluorescence spectroscopy

Intrinsic tryptophan fluorescence spectroscopy measurements were carried out using a Jasco J-815 spectropolarimeter at 25 °C in a 1-cm-pathlength cuvette. λ_{ex} was 295 nm, and the fluorescence emission spectra were recorded from 310 to 410 nm for each protein sample.

Surface plasmon resonance analysis

Measurements were carried out at room temperature in 20 mM Hepes (pH 6) and 100 mM NaCl using an L1 sensor chip on a BIAcore X100 instrument. Liposomes, containing PtdIns3*P*, PtdIns(4,5)P_2 or PE, were made as described above with an additional extrusion step using 400-nm membranes. The surface of the sensor chip was preconditioned by injecting 40 mM *N*-octyl β-D-glucopyranoside at a flow rate of 5 μl/min. The first flow cell was used as a control surface, whereas the second flow cell was employed as the active surface. Both flow cells were coated with 6000 RU (resonance units) of 1 mg/ml each of the liposomes tested at a flow rate of 2 μl/min. After liposome coating, 30 μl of 10 mM NaOH at a flow rate of 30 μl/min was used to wash away any unbound liposome. Non-specific binding sites at the sensor chip surface were then blocked with the injection of 250 μl of 0.1 mg/ml fatty-acid-free BSA (Sigma) at a flow rate of 5 μl/min. A range of concentrations of protein analytes was prepared in the same buffer and injected on both flow cell surfaces at a flow rate of 30 μl/min. Sensorgrams were obtained from at least five different concentrations of each of the tested proteins. Association and dissociation times for each protein injection were set at 120 and 600 s respectively. The remaining bound protein was washed away by the injection of 30 μl of 10 mM NaOH. The sensor chip surface was regenerated using 40 mM *N*-octyl β-D-glucopyranoside and recoated with fresh liposomes for the next protein titration. Data were analysed using BIAcore X100 evaluation software (version 2.0).

Lipid–protein overlay assay

Lipid strips were prepared by spotting 1 μl of the indicated amount of phosphoinositide dissolved in chloroform/methanol/water (65:35:8) on to Hybond-C Extra membranes (GE Healthcare). Membrane strips containing the immobilized phosphoinositide were blocked with 3 % (w/v) fatty-acid-free BSA (Sigma) in 20 mM Tris/HCl (pH 8), 150 mM NaCl and 0.1 % Tween 20 for 1 h at room temperature. Then, membranes were incubated with 0.1 μg/ml protein in the same buffer without BSA overnight at 4 °C. Following four washes with the same buffer, bound proteins were probed with rabbit anti-GST antibody (Santa Cruz Biotechnology) and donkey anti-rabbit-HRP (horseradish peroxidase) antibody (GE Healthcare). Protein binding was detected using enhanced chemiluminescence reagent (Pierce).

RESULTS

The Tollip C2 domain preferentially binds phosphoinositides

The C2 domain is a conserved module located between the N-terminal TBD and the C-terminal CUE domain in Tollip (Figure 1A). A recent report indicated that Tollip binds to both PtdIns3*P* and PtdIns(3,4,5)P_3 using the lipid–protein overlay assay [12] and that mutation at Lys^{150}, a residue located within the C2 domain, abrogates phospholipid binding [12]. To determine whether the C2 domain of Tollip is responsible for phospholipid recognition, we isolated this domain and investigated whether it binds phospholipids using liposomes, which closely resemble biological membranes. We found that the C2 domain preferentially bound to phosphoinositides compared with liposomes bearing other phospholipids, including PC, PA, PG, PS or PI (Figures 1B and 1C). These findings are in agreement with those observed in other C2 domains, which typically exhibit highly variable and relatively low lipid specificity [18]. Phospholipid binding by the C2 domain was at most ~60 % of the total protein when compared with the Vam7p PX domain (Figure 1B), a PtdIns3*P* binding domain [29]. These results indicate that the Tollip C2 domain preferentially binds phosphatidylinositol species with phosphate groups at their inositol rings.

To further validate our findings, next we compared phosphoinositide interactions using the head group of PtdIns3*P* and PtdIns(4,5)P_2, the most preferred lipid ligands of the Tollip C2 domain (Figures 1B and 1C), and NMR spectroscopy

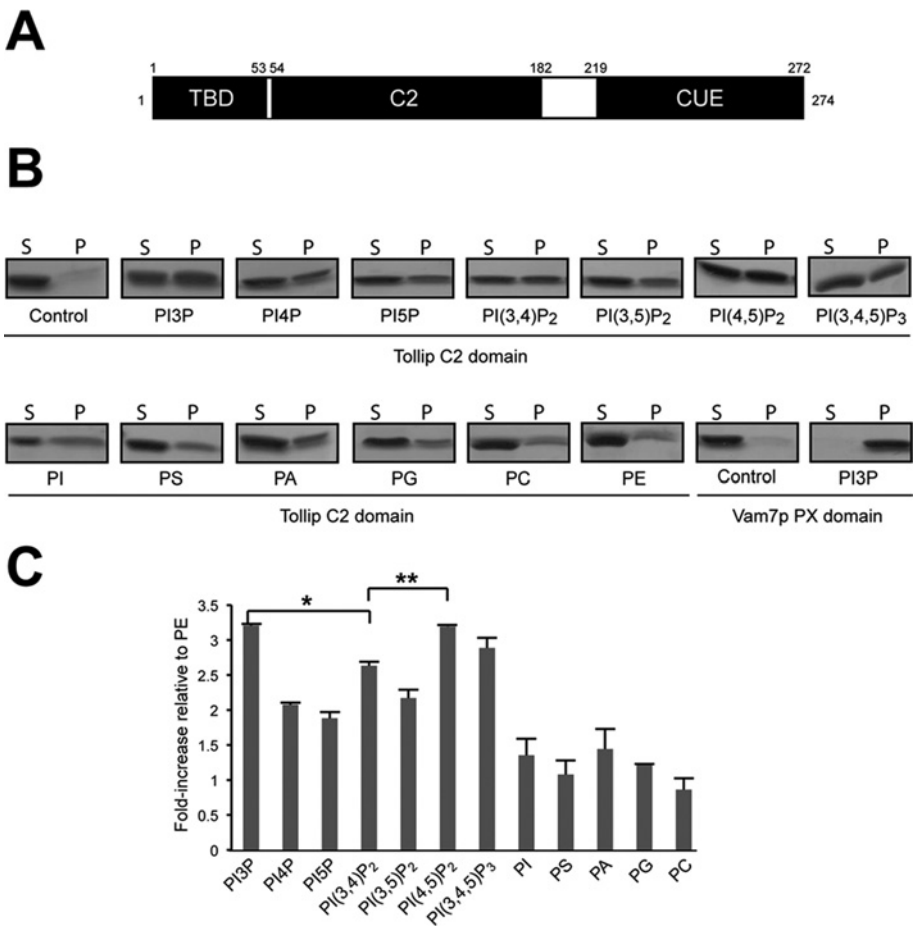

Figure 1 Lipid ligand preference of the Tollip C2 domain

(**A**) Schematic representation of the Tollip primary structure with the boundaries of each of the domains indicated above the diagram. (**B**) Phospholipid specificity of the Tollip C2 domain using liposomes containing 5 % various phospholipids and compared with control liposomes (PC/PE). The Vam7p PX domain was employed as a positive control. P and S indicate pellet and supernatant fractions respectively, after centrifugation, SDS/PAGE and Coomassie Blue staining. (**C**) Bands were quantified using Alphaimager and normalized to the liposomes control. Both * and **, $P < 0.05$. The ratios represent means + S.D. for three independent assays. PI, PtdIns.

analysis. Initial NMR titration experiments using PtdIns3*P* and PtdIns(4,5)P_2 led to significant protein precipitation (results not shown). Several chemical shift perturbations of C2 domain residues were detected after the addition of the lipid head groups, Ins(1,3)P_2 (for PtdIns3*P*; Figure 2A) and Ins(1,4,5)P_3 [for PtdIns(4,5)P_2; Figure 2B] in ^{15}N-^{1}H HSQC experiments. The rate of the association is in the fast-exchange regime and the protein exhibits a low affinity for the head group, which was anticipated, owing to the absence of a membrane interface. Most chemical-shift perturbations in each spectra are similar, suggesting that at least PtdIns3*P* and PtdIns(4,5)P_2 head groups share some binding residues. These perturbations are absent from NMR samples of the Tollip C2 domain containing an Ins1*P* head group of PI, which is composed of the core of the inositol ring of phosphoinositides, but lacks the phosphate groups at the same protein/ligand ratio (Figure 2C). Thus this result serves as a control to identify specific chemical-shift perturbations with phosphorylated inositol rings. To further determine that distinct phosphoinositides share some binding residues in the Tollip C2 domain, we performed a competition lipid–protein overlay assay. In this case, the tagged recombinant protein (as a GST-fusion) was pre-incubated with Ins(1,4,5)P_3 to allow binding, and this mixture was then added to a membrane-bound PtdIns3*P*. As shown in Figure 3(A), Ins(1,4,5)P_3 significantly reduced binding of PtdIns3*P* to the Tollip C2 domain.

Structural analysis of the Tollip C2 domain

Far-UV CD spectroscopy was used to characterize the secondary structure of the Tollip C2 domain. Figure 3(B) shows that the domain exhibits a typical spectrum of a β-sheet protein with a minimum at 218 nm. Prediction of the secondary structure content revealed that the C2 domain presents ~34 % β-sheet and negligible α-helical content (~4 %). After addition of 16-fold of Ins(1,3)P_2, the PtdIns3*P* head group did not induce any significant change in the overall secondary structure of the protein (Figure 3B and results not shown). Tryptophan, tyrosine, and phenylalanine residues are the main chromophores in the CD of the near-UV region and therefore provide information about the tertiary structure of proteins [30]. The Tollip C2 near-UV spectrum exhibits a negative peak between 278 and 310 nm with a minimum at ~292 nm, which is probably due to the contribution of its tyrosine and tryptophan side chains to the tertiary structure (Figure 3C). The overall intensity of the Tollip C2 spectrum is shifted up somewhat by the addition of Ins(1,3)P_2 (Figure 3B). Although the cause of this intensity difference is not clear, the shape similarities of the two spectra indicate that the head group does not induce a conformational change in the tertiary structure of the protein upon binding. Thus most of the chemical-shift changes observed in the Tollip C2 NMR spectrum upon addition of Ins(1,3)P_2 (Figure 2A) are likely to be a consequence of direct

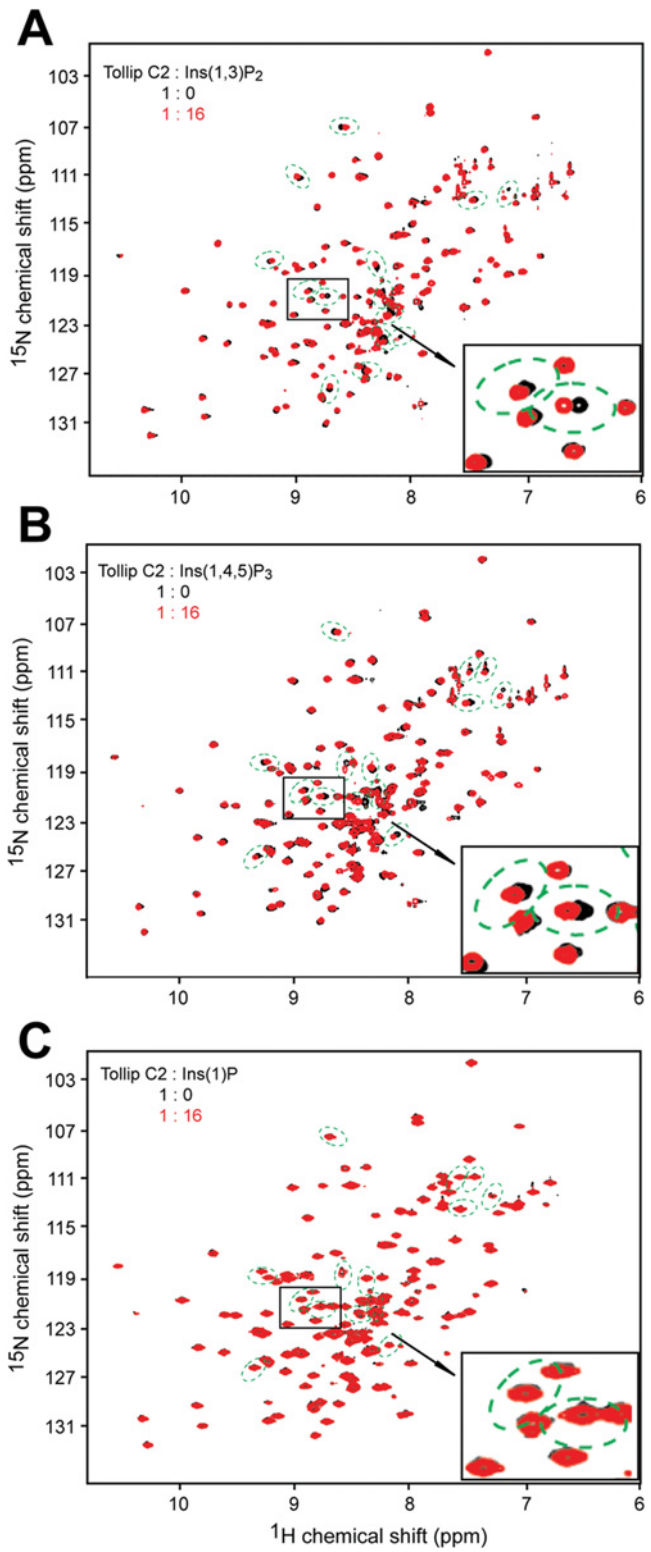

Figure 2 The Tollip C2 domain interacts with phosphorylated inositol rings at positions 3, 4 and 5

The ^{15}N-labelled Tollip C2 domain (black) was subjected to ^{1}H-^{15}N HSQC analysis following titration with Ins(1,3)P_2 (**A**), Ins(1,4,5)P_3 (**B**) or Ins1P (**C**) at a protein/lipid head group molar ratio of 1:16. Tollip C2 domain residues that shift upon head-group titration in (**A**) and (**B**) are illustrated with green broken ovals. The location of these residues is also shown in (**C**). A representative section of the HSQC titrations is magnified in each panel for clarification.

contact between the protein and the lipid head group. Recently, we reported that the CUE domain forms dimers [16] and therefore it represents a contributor of Tollip oligomerization. Some C2 domains have been reported to mediate protein dimerization [31–33]. Therefore we have also investigated the oligomeric state of the Tollip C2 domain by analytical size-exclusion chromatography. The protein eluted at a volume that corresponded to a 15.5-kDa globular protein (Figure 3D), a value close to its theoretical molecular mass (15.7 kDa). Mass spectral analysis of the protein revealed a prominent signal at 15 481 (see Figure S1 at http://www.BiochemJ.org/bj/435/bj4350597add.htm), confirming the monomeric nature of the protein. Thermal denaturation analysis indicated that the Tollip C2 domain shows two-state melting transitions, indicative of a highly co-operative unfolding transition between 50 °C and 60 °C with an apparent melting temperature of 54 °C. The fluorescence spectrum of the Tollip C2 domain exhibited a maximum at 340 nm and a further red shift of ~6 nm and reduced emission intensity after denaturation with guanidine hydrochloride (Figure 3F), indicative of a relatively buried average localization for the three tryptophan residues present in the native conformation of the protein domain.

The Tollip C2 domain binds Ca^{2+}, which is not required for phosphoinositide binding

Ca^{2+} is a physiological ligand for most C2 domains, whose binding is necessary to increase the affinity of the protein to lipids for membrane-docking events. The Tollip C2 domain presents three conserved aspartic acid residues involved in Ca^{2+} ligation found in other C2 domains [6] (see Figure 7A). Therefore we experimentally investigated whether the Tollip C2 domain binds Ca^{2+} using CD and NMR spectroscopy. The CD spectrum of the Tollip C2 domain does not exhibit any conformational change upon addition of up to 30 mM $CaCl_2$ (results not shown). However, NMR spectroscopy analysis demonstrates that Ca^{2+} selectively induces chemical-shift perturbations in the spectrum of the protein (Figure 4A). The binding also appears to be on a fast-exchange regime, indicating a low affinity for the ligand in solution. Many C2 domains have been shown to interact with lipids in a Ca^{2+}-dependent manner. Therefore we investigated whether Ca^{2+} binding contributes to phosphoinositide recognition by the Tollip C2 domain. As shown in Figure 4(B), the Tollip C2 domain did not exhibit Ca^{2+}-dependent binding to PtdIns3P, and the binding was not further changed by the presence of EGTA, a Ca^{2+} chelator. PtdIns(4,5)P_2 binding by the Tollip C2 domain was also Ca^{2+}-independent (results not shown).

Kinetic analysis of Tollip C2 domain–phosphoinositide interactions

The interaction of the Tollip C2 domain with phosphoinositide-enriched liposomes was kinetically examined by SPR (surface plasmon resonance), using tag-free Tollip C2 domain as the analyte and either PtdIns3P- or PtdIns(4,5)P_2-enriched liposomes immobilized on an L1 sensor chip as ligands. The Vam7p PX domain binds PtdIns3P [29] and was employed as a positive control. In all cases, proteins exhibited fast association and dissociation rates. The Tollip C2 domain bound phosphoinositide-enriched liposomes following a two-state conformational change model and displayed reversible binding (Figures 5A and 5B). No fitting could be obtained when plots were analysed using the 1:1 Langmuir model (results not shown). Binding affinity and kinetic properties of the proteins and their phosphoinositide ligands are summarized in Table 1. The Tollip

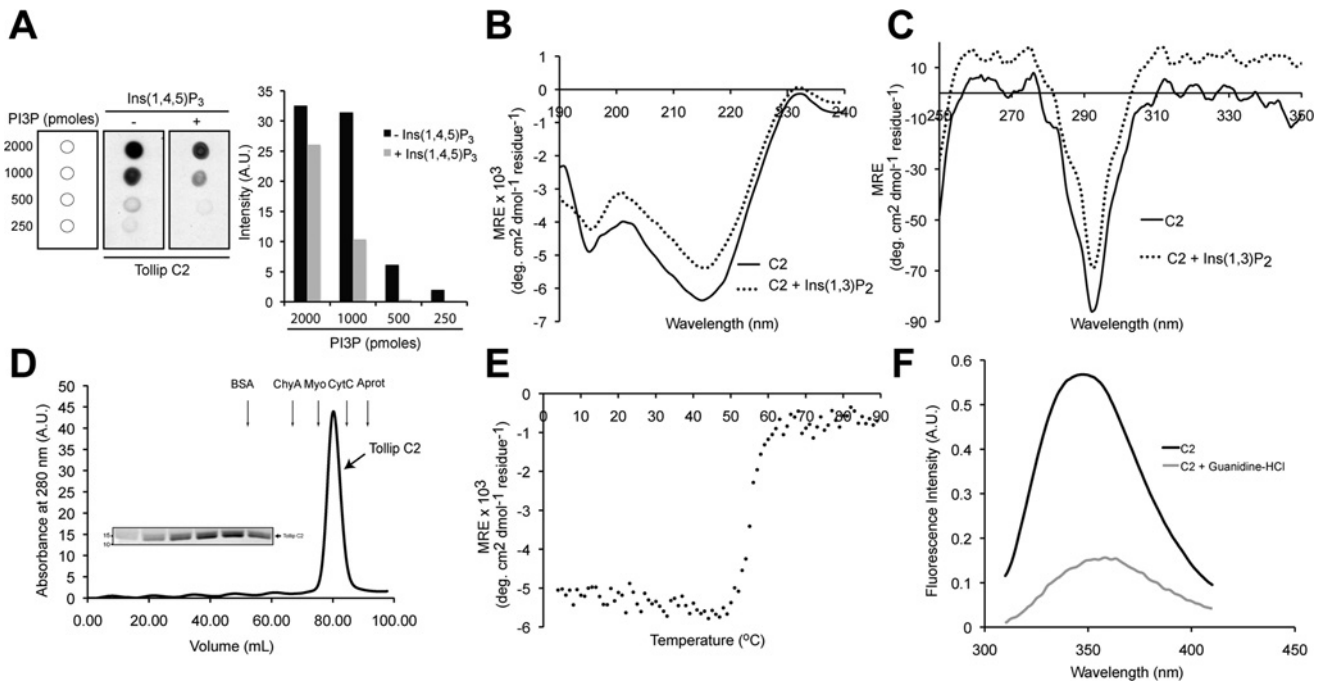

Figure 3 Structural analysis of the free and head-group-bound Tollip C2 domain

(**A**) PtdIns3*P* (PI3P) and PtdIns(4,5)P_2 compete with each other for binding to the Tollip C2 domain. The GST–Tollip C2 domain (10 μM) was pre-incubated with 50 μM Ins(1,4,5)P_3 for 30 min at room temperature and the mixture was further incubated with strips containing PtdIns3*P* at the indicated amounts and further processed as described in the Experimental section. (**B**) Far-UV CD spectra of the Tollip C2 domain in the absence or presence of 16-fold of Ins(1,3)P_2. MRE, mean residue ellipticity. (**C**) Near-UV CD spectra of the Tollip C2 domain in the absence or presence of 16-fold of Ins(1,3)P_2. (**D**) Size-exclusion chromatography elution profile of the Tollip C2 domain monitored at 280 nm. Arrows denote the positions of the molecular-mass standards (Aprot, aprotinin; ChyA, chymotrypsinogen A; CytC, cytochrome *c*; Myo, myoglobin). A.U., arbitrary units. The inset represents the fractions of the protein peak loaded on an SDS/PAGE gel and stained with Coomassie Blue. (**E**) Thermal denaturation of the Tollip C2 domain at 218 nm. (**F**) Fluorescence emission spectra of the Tollip C2 domain in the absence (black line) and presence (grey line) of 6 M guanidine hydrochloride.

Table 1 Liposome-binding parameters of the Tollip C2 domain determined from SPR analysis

k_{a1}, association rate constant; k_{a2}, forward rate constant changing complex; k_{d1}, dissociation rate complex; k_{d2}, reverse dissociation rate constant changing complex.

Ligand	k_{a1} ($M^{-1} \cdot s^{-1}$)	k_{d1} (s^{-1})	k_{a2} (s^{-1})	k_{d2} (s^{-1})	k_d (M)	Fit (χ^2)
PtdIns3*P*	$(3.3 \pm 0.2) \times 10^3$	$(3.9 \pm 0.1) \times 10^{-2}$	$(5.6 \pm 0.2) \times 10^{-4}$	$1.6 \pm 0.02 \times 10^{-2}$	1.1×10^{-5}	9.6
PtdIns(4,5)P_2	$(6.8 \pm 0.3) \times 10^4$	$(5.1 \pm 0.2) \times 10^{-1}$	$(7.1 \pm 0.1) \times 10^{-4}$	$1.1 \pm 0.04 \times 10^{-3}$	4.6×10^{-6}	7.7

C2 domain bound with dissociation constants (K_d) of 4.6 and 11 μM for PtdIns(4,5)P_2 and PtdIns3*P* liposomes respectively. These affinity values are comparable with that determined for PtdIns(4,5)P_2 binding by the C2 domain of classical PKC (protein kinase C) [34], but much lower than the affinities reported for the synaptotagmin C2b and PKCθ C2 domains for the same ligand [22,24]. On the other hand, the Vam7p PX domain bound PtdIns3*P* following a 1:1 Langmuir model (Figure 5C). The affinity of the Vam7p PX domain for PtdIns3*P* liposomes was 1000-fold higher with a K_d of 9.5 nM (see Supplementary Table S1 at http://www.BiochemJ.org/bj/435/bj4350597add.htm), a phosphoinositide affinity value similar to those determined for other PX domains [35]. The affinity differences between the proteins for phosphoinositides are reflected by plotting the log of maximum resonance units against protein concentration, in which the Tollip C2 domain exhibits a modest affinity when compared with the Vam7p PX domain (Figure 5D). However, in all titrations, phosphoinositide binding exhibited a saturable binding isotherm that is associated with specific binding (Figure 5D).

Conserved basic residues in the Tollip C2 domain play a critical role in phosphoinositide recognition

Since phosphoinositides are negatively charged, several conserved basic residues of the Tollip C2 domain (see Supplementary Figure S2 at http://www.BiochemJ.org/bj/435/bj4350597add.htm) were mutated to alanine and analysed for binding to PtdIns3*P*, one of the most preferred Tollip C2 domain ligands (see Figures 1B and 1C and [12]), using the lipid–protein overlay assay. As expected, Tollip bound to PtdIns3*P* in a lipid-mass-dependent manner (Figure 6A). Mutation of the non-conserved Lys^{150} residue (Figure S2) to glutamic acid in Tollip has been shown to abrogate lipid binding [12]. However, we found that a mutation of the same residue to a neutral amino acid reduced, but did not eliminate, PtdIns3*P* binding; rather, mutation of the conserved Lys^{162} residue to alanine almost completely abolished PtdIns3*P* binding (Figure 6A). Curiously, the isolated C2 domain consistently showed a higher binding signal when compared with the full-length Tollip protein (Figure 6A). This observation suggests that neighbouring regions may modulate phosphoinositide recognition by the C2 domain.

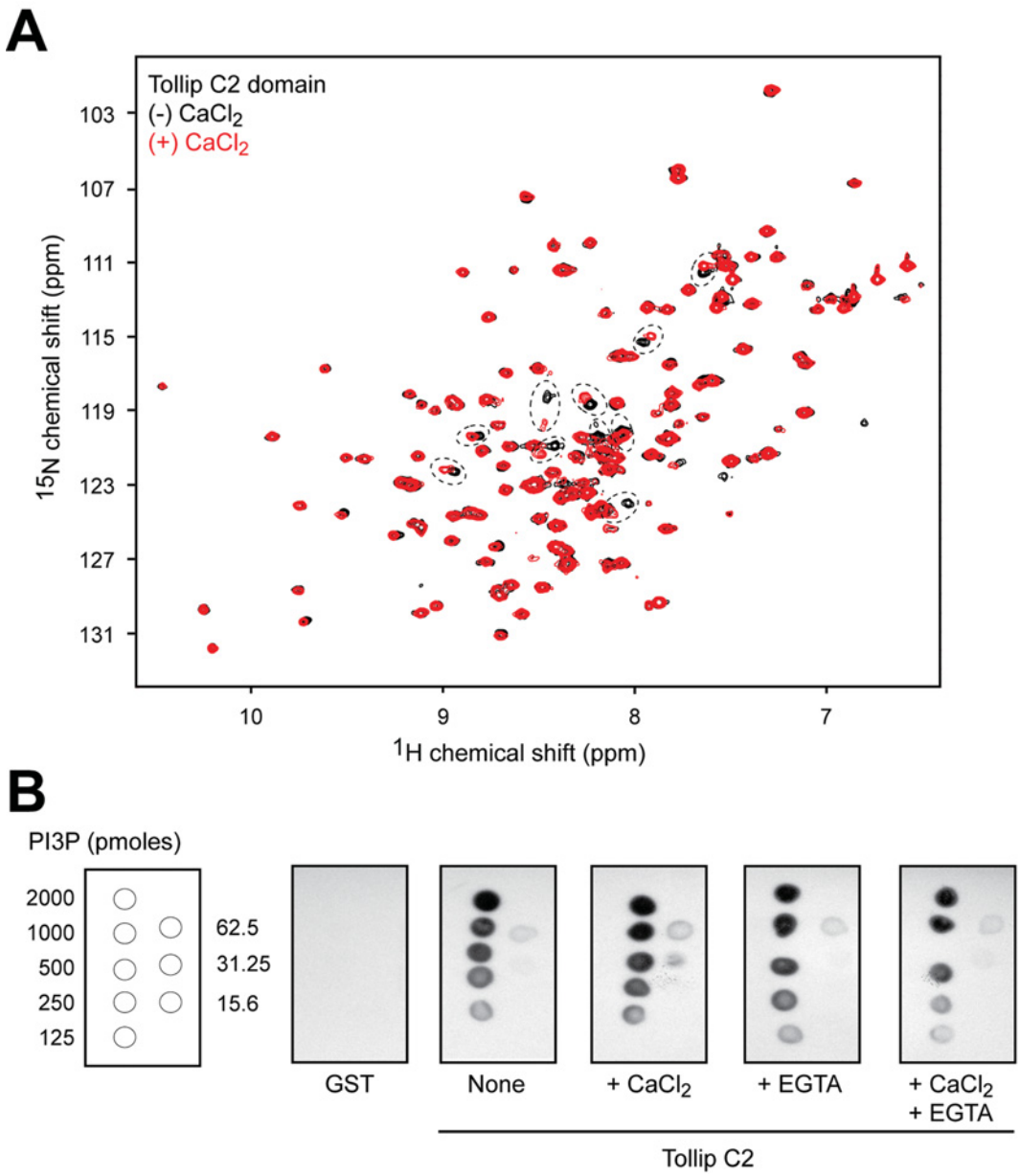

Figure 4 Ca^{2+} binding by the Tollip C2 domain and role of Ca^{2+} in phosphoinositide interactions

(**A**) Overlay of the ^{1}H-^{15}N HSQC spectra of the Tollip C2 domain in the absence (black) and presence (red) of 5 mM $CaCl_2$. Perturbed resonances are labelled with black broken ovals. (**B**) Ca^{2+}-independent phosphoinositide binding of the Tollip C2 domain determined by the lipid–protein overlay assay. Each spot contains 15.6–2000 pmol of PtdIns3*P* (PI3P). A GST–Tollip C2 domain fusion protein was incubated with lipid strips in the absence or presence of 1 mM $CaCl_2$, 1 mM EGTA, or both 1 mM $CaCl_2$ and 1 mM EGTA. GST was employed as a negative control.

We further screened for PtdIns3*P*-binding residues by site-directed mutagenesis in the Tollip C2 domain. We found that mutations to alanine at Arg^{78}, Arg^{123}, His^{135}, Arg^{157}, and Lys^{162} almost eliminated PtdIns3*P* binding, whereas mutations at Lys^{102} and Lys^{150} mirrored the strength of binding of the wild-type Tollip C2 domain for the same phosphoinositide (Figure 6A). Overall, these results indicate that specific conserved basic residues in the Tollip C2 domain play a critical role in phosphoinositide recognition. We then functionally and structurally investigated the K162A mutant of the C2 domain for simplicity. Consistent with our findings, the inability of the Tollip C2 K162A to bind PtdIns3*P* was evident using the liposome-binding assay (Figure 6B). Likewise, PtdIns3*P* binding by the Tollip C2 K162A mutant was also negligible using SPR (results not shown). Mutation at Lys^{162} did not alter the secondary structure, the tryptophan fluorescence emission, or the stability and compactness of the Tollip C2 domain (Supplementary Figure S3 at http://www.BiochemJ.org/bj/435/bj4350597add.htm and results not shown), indicating that the mutation specifically disrupts PtdIns3*P* binding. Our studies also demonstrate that Tollip bound PtdIns(4,5)P_2 and that Tollip K162A exhibited a slightly reduced, but not abolished, binding to this phosphoinositide (Figure 6C). Mutation at Lys^{150} showed no major differences from Tollip for binding to PtdIns(4,5)P_2 (results not shown). Whereas residues Arg^{78}, Arg^{123} and His^{135} in the isolated C2 domain seemed to be critical for PtdIns(4,5)P_2 binding, the Lys^{162} mutation

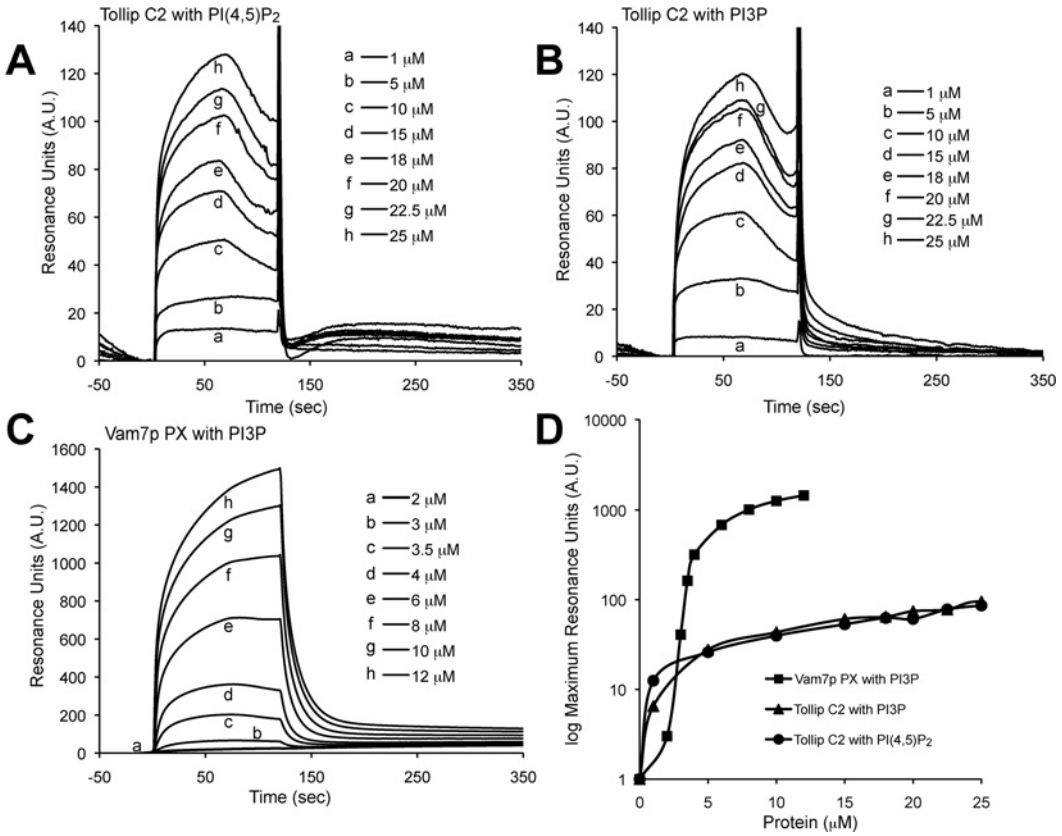

Figure 5 Kinetic analysis of Tollip C2 domain interactions with phosphoinositides

SPR sensorgrams for the binding of the Tollip C2 domain with PtdIns(4,5)P_2-containing liposomes (**A**), and with PtdIns3*P* liposomes (**B**). As a control, the Vam7p PX domain was probed against PtdIns3*P* liposomes (**C**). Various concentrations of each of the protein domains were flowed over the liposomes attached on an L1 sensor chip for 120 s. (**D***)* The strength of the associations is represented in the plot, in which the resonance units are on a logarithmic scale. Au, arbitrary units; PI, PtdIns.

exhibited only a minor reduction in binding to the same lipid (Figure 6C). PtdIns(4,5)P_2 binding by K102A and R157A C2 domains were indistinguishable to that observed for the wild-type protein (Figure 6C). Thus our findings indicate that unique Tollip C2 domain residues are able to discriminate the position of the phosphorylation(s) at the inositol ring in phosphoinositide ligands.

DISCUSSION

Tollip is a key regulator of TLR-dependent signalling pathways [36]. To exert this function, Tollip binds to the tail of TLR proteins in association with adaptor proteins at the boundaries of the cytosolic face of the plasma membrane and endosomes to inhibit IRAK function. However, the determinants by which Tollip associates with these proteins at the membrane boundaries still remain unclear. In the present paper, we show for the first time that Tollip preferentially binds to phosphoinositides by its conserved C2 domain. Phosphatidylinositols represent less than 15 % of the total phospholipids present in eukaryotes, with PtdIns4*P* and PtdIns(4,5)P_2 being the most abundant phosphoinositides in mammalian cells [37]. Each of the seven phosphoinositides found in these cells exhibits distinctive subcellular membrane localization. For example, PtdIns(4,5)P_2 and PtsIns(3,4,5)P_3 are enriched at the plasma membrane, whereas PtsIns3*P* is found exclusively in endosomes [37]. Remarkably, the subcellular localization of these phospholipids correlates with the reported subcellular localization of Tollip. Tollip is localized on early endosomes, multivesicular bodies [8] and the Golgi apparatus [12]. Thus the subcellular localization of Tollip and its ability to bind phosphoinositides and ubiquitin suggest that it may be involved in the recognition and transport of ubiquitinated proteins in endocytic pathways. TLR proteins signal from both plasma membranes and endosomes [2]. Thus, given the broad phosphoinositide specificity of its C2 domain, it is conceivable that Tollip is phosphoinositide-dependently partitioned in different subcellular membrane pools to control TLR function through MyD88-dependent pathways. We speculate that the broad specificity of the Tollip C2 domain to phosphoinositides may also increase the membrane affinity of Tollip or it may help to properly orient Tollip at the membrane.

Phospholipid-binding domains, including C2, PX, FYVE, PH and ENTH domains, are modules engaged in membrane trafficking by recruiting signalling peripheral proteins to specific cell membrane surfaces. These domains exhibit diverse affinity and specificity to negatively charged phospholipids found at the membrane and present a strong positive potential on their surface that promotes these associations. Of these, members of the PH and C2 domains are most commonly found in eukaryotes. Despite its ubiquitous presence, the C2 domain, unlike other lipid-binding modules, does not exhibit a well-defined lipid-binding site nor a conserved cationic patch [18]. Moreover, not all C2 domains can be easily identified by sequence homology. Another level of complexity is that C2 domains are present in soluble and transmembrane proteins, they bind lipids either in a Ca^{2+}-dependent

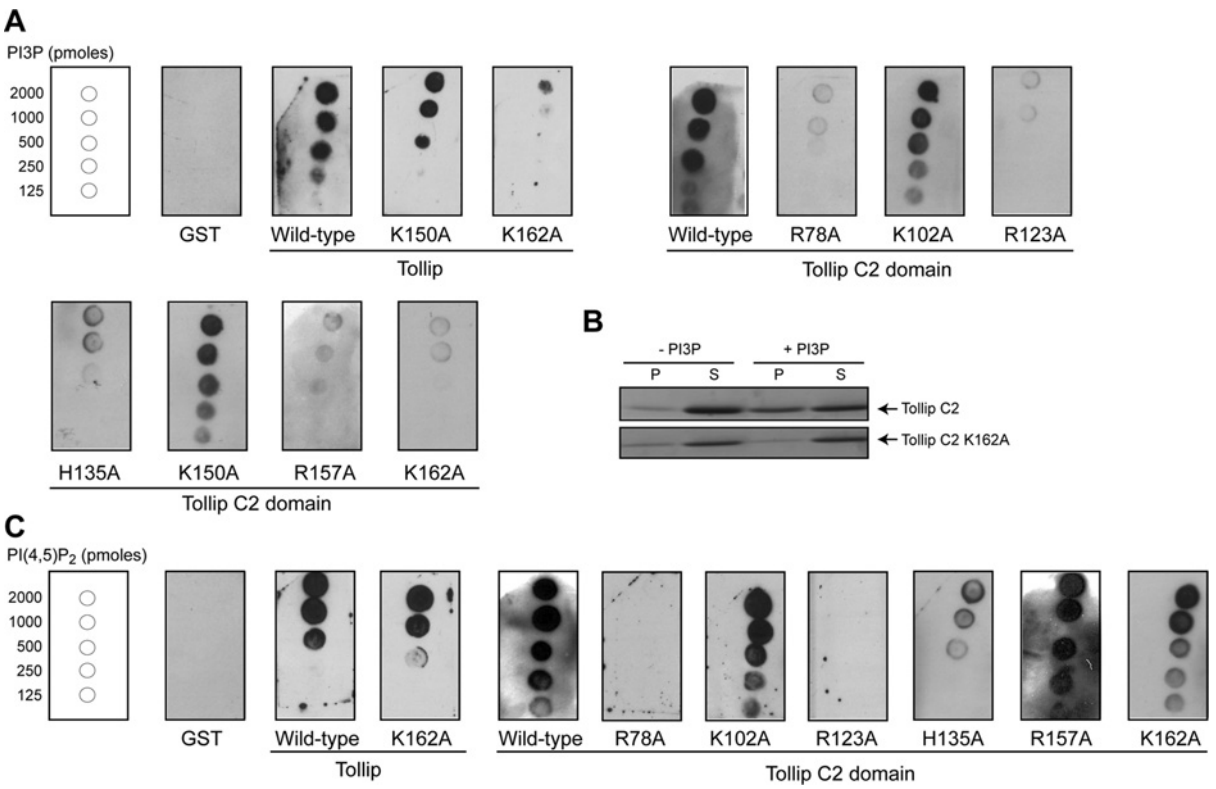

Figure 6 Identification of the Tollip residues critical for PtdIns3*P* and PtdIns(4,5)P_2 binding

(**A**) Lipid–protein overlay assay of immobilized PtdIns3*P* at the indicated amounts and GST-fusion Tollip, C2 domain and mutants in basic residues within the C2 domain. GST was used as a negative control. (**B**) Liposome-binding assay of wild-type Tollip C2 domain or its K162A mutant with liposomes without or with PtdIns3*P*. P and S represent pellet and supernatant fractions respectively after centrifugation, SDS/PAGE and Coomassie Blue staining. PI, PtdIns. (**C**) Lipid–protein overlay assay of immobilized PtdIns(4,5)P_2 at the indicated amounts and GST-fusion Tollip, C2 domain and mutants in conserved basic residues within the C2 domain.

or -independent fashion, and they can either bind strongly or weakly to biological membranes [18]. Therefore, sequence homology is unlikely to predict the biological function of an uncharacterized C2 domain on the basis of studies performed with the same module found in unrelated proteins. From our present studies, the Tollip C2 domain exhibited the highest preference of binding to liposomes enriched with the phosphoinositides PtdIns3*P*, PtdIns(4,5)P_2, and PtdIns(3,4,5)P_3 (Figures 1B and 1C). Therefore we investigated further the Tollip-binding properties of two of these ligands [PtdIns3*P* and PtdIns(4,5)P_2], given their strength of binding as well as the different locations of the phosphate groups at their inositol rings. Titration of the Tollip C2 domain with the head groups of PtdIns3*P* and PtdIns(4,5)P_2 showed chemical-shift deviations for restricted sets of NH signals (Figure 2). We were unable to assign the residues associated with these NMR chemical shifts due to the insolubility of the Tollip C2 domain at high concentrations. However, comparison of chemical-shift perturbations of the protein NMR spectrum by the addition of Ins(1,3)P_2 and Ins(1,4,5)P_3 suggest that phosphoinositide ligands share some residues in their binding sites. Competition analysis further confirmed this observation (Figure 3A). These results are not surprising given the intrinsic nature of C2 domains in recognizing a broad range of phospholipids [18]. Some C2 domains exhibit a dual lipid-recognition mechanism, in which multiple lipid ligands must be present at the membrane to achieve high affinity and to properly localize intracellularly [17]. However, our experimental results suggest that two Tollip C2 domain lipid ligands, PtdIns3*P* and PtdIns(4,5)P_2, overlap their binding sites (Figures 2 and 3A).

Far-UV CD spectroscopy analysis of the Tollip C2 domain support the presence of β-sheet secondary structure and that the protein lacks any major conformational change upon Ins(1,3)P_2 binding (Figure 3B and results not shown). In addition, a co-operative unfolding transition is observed in the protein with a relatively low-temperature midpoint ($\sim$54 °C). Similar properties are displayed by the synaptotagmin I C2A domain [38]. The near-UV spectrum of the Tollip C2 domain is unaffected by the presence of the lipid head group, indicating that no major changes in the tertiary folding of the protein are induced upon ligand binding. This is in agreement with the observation of selected NMR cross-peaks perturbed by the addition of phosphoinositide head groups (Figure 3).

A proposed Ca^{2+}-binding role has been shed by the observation that CBRs are usually surrounded by positively charged residues [39,40], amino acids that are also found near the second aspartic acid-rich region in Tollip (see Figure 7A). However, the presence of only three of the five aspartic acid residues required for Ca^{2+} binding suggests that Tollip may not bind Ca^{2+} (Figure 7A). Nonetheless, we experimentally demonstrate that the Tollip C2 domain binds Ca^{2+}, but that the ion seems to be dispensable for phosphoinositide binding. This result is not surprising, since similar observations were reported for the C2A domain of dysferlin, which contains four negatively charged residues of five required for Ca^{2+}-binding proteins [41]. Intriguingly, the synaptotagmin IV C2B domain contains all five aspartic residues, but is still unable to bind Ca^{2+} [23]; therefore Ca^{2+}-binding properties cannot be predicted from sequence analysis. As a Ca^{2+}-independent lipid-binding protein, basic residues at the surface of the Tollip C2 domain could make direct membrane contact, as

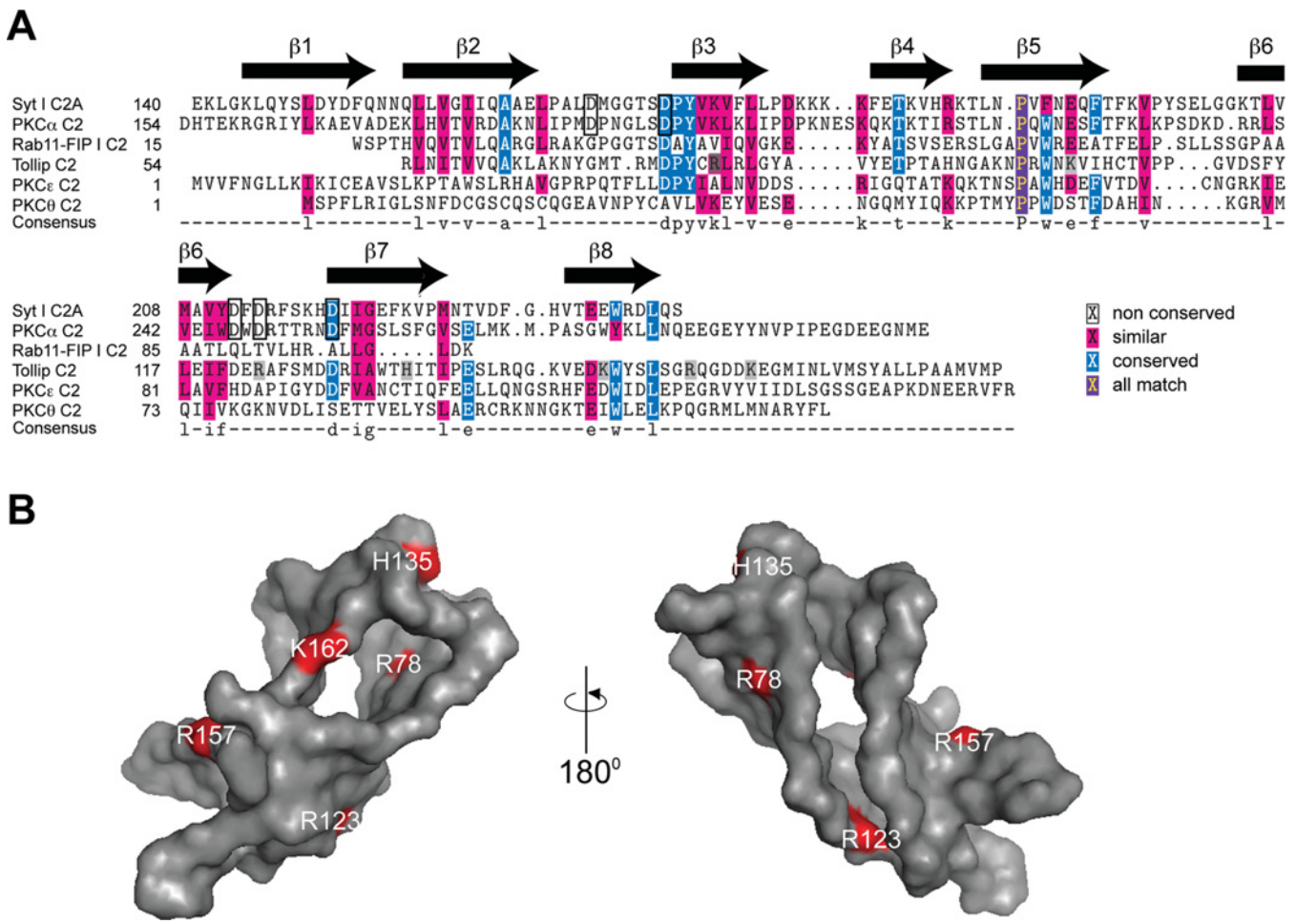

Figure 7 Sequence alignment, structural properties and location of critical basic residues in the modelled structure of the Tollip C2 domain

(**A**) Sequence alignment of the C2A domain of human synaptotagmin I (Syt I) (GenBank® accession number NP_005630), the C2 domain of human PKCα (GenBank® accession number NP_002728), the C2 domain of the human Rab11 family of interacting proteins (FIP) (GenBank® accession number NP_079427), the C2 domain of human Tollip (GenBank® accession number CAG38508), the C2 domain of human PKCε (GenBank® accession number CAA46388) and the C2 domain of human PKCθ (GenBank® accession number NP_006248) constructed from the Biology WorkBench database (http://workbench.sdsc.edu). Boxes indicate the conserved aspartic acid residues engaged in Ca^{2+} ligation in both the synaptotagmin I and PKCα C2 domains. The secondary-structure content determined for the synaptotagmin I C2 domain is depicted above the sequence alignment. Mutated Tollip C2 domain residues from the present study are labelled in grey. (**B**) Two views of the predicted tertiary structure of the Tollip C2 domain constructed from the AL2TS database (http://proteinmodel.org/AS2TS/al2ts.html) using the C2A domain of synaptotagmin I as a template and depicted using PyMol (http://www.pymol.org). Experimentally determined PtdIns3*P*-binding residues are labelled in red on the predicted Tollip C2 domain tertiary structure.

proposed for other C2 domains [18]. A distinct C2 family, related to the phosphoinositide 3-kinase C2 domain, has recently been proposed to interact with negatively charged lipids in a Ca^{2+}-independent manner through a patch of basic and hydrophobic residues located at the concave surface of the upper β-sheet that makes a PtdIns(4,5)P_2-binding and membrane-penetration site [42]. However, this region, located between β-strands 5 and 6 in C2 domains, does not exhibit a conserved basic and hydrophobic signature in Tollip (Figures 7A and S2). The CBR of Ca^{2+}-independent lipid-binding C2 domains has been proposed to play a role in lipid binding and specificity [43–45]. Further investigation is required to determine the role of Ca^{2+} binding by the Tollip C2 domain, which is beyond the scope of the present study.

SPR experiments allowed us to characterize the kinetics of Tollip C2 domain binding to phosphoinositides. The protein binds to PtdIns3*P* and PtdIns(4,5)P_2 with K_d values of 11 and 4.6 μM respectively, following a conformational change model. This may be the general mechanism by which Tollip binds to TLRs through a first association step with phosphoinositide-enriched membranes accompanied by a conformational change of the protein that further enhances binding to TLRs. For comparison purposes, we also measured the affinity of the Vam7p PX domain to PtdIns3*P*, which resulted in 1000-fold higher affinity than that of the C2 domain and the mode of binding followed a one-to-one interaction model. Despite the fact that both Tollip and Vam7p proteins are found in endosomes, differences in affinity can be explained by the low phospholipid specificity exhibited by the Tollip C2 domain. Our investigation indicates that the isolated C2 domain binds phosphoinositides more strongly than Tollip, suggesting that other domains (i.e. TBD and CUE) in the protein may exert a modulatory function. The C2 domain of the cytosolic phospholipase 2α binds more prominently than the full-length protein, and a local effect on the C2 domain was proposed [22]. Likewise, the PtdIns(4,5)P_2-binding ubiquitin ligase Smurf2 protein exhibits auto-inhibitory properties by intramolecular interaction between its C2 and HECT domains, leading to a reduction of its enzymatic activity and the stabilization of the protein levels in the cell [46].

In the present work, we have identified for the first time conserved basic amino acids critical for Tollip C2 domain interactions with PtdIns3*P* and PtdIns(4,5)P_2. Many structures of Ca^{2+}-dependent C2 domains have been solved in detail, and they exhibit a common fold with a well-defined cationic β-groove and with the CBR in the protein engaged in lipid binding [18]. A phosphoinositide-binding site has also been mapped in the C2B domain of rabphilin-3A, which shows that its polar C-terminal region, as well as its β-strands 3, 4, 6 and 7, are critically involved in lipid recognition in a Ca^{2+}-independent manner [47]. Our mutational analysis indicates that the Tollip C2 domain could bind phosphoinositides in a similar fashion (Figure 7B). Mutation of Lys^{150} to glutamic acid has been shown to abolish phospholipid binding by Tollip [12]. We mutated this residue to alanine, since this amino acid would not cause a change in the overall charge of the protein. Both Tollip and C2 domain K150A mutants exhibited indistinguishable binding to phosphoinositides (Figure 6A and results not shown). This result is supported by the fact that the residue is not conserved among Tollip proteins (Figure S2). Also, we found that some mutations in basic residues in the Tollip C2 domain abolished PtdIns3*P*, but not PtdIns(4,5)P_2, binding. However, these lipids compete with each other for binding to the Tollip C2 domain. Therefore it is conceivable that phosphoinositide-binding sites overlap in Tollip, but that distinctive residues provide broad specificity of the protein for phosphoinositides. Binding between the Tollip C2 domain and the evaluated phosphoinositides is with moderated affinity, which can be explained from the proposed shallow, surface-exposed, PtdIns3*P*-binding residues in the modelled structure of the protein (Figure 7B). Overall, we propose that, together with Ca^{2+}, a variety of hydrophobic and electrostatic forces can contribute to the Tollip–phosphoinositide interactions with biological membranes necessary for Tollip to modulate TLR signalling. Given the role of Tollip in recruiting adaptor proteins at the cytosolic tail of TLRs by its CUE domain, formation of such complexes may be further enhanced by initial Tollip interactions with phosphoinositides and membranes by its C2 domain. Further molecular studies are necessary to address how Tollip modulates TLR signalling. We are currently investigating the co-ordination between the C2, TBD and CUE domains for their molecular interactions, which will provide new insights into understanding the multimodular nature of Tollip.

AUTHOR CONTRIBUTION

Gayatri Ankem performed the purification of proteins and carried out liposome-binding assays, NMR titrations, CD measurements and protein–lipid overlay assays. Sharmistha Mitra carried out size-exclusion chromatography analysis, lipid–protein overlay assays and SPR experiments. Furong Sun and Anna Moreno purified proteins. Boonta Chutvirasakul designed constructs and purified proteins. Hugo Azurmendi carried out NMR experiments. Liwu Li provided reagents. Daniel Capelluto conceived the study, designed experiments, analysed data and wrote the manuscript.

ACKNOWLEDGEMENTS

We are grateful to Dr Kae-Jung Hwang and Rebecca Lehman for their contribution in the initial phase of this work, to Jeff Ellena for his assistance during the NMR titration experiments performed at the University of Virginia, and to Dr Carla V. Finkielstein and Dr Janet Webster for thoughtful comments on the manuscript.

FUNDING

This work was supported by the American Heart Association [grant number 086077E (to D.C.)].

REFERENCES

1 Kawai, T. and Akira, S. (2010) The role of pattern-recognition receptors in innate immunity: update on Toll-like receptors. Nat. Immunol. **11**, 373–384
2 Barton, G. M. and Kagan, J. C. (2009) A cell biological view of Toll-like receptor function: regulation through compartmentalization. Nat. Rev. Immunol. **9**, 535–542
3 Bowie, A. and O'Neill, L. A. (2000) The interleukin-1 receptor/Toll-like receptor superfamily: signal generators for pro-inflammatory interleukins and microbial products. J. Leukoc. Biol. **67**, 508–514
4 Frantz, S., Ertl, G. and Bauersachs, J. (2007) Mechanisms of disease: Toll-like receptors in cardiovascular disease. Nat. Clin. Pract. **4**, 444–454
5 Gan, L. and Li, L. (2006) Regulations and roles of the interleukin-1 receptor associated kinases (IRAKs) in innate and adaptive immunity. Immunol. Res. **35**, 295–302
6 Burns, K., Clatworthy, J., Martin, L., Martinon, F., Plumpton, C., Maschera, B., Lewis, A., Ray, K., Tschopp, J. and Volpe, F. (2000) Tollip, a new component of the IL-1RI pathway, links IRAK to the IL-1 receptor. Nat. Cell Biol. **2**, 346–351
7 Zhang, G. and Ghosh, S. (2002) Negative regulation of toll-like receptor-mediated signaling by Tollip. J. Biol. Chem. **277**, 7059–7065
8 Katoh, Y., Shiba, Y., Mitsuhashi, H., Yanagida, Y., Takatsu, H. and Nakayama, K. (2004) Tollip and Tom1 form a complex and recruit ubiquitin-conjugated proteins onto early endosomes. J. Biol. Chem. **279**, 24435–24443
9 Yamakami, M., Yoshimori, T. and Yokosawa, H. (2003) Tom1, a VHS domain-containing protein, interacts with tollip, ubiquitin, and clathrin. J. Biol. Chem. **278**, 52865–52872
10 Brissoni, B., Agostini, L., Kropf, M., Martinon, F., Swoboda, V., Lippens, S., Everett, H., Aebi, N., Janssens, S., Meylan, E. et al. (2006) Intracellular trafficking of interleukin-1 receptor I requires Tollip. Curr. Biol. **16**, 2265–2270
11 Ciarrocchi, A., D'Angelo, R., Cordiglieri, C., Rispoli, A., Santi, S., Riccio, M., Carone, S., Mancia, A. L., Paci, S., Cipollini, E. et al. (2009) Tollip is a mediator of protein sumoylation. PLoS ONE **4**, e4404
12 Li, T., Hu, J. and Li, L. (2004) Characterization of Tollip protein upon lipopolysaccharide challenge. Mol. Immunol. **41**, 85–92
13 Shih, S. C., Prag, G., Francis, S. A., Sutanto, M. A., Hurley, J. H. and Hicke, L. (2003) A ubiquitin-binding motif required for intramolecular monoubiquitylation, the CUE domain. EMBO J. **22**, 1273–1281
14 Prag, G., Misra, S., Jones, E. A., Ghirlando, R., Davies, B. A., Horazdovsky, B. F. and Hurley, J. H. (2003) Mechanism of ubiquitin recognition by the CUE domain of Vps9p. Cell **113**, 609–620
15 Kang, R. S., Daniels, C. M., Francis, S. A., Shih, S. C., Salerno, W. J., Hicke, L. and Radhakrishnan, I. (2003) Solution structure of a CUE-ubiquitin complex reveals a conserved mode of ubiquitin binding. Cell **113**, 621–630
16 Azurmendi, H., Mitra, S., Ayala, I., Li, L., Finkielstein, C. V. and Capelluto, D. G. S. (2010) Backbone ^{1}H, ^{15}N, and ^{13}C resonance assignments and secondary structure of the Tollip CUE domain. Mol. Cells **30**, 581–585
17 Stahelin, R. V. (2009) Lipid binding domains: more than simple lipid effectors. J. Lipid Res. **50**, S299–S304
18 Cho, W. and Stahelin, R. V. (2006) Membrane binding and subcellular targeting of C2 domains. Biochim. Biophys. Acta **1761**, 838–849
19 Nalefski, E. A., Wisner, M. A., Chen, J. Z., Sprang, S. R., Fukuda, M., Mikoshiba, K. and Falke, J. J. (2001) C2 domains from different Ca^{2+} signaling pathways display functional and mechanistic diversity. Biochemistry **40**, 3089–3100
20 Ochoa, W. F., Garcia-Garcia, J., Fita, I., Corbalan-Garcia, S., Verdaguer, N. and Gomez-Fernandez, J. C. (2001) Structure of the C2 domain from novel protein kinase Cε. A membrane binding model for Ca^{2+}-independent C2 domains. J. Mol. Biol. **311**, 837–849
21 Lindsay, A. J. and McCaffrey, M. W. (2004) The C2 domains of the class I Rab11 family of interacting proteins target recycling vesicles to the plasma membrane. J. Cell Sci. **117**, 4365–4375
22 Melowic, H. R., Stahelin, R. V., Blatner, N. R., Tian, W., Hayashi, K., Altman, A. and Cho, W. (2007) Mechanism of diacylglycerol-induced membrane targeting and activation of protein kinase Cθ. J. Biol. Chem. **282**, 21467–21476
23 Dai, H., Shin, O. H., Machius, M., Tomchick, D. R., Sudhof, T. C. and Rizo, J. (2004) Structural basis for the evolutionary inactivation of Ca^{2+} binding to synaptotagmin 4. Nat. Struct. Mol. Biol. **11**, 844–849
24 Fukuda, M., Kojima, T., Aruga, J., Niinobe, M. and Mikoshiba, K. (1995) Functional diversity of C2 domains of synaptotagmin family. Mutational analysis of inositol high polyphosphate binding domain. J. Biol. Chem. **270**, 26523–26527
25 Delaglio, F., Grzesiek, S., Vuister, G. W., Zhu, G., Pfeifer, J. and Bax, A. (1995) NMRPipe: a multidimensional spectral processing system based on UNIX pipes. J. Biomol. NMR **6**, 277–293

26 Garrett, D. S., Powers, R., Gronenborn, A. M. and Clore, G. M. (1991) A common-sense approach to peak picking in 2-dimensional, 3-dimensional, and 4-dimensional spectra using automatic computer-analysis of contour diagrams. J. Magn. Reson. **95**, 214–220

27 Whitmore, L. and Wallace, B. A. (2004) DICHROWEB, an online server for protein secondary structure analyses from circular dichroism spectroscopic data. Nucleic Acids Res. **32**, W668–W673

28 Sreerama, N. and Woody, R. W. (2004) Computation and analysis of protein circular dichroism spectra. Methods Enzymol. **383**, 318–351

29 Cheever, M. L., Sato, T. K., de Beer, T., Kutateladze, T. G., Emr, S. D. and Overduin, M. (2001) Phox domain interaction with PtdIns(3)P targets the Vam7 t-SNARE to vacuole membranes. Nat. Cell Biol. **3**, 613–618

30 Kelly, S. M., Jess, T. J. and Price, N. C. (2005) How to study proteins by circular dichroism. Biochim. Biophys. Acta **1751**, 119–139

31 Guan, R., Dai, H., Tomchick, D. R., Dulubova, I., Machius, M., Sudhof, T. C. and Rizo, J. (2007) Crystal structure of the RIM1α C2B domain at 1.7 Å resolution. Biochemistry **46**, 8988–8998

32 Gerber, S. H., Garcia, J., Rizo, J. and Sudhof, T. C. (2001) An unusual C_2-domain in the active-zone protein piccolo: implications for Ca^{2+} regulation of neurotransmitter release. EMBO J. **20**, 1605–1619

33 Liu, L., Song, X., He, D., Komma, C., Kita, A., Virbasius, J. V., Huang, G., Bellamy, H. D., Miki, K., Czech, M. P. and Zhou, G. W. (2006) Crystal structure of the C2 domain of class II phosphatidylinositide 3-kinase C2α. J. Biol. Chem. **281**, 4254–4260

34 Guerrero-Valero, M., Marin-Vicente, C., Gomez-Fernandez, J. C. and Corbalan-Garcia, S. (2007) The C2 domains of classical PKCs are specific PtdIns(4,5)P_2-sensing domains with different affinities for membrane binding. J. Mol. Biol. **371**, 608–621

35 Stahelin, R. V., Karathanassis, D., Bruzik, K. S., Waterfield, M. D., Bravo, J., Williams, R. L. and Cho, W. (2006) Structural and membrane binding analysis of the Phox homology domain of phosphoinositide 3-kinase-C2α. J. Biol. Chem. **281**, 39396–39406

36 Abreu, M. T. (2010) Toll-like receptor signalling in the intestinal epithelium: how bacterial recognition shapes intestinal function. Nat. Rev. Immunol. **10**, 131–144

37 Di Paolo, G. and De Camilli, P. (2006) Phosphoinositides in cell regulation and membrane dynamics. Nature **443**, 651–657

38 Shao, X., Li, C., Fernandez, I., Zhang, X., Sudhof, T. C. and Rizo, J. (1997) Synaptotagmin-syntaxin interaction: the C2 domain as a Ca^{2+}-dependent electrostatic switch. Neuron **18**, 133–142

39 Sutton, R. B., Davletov, B. A., Berghuis, A. M., Sudhof, T. C. and Sprang, S. R. (1995) Structure of the first C2 domain of synaptotagmin I: a novel Ca^{2+}/phospholipid-binding fold. Cell **80**, 929–938

40 Verdaguer, N., Corbalan-Garcia, S., Ochoa, W. F., Fita, I. and Gomez-Fernandez, J. C. (1999) Ca^{2+} bridges the C2 membrane-binding domain of protein kinase Cα directly to phosphatidylserine. EMBO J. **18**, 6329–6338

41 Therrien, C., Di Fulvio, S., Pickles, S. and Sinnreich, M. (2009) Characterization of lipid binding specificities of dysferlin C2 domains reveals novel interactions with phosphoinositides. Biochemistry **48**, 2377–2384

42 Zhang, D. and Aravind, L. (2010) Identification of novel families and classification of the C2 domain superfamily elucidate the origin and evolution of membrane targeting activities in eukaryotes. Gene **469**, 18–30

43 Ananthanarayanan, B., Das, S., Rhee, S. G., Murray, D. and Cho, W. (2002) Membrane targeting of C2 domains of phospholipase C-δ isoforms. J. Biol. Chem. **277**, 3568–3575

44 Das, S., Dixon, J. E. and Cho, W. (2003) Membrane-binding and activation mechanism of PTEN. Proc. Natl. Acad. Sci. U.S.A. **100**, 7491–7496

45 Dunn, R., Klos, D. A., Adler, A. S. and Hicke, L. (2004) The C2 domain of the Rsp5 ubiquitin ligase binds membrane phosphoinositides and directs ubiquitination of endosomal cargo. J. Cell Biol. **165**, 135–144

46 Wiesner, S., Ogunjimi, A. A., Wang, H. R., Rotin, D., Sicheri, F., Wrana, J. L. and Forman-Kay, J. D. (2007) Autoinhibition of the HECT-type ubiquitin ligase Smurf2 through its C2 domain. Cell **130**, 651–662

47 Montaville, P., Coudevylle, N., Radhakrishnan, A., Leonov, A., Zweckstetter, M. and Becker, S. (2008) The PIP_2 binding mode of the C2 domains of rabphilin-3A. Protein Sci. **17**, 1025–1034

Received 5 January 2011/1 February 2011; accepted 7 February 2011
Published as BJ Immediate Publication 7 February 2011, doi:10.1042/BJ20102160

Biochem. J. (2011) **435**, 597–608 (Printed in Great Britain) doi:10.1042/BJ20102160

SUPPLEMENTARY ONLINE DATA

The C2 domain of Tollip, a Toll-like receptor signalling regulator, exhibits broad preference for phosphoinositides

Gayatri ANKEM*[1], Sharmistha MITRA*[1], Furong SUN*, Anna C. MORENO*, Boonta CHUTVIRASAKUL*[2], Hugo F. AZURMENDI‡, Liwu LI† and Daniel G. S. CAPELLUTO*[3]

*Protein Signaling Domains Laboratory, Department of Biological Sciences, Virginia Tech, Blacksburg, VA 24061, U.S.A., †Laboratory of Innate Immunity and Inflammation, Department of Biological Sciences, Virginia Tech, Blacksburg, VA 24061, U.S.A., and ‡Department of Chemistry, Virginia Tech, Blacksburg, VA 24061, U.S.A.

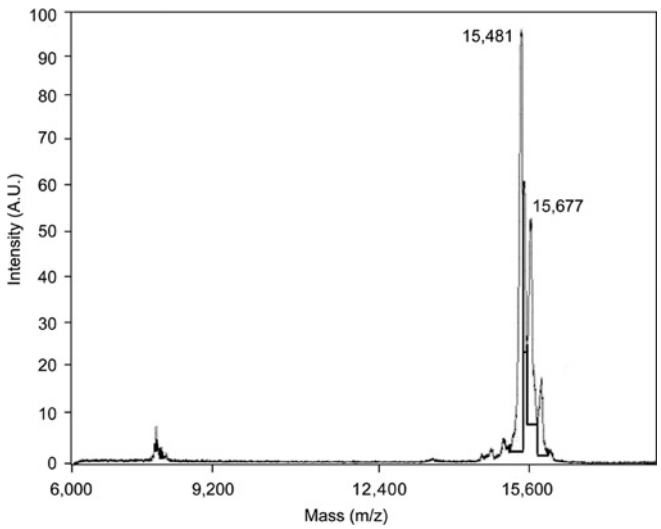

Figure S1 MS analysis of the Tollip C2 domain

A.U., arbitrary units.

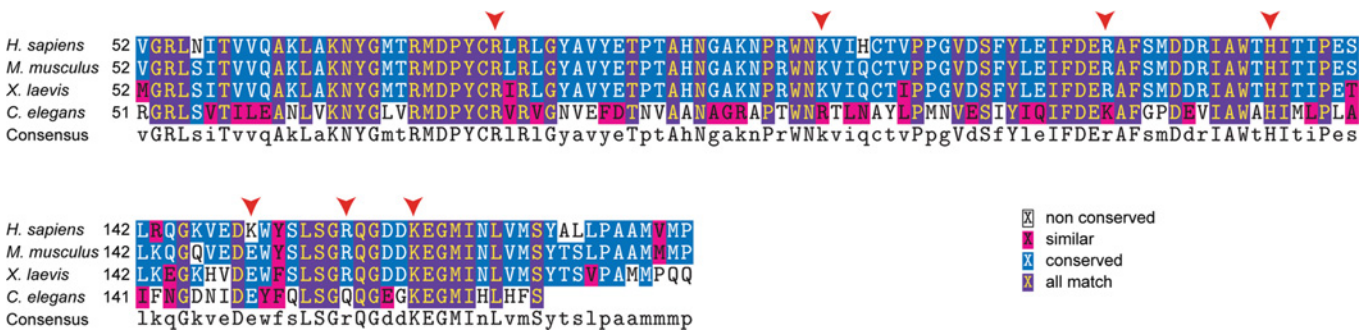

Figure S2 Sequence alignment of the Tollip C2 domains

Sequences are from *Homo sapiens* (GenBank® accession number CAG38508), *Mus musculus* (GenBank® accession number CAB58121), *Xenopus laevis* (GenBank® accession number NP_001085420) and *Caenorhabditis elegans* (GenBank® accession number NP_492757). The engineered mutations on the human Tollip C2 domain are indicated with red arrowheads above the sequences.

[1] These authors contributed equally to this work.
[2] Present address: Department of Pharmaceutical Chemistry and Pharmacognosy, Srinakharinwirot University, Nakornnayok 26120, Thailand.
[3] To whom correspondence should be addressed (email capellut@vt.edu).

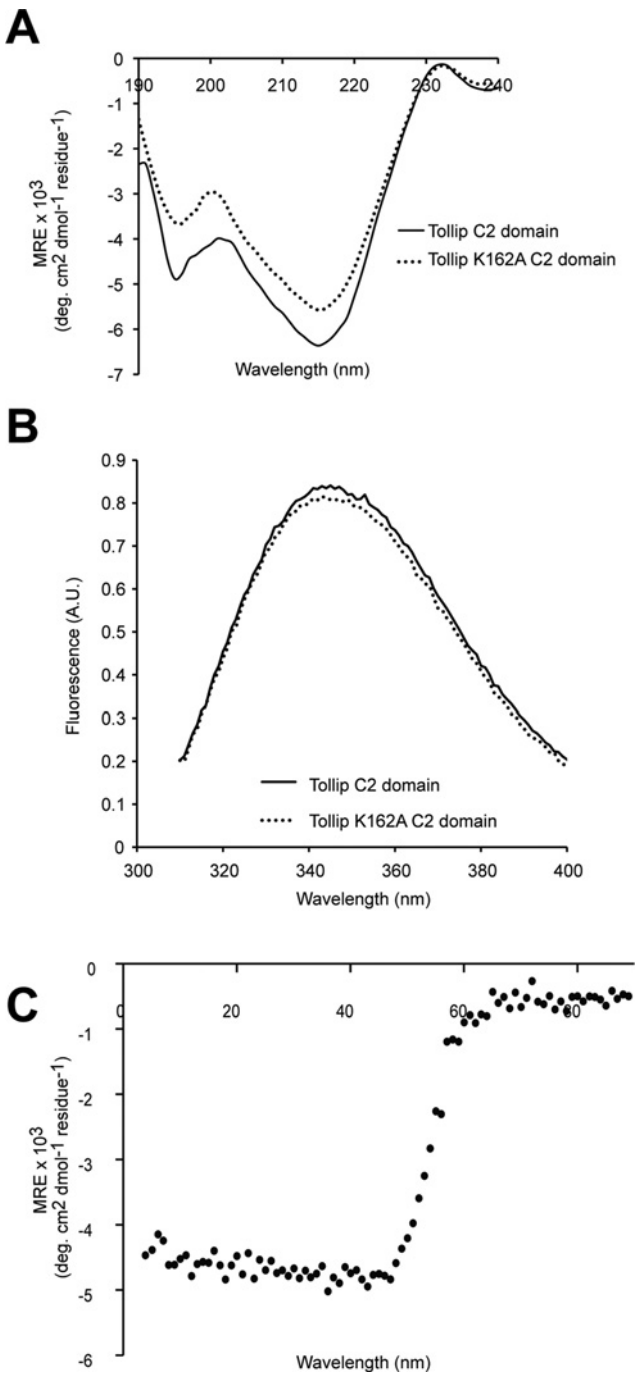

Figure S3 Structural analysis of the effects of a lipid-binding mutation on the Tollip C2 domain

(**A**) Far-UV CD spectra of the Tollip C2 domain (solid line) and K162A mutant (broken line). (**B**) Tryptophan fluorescence spectra of the Tollip C2 domain (solid line) and K162A mutant (broken line). (**C**) Thermal denaturation of the Tollip C2 K162A mutant. MRE, mean residue ellipticity.

Table S1 Apparent kinetic constants of the binding of the Vam7p PX domain to PtdIns3*P* liposomes using SPR detection

The constants and error values of the fitting were obtained from a single titration experiment of a representative data set. k_a, association rate constant; k_d, dissociation rate constant.

Ligand	k_a ($M^{-1} \cdot s^{-1}$)	k_d (s^{-1})	K_d (M)	Fit (χ^2)
PtdIns3*P*	$(2.4 \pm 0.8) \times 10^5$	$(2.7 \pm 1.3) \times 10^{-2}$	1.1×10^{-7}	12.8

Received 5 January 2011/1 February 2011; accepted 7 February 2011
Published as BJ Immediate Publication 7 February 2011, doi:10.1042/BJ20102160